



Democratic and Popular Republic of Algeria  
Ministry of Higher Education and Scientific Research  
University of Med Khider Biskra  
Faculty of Exact Sciences of Nature and Life



Department of Matter Sciences

Thesis

Presented to obtain the Degree of

Doctorate

Speciality: thin films

***Tin dioxide  $SnO_2$  thin films deposited by  
ultrasonic spray technique:  
Properties and Applications***

Presented by:

***Khelifi Chafia***

To the Jury composed by:

*Zerarka Abdel Ouahab*

*Attaf Abdallah*

*Chala Abdelouahad*

*Attaf Nadhir*

*Benhaoua Boubaker*

*Professor*

*Professor*

*Professor*

*Professor*

*Professor*

*University Med Khider of Biskra*

*University Med Khider of Biskra*

*University Med Khider of Biskra*

*University Mentouri of Constantine I*

*University Hama lakhder of El-Oued*

*President*

*Reporter*

*Examiner*

*Examiner*

*Examiner*

# Acknowledgement

*Firstly, I would like to thanks Allah for*

*Ever grace given to me*

*My parents, who are, support and filling me with love*

*Then with their prayers.*

*A great respect to my supervisor Pr. Abdallah Attaf*

*For his kindness, patience and his excellent ideas*

*Throughout my study.*

*To the president Pr. Ab. Zrarka for his honor that makes to me*

*To my examiners Pr. Chala Abdelouahad, Pr. Attaf Nadir,*

*Pr. Benhaoua Boubaker*

*Many thanks are given to all my teachers, especially Pr. S.*

*Rahmane and Dr T. Tibermacine for all valuable*

*informations and advices are giving to me.*

*To all the members of our laboratory*

*Finally I would like to acknowledge all my friends and*

*Ever one helps or supports me*

# *Dedicate*

*I dedicate this modest work to:*

*My parents treasured, I ask Allah to protect  
and join them in highest paradise*

*To my brothers and all my family*

*To my teachers ever one by his name*

*To all my friends.*



# Table of Contents

<b>DEDICATE .....</b>	<b>I</b>
<b>TABLE OF CONTENTS .....</b>	<b>II</b>
<b>INTRODUCTION .....</b>	<b>V</b>
<b>CHAPTER I: GENERALITIES ABOUT TCO, SnO<sub>2</sub>, THIN FILMS AND THESE CHARACTERIZATIONS</b>	
<b>I.1 TRANSPARENT CONDUCTING OXIDES .....</b>	<b>1</b>
<b>I.1.1 Applications of TCOs materials.....</b>	<b>2</b>
<b>I.2 TIN DIOXIDE.....</b>	<b>2</b>
<b>I.2.1 Definition.....</b>	<b>2</b>
<b>I.2.2 Crystalline Structure .....</b>	<b>3</b>
<b>I.2.3 The different phases of tin oxide.....</b>	<b>3</b>
<b>I.3 THIN FILMS .....</b>	<b>4</b>
<b>I.3.1 Thin film deposition processes .....</b>	<b>5</b>
<b>I.3.1.1 Physical Vapor Deposition (PVD) .....</b>	<b>5</b>
<b>I.3.1.1.a Pulsed Laser Deposition (PLD).....</b>	<b>5</b>
<b>I.3.1.1.b. Ion Beam Assisted Deposition.....</b>	<b>6</b>
<b>I.3.1.2 Chemical Vapor Deposition (CVD).....</b>	<b>8</b>
<b>I.3.1.2.a Sol-gel technique .....</b>	<b>8</b>
<b>I.3.1.2.b Pyrolysis spray technique (SP) .....</b>	<b>9</b>
<b>I.3.1.2.b.1 Classification of spray pyrolysis techniques .....</b>	<b>10</b>
<b>I.3.1.2.b.2 Advantages of spray pyrolysis.....</b>	<b>11</b>
<b>I.4.CHARACTERIZATION TECHNIQUES OF THIN FILMS .....</b>	<b>12</b>
<b>I.4.1 Adhesion Test .....</b>	<b>12</b>
<b>I.4.2 Micro structural and Phase Characterization.....</b>	<b>12</b>
<b>I.4.2.1 Scanning Electron Microscope .....</b>	<b>12</b>
<b>I.4.2.2 Energy dispersive X-ray spectroscopy.....</b>	<b>13</b>
<b>I.4.2.3 X-ray diffraction.....</b>	<b>13</b>
<b>I.4.2.3.a Determination of the grains size .....</b>	<b>14</b>
<b>I.4.3 Optical characterization and measurement.....</b>	<b>14</b>
<b>I.4.3.1. Ultraviolet visible spectroscopy .....</b>	<b>14</b>
<b>I.4.3.1.a Film thickness.....</b>	<b>15</b>
<b>I.4.3.1.a .1 Swanepoel method.....</b>	<b>15</b>



<b>III.3. CONCLUSION.....</b>	<b>50</b>
<b>CHAPTER VI: INVESTIGATION OF F DOPED SnO<sub>2</sub> THIN FILMS PROPERTIES</b>	
<b>VI.1. EXPERIMENTAL METHODOLOGY.....</b>	<b>51</b>
<b>VI.2 RESULTS AND DISCUSSION.....</b>	<b>51</b>
<b>VI.2.1 Growth Velocity .....</b>	<b>51</b>
<b>VI.2.2 Scanning Electron Microscopy .....</b>	<b>52</b>
<b>VI.2.3 Structural Characteristics .....</b>	<b>54</b>
<b>VI.2.4 Texture Coefficient (TC) .....</b>	<b>55</b>
<b>VI.2.5 Crystallite Size and Dislocation Density.....</b>	<b>57</b>
<b>VI.2.6 The transmittance .....</b>	<b>58</b>
<b>VI.2.6.1 Figure of Merit.....</b>	<b>59</b>
<b>VI.2.6.2 Band Gap Energy .....</b>	<b>60</b>
<b>VI.2.7 Photoluminescence .....</b>	<b>62</b>
<b>VI.2.8 Electrical properties.....</b>	<b>63</b>
<b>VI.3. CONCLUSION .....</b>	<b>64</b>
<b>CHAPTER V: TUNING THE OPTO-ELECTRICAL PROPERTIES OF SnO<sub>2</sub> THIN FILMS BY F AND TI CO-DOPING</b>	
<b>V.1. EXPERIMENTAL METHODOLOGY .....</b>	<b>65</b>
<b>V.2 RESULTS AND DISCUSSION .....</b>	<b>65</b>
<b>V.2.1 Growth Velocity .....</b>	<b>65</b>
<b>V.2.2 Scanning Electron Microscopy .....</b>	<b>67</b>
<b>V.2.3 Structural Characteristics.....</b>	<b>69</b>
<b>V.2.4 Crystallite Size .....</b>	<b>71</b>
<b>V.2.5 The transmittance .....</b>	<b>72</b>
<b>V.2.5.1 Figure of Merit .....</b>	<b>74</b>
<b>V.2.5.2 Band Gap Energy .....</b>	<b>75</b>
<b>V.2.6 Photoluminescence.....</b>	<b>77</b>
<b>V.2.7 Electrical properties .....</b>	<b>78</b>
<b>V.3. CONCLUSION .....</b>	<b>80</b>
<b>GENERAL CONCLUSION .....</b>	<b>81</b>
<b>BIBLIOGRAPHY.....</b>	<b>83</b>

# Introduction

Transparent conducting oxides (TCOs) constitute a unique class of materials, which combine two physical properties together: high optical transparency and high electrical conductivity. TCOs films like SnO<sub>2</sub> [1], ZnO [2], In<sub>2</sub>O<sub>3</sub> have attracted the attention of many research workers due to their wide range of applications, Such as solar cells, Flat panel Displays, gas sensors,....

Tin dioxide is an inorganic compound with the chemical formula SnO<sub>2</sub>. It is n-type semiconductor with high transparency and very good electrical conductivity; the films are chemically inert, mechanically hard and can resist high temperature. It mainly occurs in the mineral cassiterite, and crystallizes with a tetragonal structure.

In this work, we investigate the effect of flow rate and doped with both of F and Ti on the properties of pure SnO<sub>2</sub> films, in order to define in which applications they are better.

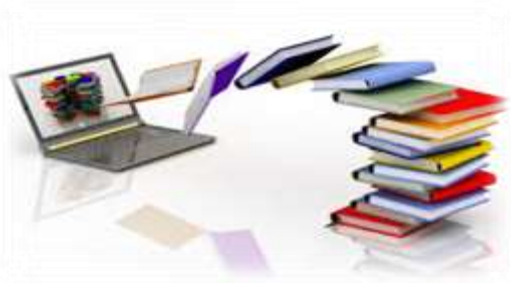
In the first chapter, we present fundamental physical properties of Transparent Conducting Oxides materials (optical, electrical...) with their applications, and SnO<sub>2</sub> thin films characteristics. More that the depositions techniques used to develop TCOs films, such as spray pyrolysis, which is very attractive for making functionally graded films. In addition, we describe the various methods adopted for characterizations of their structural, optical and electrical properties.

The second chapter contain the effect of solution flow rate of tin dioxide thin films prepared by spray pyrolysis technique onto glass substrate, at different flow rates ranging from 50 to 175 ml/h with steps of 25 ml/h. In addition, we have to characterize the structural, optical and electrical properties of those films.

The third chapter based on Ti doped SnO<sub>2</sub> thin films prepared at different Ti concentration ranging from 1 to 5 at%. More that we have their characteristics by different techniques as XRD, SEM, PL, UV-vis ....

The fourth chapter analyze the effect of the F dopant on the properties of SnO<sub>2</sub> films, deposited at different F concentration ranging from 2 to 5 at%. The characteristic were done using the previous different characterization techniques.

The fifth chapter is about F-Ti: SnO<sub>2</sub> Co-doping thin films. In order to have both of high transparency and conductivity, then we study how the inclusion of Ti and F to the pure SnO<sub>2</sub> affect its structural, optical and electrical properties.



## ***Chapter I:***

# ***Generalities about TCO, SnO<sub>2</sub>, thin films and these characterizations***

**T**his chapter presents the fundamental physical properties of Transparent Conducting Oxides materials with their applications and tin dioxide characteristics.

## **I.1 transparent conducting oxides**

Transparent conducting oxides (TCO) constitute a unique class of materials, which combine two physical properties together; high optical transparency and high electrical conductivity. Studies of transparent and conducting semiconducting oxide films have attracted the attention of many research workers due to their wide range of applications. Such as solar cells and gas sensors [3].

TCOs have been known for nearly a century. Indeed, the first TCO film, cadmium oxide, was synthesized and characterized as early as 1907 [4]. The first TCO patents for undoped and doped tin oxide (SnO<sub>2</sub>) films were filed respectively in 1931 and 1942. Such films were employed as aircraft windshield deicers in World War II. The following decades saw the development of In<sub>2</sub>O<sub>3</sub> and ZnO-based TCOs. It included indium-tin oxide (ITO) and the first Al-doped ZnO films, which was reported in the same year (1971) as the first ZnO-based varistor. Since that time, there has been steady improvement in the deposition and properties of SnO<sub>2</sub>, In<sub>2</sub>O<sub>3</sub>, and ZnO-based films [5].

Transparent conducting oxides, such as Sn-doped In<sub>2</sub>O<sub>3</sub> (indium doped tin oxide, ITO), Al-doped ZnO (AZO), Sb-doped SnO<sub>2</sub> (ATO), and F-doped SnO<sub>2</sub> (FTO), have the unique feature of combining optical transparency in the visible region (colorless state) with metal type electrical conductivity [3].

A TCO is a semiconductor with a wide band energy gap ( $\geq 3$  eV), which confers the optical transparency. It has also quasi free electrons in its wide conduction band of s-character; the free electrons confer the metal type conductivity. These arise either from defects in the material or from extrinsic dopants which introduce electron donor centers that underlie the conduction band edge.

During the last thirty to forty years, the dominant doped TCOs have been based on tin oxide (SnO<sub>2</sub>), indium oxide (In<sub>2</sub>O<sub>3</sub>), and zinc oxide (ZnO) [6].

### I.1.1 Applications of TCOs materials

For their luminescence properties introduction TCO films have been widely used as a transparent conducting thin film materials for application in various fields such as solar cells, flat panel displays, smart windows, touch screens, [7]optoelectronic devices, heat mirrors, for liquid crystal displays (LCDs), organic light emitting diodes (OLEDs) and gas sensors[8], ... etc. (Fig. I.1).



**Fig.I.1.**Some applications of TCOs.

## I.2 Tin dioxide

### I.2.1 Definition

Tin dioxide is an inorganic compound with the chemical formula SnO<sub>2</sub>. It mainly occurs in the mineral cassiterite and crystallizes with a tetragonal structure. It is a colorless, amphoteric and diamagnetic solid. That is usually thought of, as an oxygen deficient n-type semiconductor. It is insoluble in water, but dissolves in alkalis and acids.

Tin dioxide is purified by reduction of the metal and burning tin in air [9].

### **I.2.2 Crystalline Structure**

SnO<sub>2</sub> has the tetragonal structure it is means ( $a = b = 4.738 \text{ \AA}$  and  $c = 3.186 \text{ \AA}$ ).

The cell contains six atoms, four oxygen atoms, and two of tin atoms. In this system each oxygen atom is surrounded by three of the tin atoms and each tin atom is surrounded by six oxygen atoms[10] (Fig.I.2).

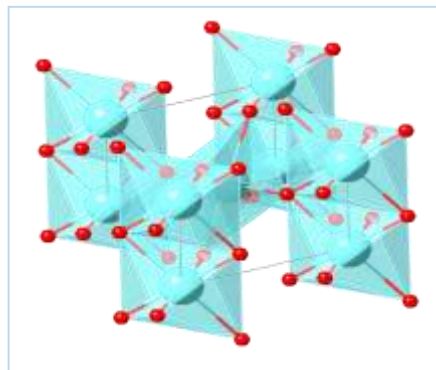


**Fig.I.2** Geometry of tin dioxide.

### **I.2.3 The different phases of tin oxide**

The tin dioxide films are amorphous when deposited at lower temperatures than 350 °C. It is only from this, the crystallization temperature of the films begins. The thin tin oxide films prepared by the various synthetic techniques are generally non-stoichiometric, and exhibit metastable phases such as SnO and Sn<sub>3</sub>O<sub>4</sub>. The SnO phase appears at the deposition temperature of 400 °C and disappears at a temperature of 500 °C. This phase is divided into SnO<sub>2</sub> and Sn at temperature of 450 °C annealing. This shows that annealing of the films at 500 °C is required to have a good stoichiometry SnO<sub>2</sub> [10].

Tin dioxide thin films are n-type semiconductors with high transparency and very good electrical conductivity; the films are chemically inert, mechanically hard and can resist high temperature. Owing to its low resistivity and high transmittance SnO<sub>2</sub> is one of the most important transparent conductive oxide materials, which are attractive from scientific and technological point of view due to its interesting properties. Many workers have tried to improve the physical properties of tin oxide films by doping the films with different dopants such as antimony, fluorine and titanium. There are many applications have been used from depositing these films such as gas sensors, transparent electrodes, solar cells and liquid crystal displays,...[11].

The high transparency of tin oxide semiconductors, combined with their mechanical hardness adherence and good environmental stability, has opened up numerous applications for them. Many techniques can be used to produce tin oxide films such as evaporation, sputtering, pulsed laser ablation and spray pyrolysis. Among these techniques, spray pyrolysis deposition method, it is particularly attractive because of its simplicity. It is fast, inexpensive, vacuum less, and suitable for mass production. Moreover, this technique would make it possible for the developing countries to apply this technique by their own means [12].

It is well known that appropriate doping can enhance the conductivity of tin oxide films; this enhancement has not been explained fully. Recently, some reports have suggested that the structure plays a major role in this behavior.

### I.3 Thin films

Thin films are material layers with thicknesses ranging from one atomic layer up to several micrometers. They are ubiquitous in the modern world and can be found in such diverse applications as mirrors, cutting tools[13], eyeglasses, microelectronics, window glass and solar cells[14]. It has great importance and significance for a large variety of industrial applications that can meet a very wide range of requirements for specific industrial or scientific applications.

While remarkable advances in thin film technology have been made. Some of the important applications are wear, corrosion and resistant coatings however; the selection of a specific technology for the deposition of thin films can be based on a variety of considerations. A multitude of thin films of different materials can be deposited for a large variety of applications; hence, no general guidelines can be given of what the most suitable deposition technology should be. In selecting an appropriate deposition technology for a specific application, several criteria have to be considered [15].

Generally, thin films are used when there is a need to enhance or change the properties of the surface of an object - usually referred to as a substrate - by adding or changing its functionality in some way.

It is clear that the current activity around thin films technologies is likely to continue seeing more innovation in the near future as showing in the Fig. I.3:

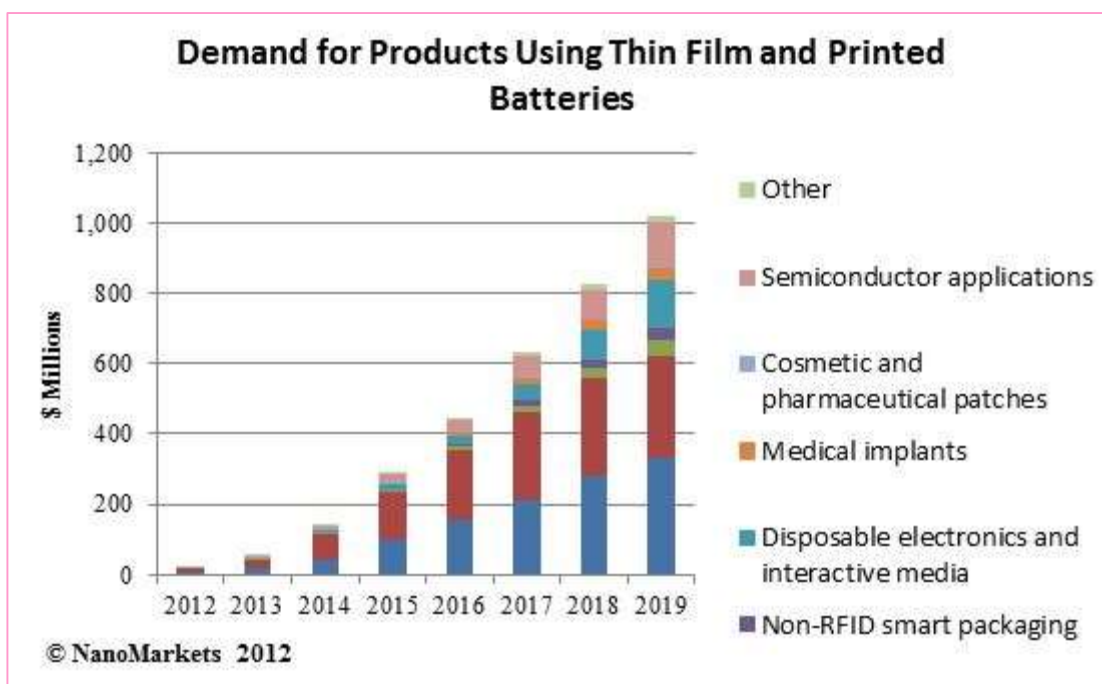


**Fig.I.3** The demand for products using thin films and printed batteries.

### **I.3.1 Thin film deposition processes**

Thin films can be deposited by multiple methods, e.g. from liquids, using for example electrochemistry, or from vapors. Vapor deposition methods are roughly divided in two categories, chemical vapor deposition (CVD) and physical vapor deposition (PVD), although hybrid processes are not unheard of. PVD and CVD processes are differentiated by how material transport and film deposition is facilitated.

In CVD, the deposition material is transported as components of gaseous compounds that are driven to react on the substrate, usually by heating the substrate at high temperatures, leaving a film of the desired material and reactant gases. A film property closely related to the deposition conditions is the intrinsic stress of the film. It is also very important for other film properties such as hardness, electrical properties and film adhesion. The common reason for film stresses is differences in contraction between the film and the substrate leading to tension or compression of the film upon cooling after deposition at elevated temperatures [14].

The PVD process can be carried out at lower deposition temperatures and without corrosive products [20]. It is high wear resistance, low frictional coefficient; great variety of coatings can be produced and no toxic reaction products but deposition rates are typically lower [16].

#### **I.3.1.1 Physical Vapor Deposition (PVD)**

##### **I.3.1.1.a Pulsed Laser Deposition (PLD)**

The principle of pulsed laser deposition, in contrast to the simplicity of the system set-up, is a very complex physical phenomenon. It does not only involve the physical process of the laser material interaction of the impact of high power pulsed radiation on solid target, but also the formation plasma plume with high energetic species and even the transfer of the ablated material through the plasma plume onto the heated substrate surface. Thus, the thin film formation process in PLD generally can be divided into the following four stages [16]:

- ✚ Laser radiation interaction with the target
- ✚ Dynamic of the ablation materials
- ✚ Deposition of the ablation materials with the substrate
- ✚ Nucleation and growth of a thin film on the substrate surface
- ✚ Each stage in PLD is critical to the formation of quality epitaxial crystalline, stoichiometric, uniform and small surface roughness thin film.

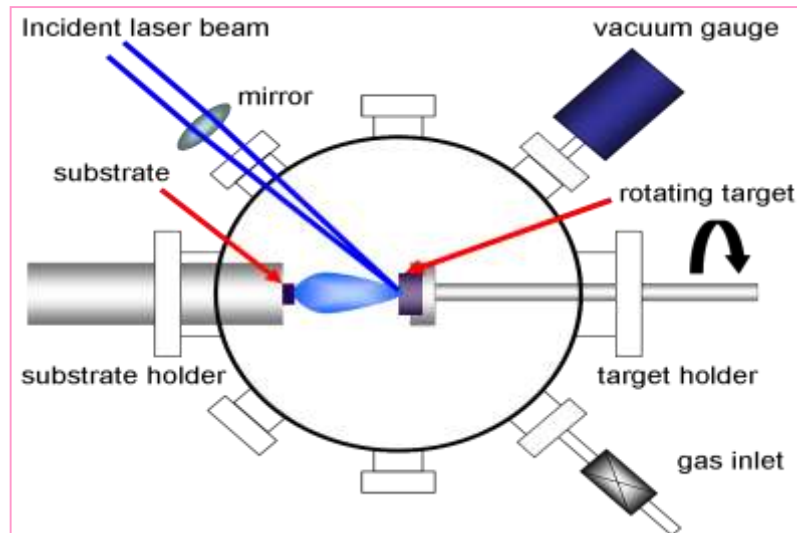


Fig.I.4. PLD system setup [16].

### I.3.1.1.b. Ion Beam Assisted Deposition

Ion Beam Assisted Deposition (IBAD) is a powerful new technique for producing adherent surface coatings with special properties. A facility for this technique is described. It consists of a cylindrical vacuum chamber, a rotating cooled target holder, an electron gun with evaporation source, a duoplasmatron ion source for gaseous ions, and the necessary power supplies and controls (Fig.I.5). Evaporation and bombardment are possible in sequence or simultaneously. The ion source delivers ions up to 30 keV energy directed at the component surface. The component is situated at the intersection of evaporate and ion beam. The maximum beam current is  $\sim 7$  mA for argon [17].

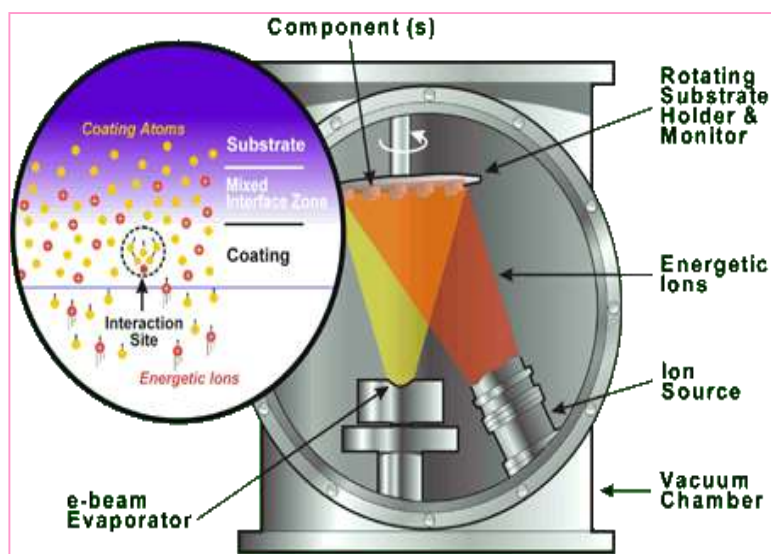


Fig I.5. IBAD system setup.

The concurrent ion bombardment differentiates IBAD from other thin film deposition techniques. It significantly improves adhesion, and permits control over film properties such as morphology, density, stress level, crystalline, and chemical composition. Ion bombardment is capable of depositing many different types of metallic and ceramic coatings. Examples of metallic coatings include silver, gold, platinum[18], and titanium[19].

### I.3.1.2 Chemical Vapor Deposition (CVD)

#### I.3.1.2.a Sol-gel technique

- **Sol**: a stable suspension of colloidal solid particles or polymers in a liquid.
- **Gel**: porous, three dimensional, continuous solid network surrounding a continuous liquid phase

Sol-gel is a chemical synthesis technique for preparing glasses, gels and ceramic powders. For the purposes of many thesis, it will serve as an easy way to make high purity glass in solution form at room temperature. In the sol-gel process, a system of colloidal particles in a solution (sol) becomes a macroscopic material (gel), which is interpenetrated by a liquid.

Once the liquid evaporates, a strong glass like material remains. The basic sol-gel reaction, shown in Fig.I.6, consists of two chemical reactions that produce a thin film when the sol is applied to a substrate. The first is a hydrolysis reaction and the second is a condensation reaction. The hydrolysis reaction produces the sol and then, in the condensation reaction, a macroscopic gel is formed on the substrate producing a thin film [20].

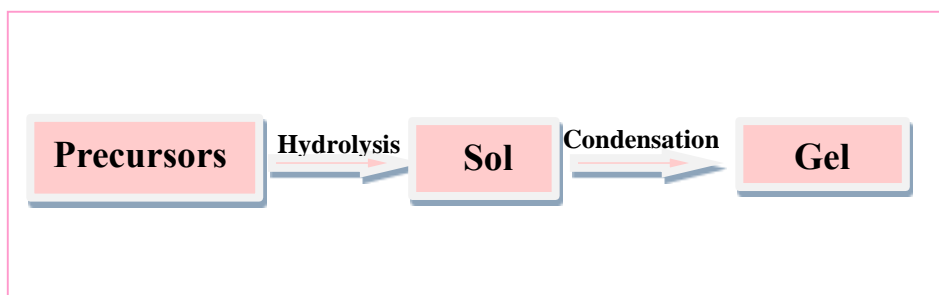


**Fig.I.6.**The basic sol-gel reaction

There are different sol-gel methods:

- ✚ The "spin-coating" or centrifugation (Fig.I.7) consists in pouring the sol or gel on the substrate that rotated by a spin coater. Excess liquid is ejected under the action of centrifugal force and the deposition thickness is a function of the rotational speed of the substrate and the deposition time [21].
- ✚ The "dip-coating" or tempered: process less used, it is to dip the substrate in the solution to deposit on it, and then draw it at a constant speed which determines the thickness of the deposit. After the deposit is dried and then annealed for crystallization [22].

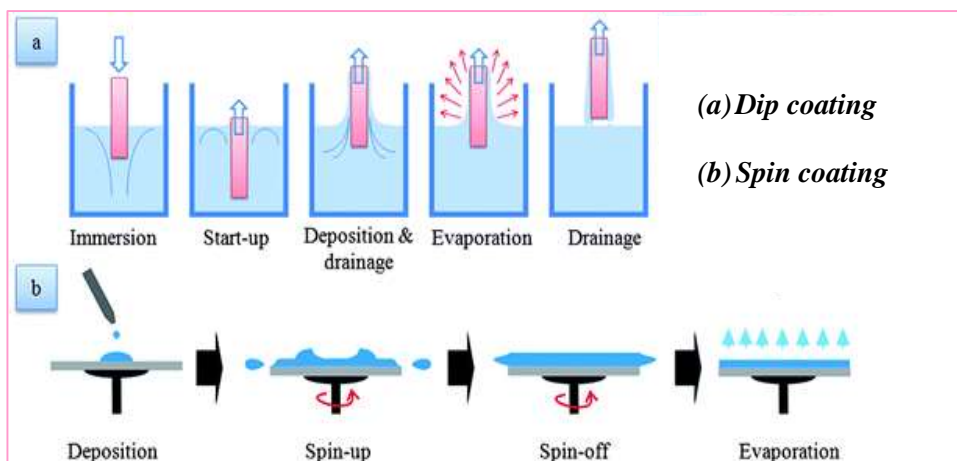


**Fig I.7** Schema of Sol-Gel process.

### **I.3.1.2.b Pyrolysis spray technique (PS)**

Pyrolysis spray is a processing technique being considered in research to prepare thin and thick films, ceramic coatings and powders (Fig.I.8). Unlike many other film deposition techniques, spray pyrolysis represents a very simple and relatively cost-effective processing method (especially with regard to equipment costs). It offers an extremely easy technique for preparing films of any composition. Spray pyrolysis does not require high-quality substrates or chemicals. The method has been employed for the deposition of dense films, porous films and for powder production. Even multilayered films can be easily prepared using this versatile technique [23].

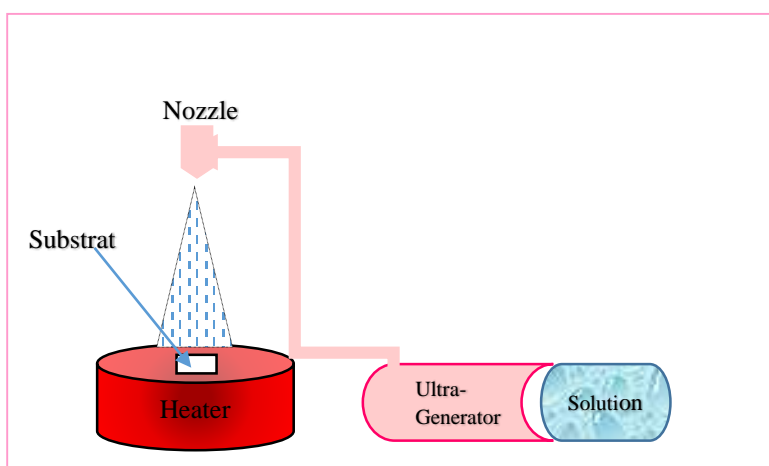


**Fig.I.8** General Schematic of ultrasonic spray process.

### **I.3.1.2.b.1 Classification of spray pyrolysis techniques**

Spray pyrolysis is a versatile processing technique for preparation of dense and porous single and multilayered films and powders of various materials and morphologies. Classification of different spray processes could be made in one way based on the type of energy source for the precursor reaction; such as spray pyrolysis in a tubular reactor (SP), vapor flame reactor (VFSP), the emulsion combustion method (ECM) and flame spray pyrolysis (FSP); or the method of atomizing the precursor, namely air pressurized, electrostatic and ultrasonic spray pyrolysis. In the case that the energy source for precursor reaction is an external energy supply and not from the spray itself, (as in SP and VFSP), method is less sensitive to the choice of precursors and solvent [24].

Different types of solvents are used in spray pyrolysis depending on the type and solubility of the precursors and economic aspects. Nitrates, chlorides and acetates are typically chosen as the metal oxide precursors that can be dissolved in aqueous and alcoholic solvents

The other classification for the type of spray pyrolysis is usually attributed to the type of the atomizer that is used in the system. In addition, the droplet size of the aerosol is generally dependent on the atomization method, which in turn determines the film quality. There are three major types of atomizers: air blast, electrostatic and the ultrasonic. The spray pyrolysis technique using the electrostatic atomizer is called Electrostatic Spray Deposition (ESD), the technique using the air blast atomizer is named Pressurized Spray Deposition (PSD) and the technique using Ultrasonic atomizer is generally recognized as the ultrasonic or normal Spray Pyrolysis [25].

**Table.I.1** Characteristics of atomizers commonly used in spray pyrolysis:

<b>Atomizer</b>	<b>Droplet size (<math>\mu\text{m}</math>)</b>	<b>Atomization rate (<math>\text{cm}^3/\text{min}</math>)</b>
<b>Pressure</b>	10-100	3- no limit
<b>Nebulizer</b>	0.1-2	0.5-5
<b>Ultrasonic</b>	1-100	< 2
<b>electrostatic</b>	0.1-10	/

Thin film deposition using spray pyrolysis can be divided into four types of processes [25] that may occur during deposition are showing in Fig.I.9:

- In process 1: the droplet splashes on the substrate, vaporizes and leaves a dry precipitate in which decomposition occurs.

- In process 2: the solvent evaporates before the droplet reaches the surface and the precipitate impinges upon the surface where decomposition occurs.
- In process 3: the solvent vaporizes as the droplet approaches the substrate then the solid melts vaporizes (or sublimates) and the vapor diffuses to the substrate to undergo a heterogeneous reaction there, this is true CVD.
- In process 4: at the highest temperatures the chemical reaction takes place in the vapor phase.

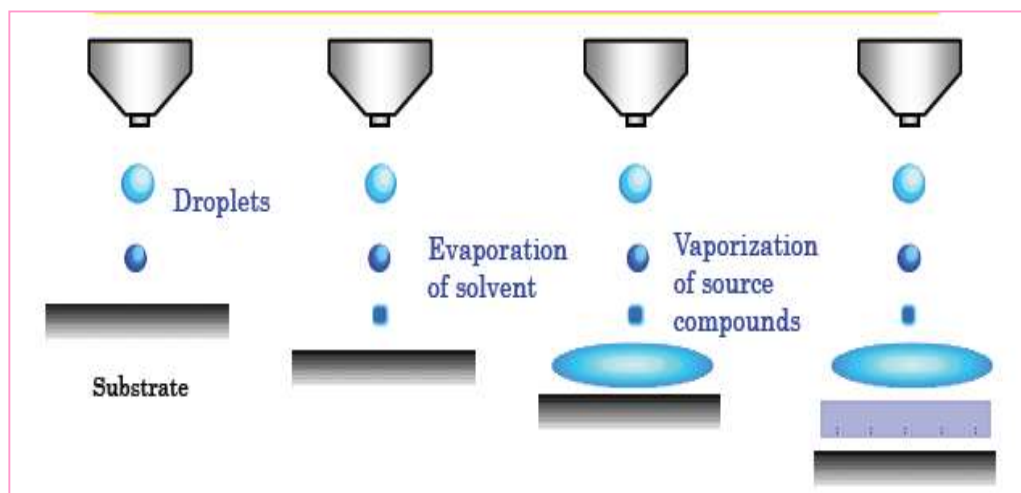


**Fig.I.9.** spray process [26].

### **I.3.1.2.b.2 Advantages of spray pyrolysis**

In comparison with other thin film deposition methods, spray pyrolysis has many advantages including: open-atmosphere process, open reaction chamber, easy access to observe the deposition process and adjustment during the experiment. It has also the multi-layer fabrication capability, which is very attractive for making functionally graded films. The composition of the film can be adjusted by changing the precursor solutions. Films can be also obtained on large surfaces at temperatures  $\sim 500$  °C. One of the major advantages of spray pyrolysis over the vapor phase routes is the possibility of producing multi component particles with exact desirable stoichiometry in the final product. Depending on the substrate temperature, precursor type and the nozzle-substrate distance, the droplets can evaporate or decompose completely before reaching the substrate, resulting in a process resembling to CVD or the liquid is deposited without evaporation. Burning a flammable precursor may also result in forming a particulate spray or to obtain higher deposition temperatures [25].

## I.4.Characterization techniques of thin films

### I.4.1 Adhesion Test

Before doing any characterization on the prepared films, adhesion strength between the films and the substrates were evaluated by applying the Stick tape test on the deposited films.

Generally, adhesion strength is considered to be "good" if the film adheres to the substrate and it doesn't peel off the substrate.

### I.4.2 Micro structural and Phase Characterization

#### I.4.2.1 Scanning Electron Microscope

The scanning microscope is mainly used in biology, in material science and in the field of research. SEM will enable to observe the surface topography of bulk samples by sweeping this surface using a probe (here an electron beam) and by analyzing the information obtained. It shows the samples in three dimensions. It provides information on the relationships between the different structures of the tissue and also get a picture of composition of the material studied. It allows the observation of macro and microscopic object minimum retail obtained depends on the size of the probe. The size of the probe is determined by the optical aberrations of the microscope.

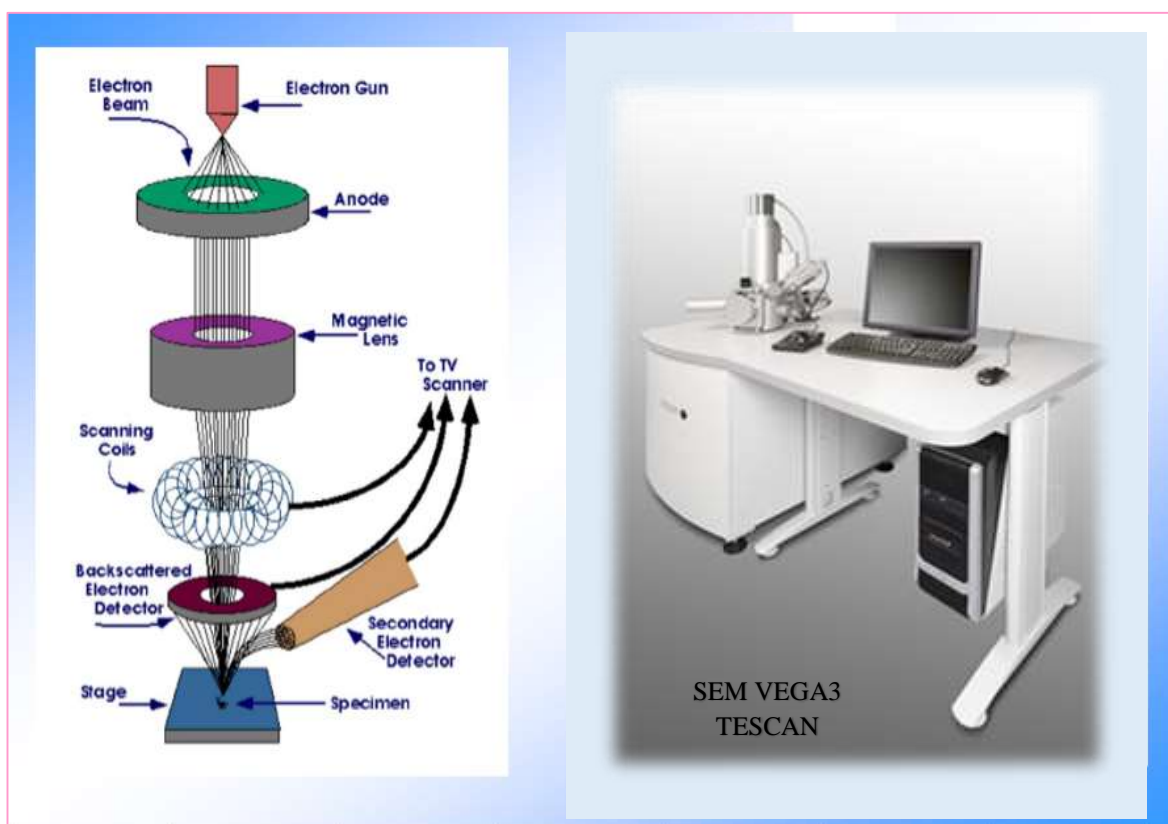


**Fig.I.10.**The Scanning Electron Microscopy VEGA3 TESCAN of LPCMA laboratory, Biskra University.

### I.4.2.2 Energy dispersive X-ray spectroscopy

Energy Dispersive X-Ray Spectroscopy was used for the elemental analysis and chemical characterization of a sample. Compositional homogeneity of the film was also analyzed via recording the composition maps [25].

### I.4.2.3 X-ray diffraction

X-ray diffraction has been used to identify the crystalline phases of the materials based on the Bragg's law. As shown in Fig I.11, condition at which diffraction occurs in a crystalline material satisfying the Bragg's law is described as [27]:

$$n\lambda = 2d \sin\theta$$

Where:

$\lambda$  : is the wave length of the X-ray beam.

$d$ : is the spacing between the planes in the atomic lattice.

$\theta$ : is the angel between the incident ray and the scattering planes.

$n$ : is the order of diffraction.

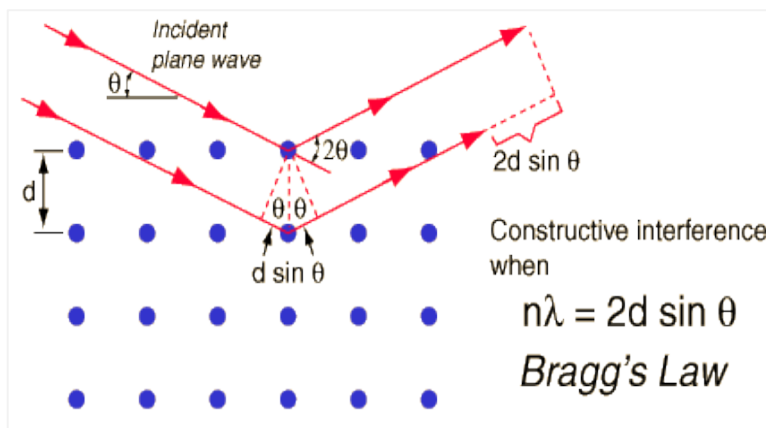


**Fig.I.11.** the X-ray Diffraction D8-ADVANCE

Instrument of Biskra University.

### I.4.2.3.a Determination of the grains size

The of crystallites was calculated using a well-known Scherrer's formula [28]:

$$D = \frac{0.9 \lambda}{\beta \cos \theta}$$

Where:

**D** is the of crystallite,  $\lambda$  (=1.5405 Å) used the wavelength of X-rays,  $\beta$  the broadening of diffraction line measured at half maximum intensity in radians (Fig.I.12) and  $\theta$  is the angle of diffraction.

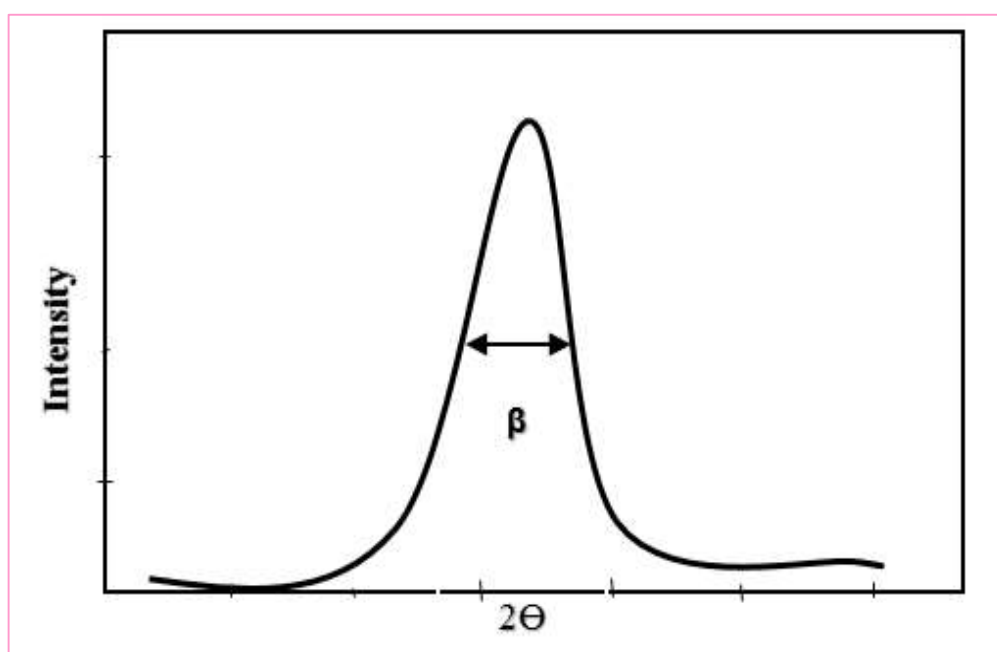


**Fig.I.12** Illustration showing the definition of  $\beta$  from the diffraction curve of the X-ray.

## I.4.3 Optical characterization and measurement

### I.4.3.1. Ultraviolet visible spectroscopy

Ultraviolet visible spectroscopy or ultraviolet-visible spectrophotometry (UV-Vis or UV/Vis) (Fig.I.13) refers to absorption spectroscopy or reflectance spectroscopy in the ultraviolet visible spectral region. The absorption or reflectance in the visible range directly affects the perceived color of the chemicals involved, it measures the intensity of light passing through a sample ( $I$ ) and compares it to the intensity of light before it passes through the sample ( $I_0$ ). The ratio ( $\frac{I}{I_0}$ ) is called the transmittance and it is usually expressed as a percentage (T %).

The absorbance,  $A$  is based on the transmittance [29]:

$$A = -\log\left(\frac{T}{100}\right)\%$$

The UV-visible spectrophotometer can be also configured to measure reflectance. In this case, the spectrophotometer measures the intensity of light reflected from a sample ( $I$ ), and compares it to the intensity of light reflected from a reference material ( $I_0$ ) (such as a white tile).

The ratio ( $\frac{I}{I_0}$ ) is called the reflectance, and is usually expressed as a percentage (R %) [29].

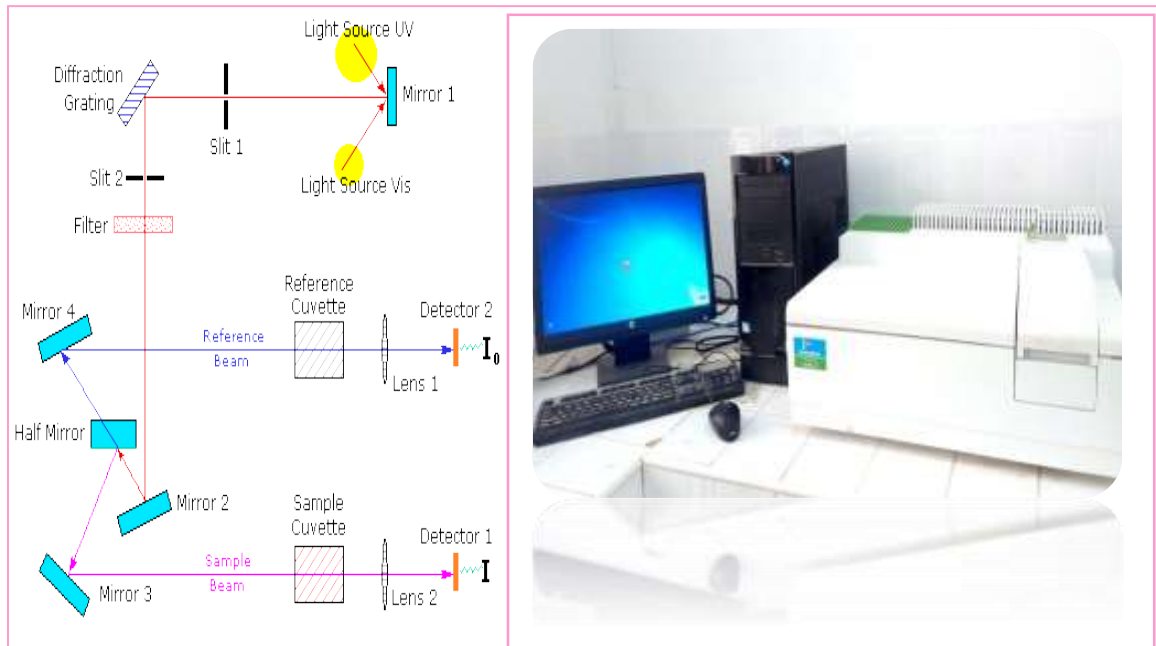


**Fig.I.13** the principle of operation of UV-visible spectrophotometer.

### **I.4.3.1.a Film thickness**

#### **I.4.3.1.a .1 Swanepoel method**

Thickness of deposited samples prepared at different solution flow rates and at different doping was calculated using modified Swanepoel envelop method (an envelope was drawn using the maxima and minima of each curve and also used value of refractive index  $n_s$  of quartz glass was 1.52) Fig.I.14 [30], the film thickness:

$$t = \frac{\lambda_1 \lambda_2}{2(\lambda_1 n_2 - \lambda_2 n_1)}$$

Where  $\lambda_1$  and  $\lambda_2$  are the wavelengths at which two successive maxima or minima occur and  $n_1$  and  $n_2$  are the corresponding refractive indices [31]:

$$n = [N + (N^2 - n_s^2)^{1/2}]^{1/2}$$

Moreover,  $N$  obtained by this relation [32]:

$$N = 2n_s \frac{(T_M - T_m)}{T_M T_m} + \frac{(n_s^2 + 1)}{2}$$

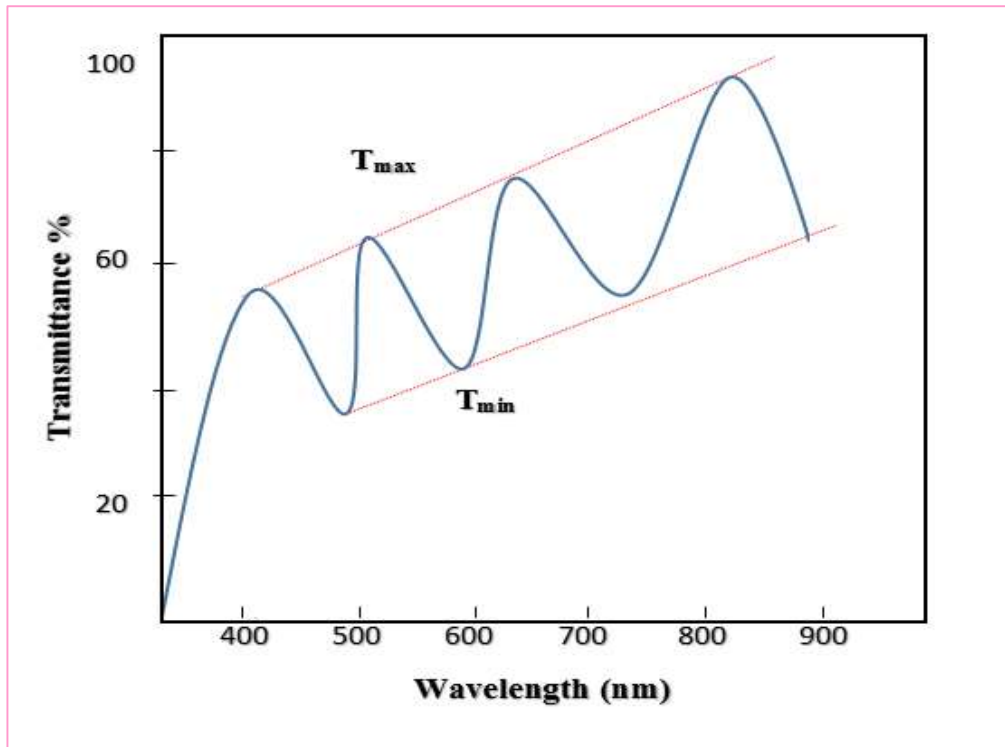


Fig.I.14 Method of interference fringes to determinate the thickness.

#### I.4.3.1.a .2 Gravimetric Method

These method based on the determination of mass. The film thickness  $t$  can be calculated from the mass of the coating  $m$  if the density  $\rho$  and the area  $A$  on which the material is deposited are known:

$$t = m/A\rho$$

For this method, one has to bear in mind that the density of a coating may deviate significantly from that of the bulk (e.g. due to porosity or implanted interstitial atoms). For exact measurements, calibration is necessary [33].

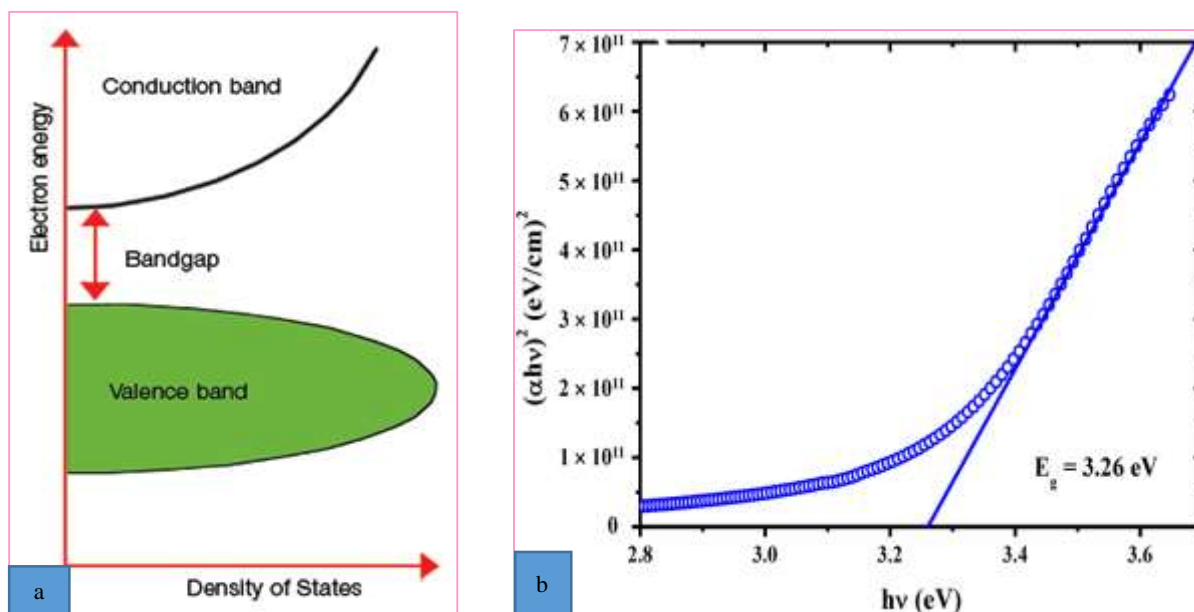
### I.4.3.1.b. Band gap

The measurement of the band gap of materials is important in the semiconductor, nanomaterial and solar industries. This note demonstrates how the band gap of a material can be determined from its UV absorption spectrum.

The term “band gap” refers to the energy difference between the top of the valence band to the bottom of the conduction band (Fig.I.15); electrons are able to jump from one band to another. In order for an electron to jump from a valence band to a conduction band, it requires a specific minimum amount of energy for the transition, the band gap energy. A diagram illustrating the band gap is shown in Fig. I.15.a [34].

The band gap energy of insulators is large ( $> 4\text{eV}$ ), but lower for semiconductors ( $< 3\text{eV}$ ).

From the transmittance spectrum in the UV-visible the variation of  $(\alpha h\nu)^2$  with photon energy  $h\nu$  for thin film is shown in Fig.I.15.b. It has been observed that the plots of  $(\alpha h\nu)^2$  versus  $h\nu$  are linear over a wide range of photon energies indicating the direct type of transitions. The intercepts (extrapolations) of these plots (straight lines) on the energy axis give the energy band gaps [28].



**FigI.15** Explanation of band gap [34].

### I.4.3.1.c Disorder calculating (Urbach Energy)

Ultrasonic Spray Pyrolysis is a deposition method which growth of the film is by condensation. In this situation, the atoms arriving on the substrate can stick to the point of landing. Therefore, the atoms in the film of the network are not usually in an ideal position, hence, the appearance of the gaps in the width of the SnO<sub>2</sub> bond, in this case, the strip edges disclosed in the case of crystal lattices and delimited by  $E_v$  and  $E_c$  may disappear. We observe localized states formed band tails border of the band gap in the valence band and conduction. For energies above and below  $E_v$ ,  $E_c$  are the extended states, this difference known as the disorder or Urbach Energy; According to Urbach law, the absorption coefficient  $\alpha$  is [35]:

$$\alpha = \alpha_0 \exp \frac{h\nu}{E_{00}}$$

By plotting ( $\ln \alpha$ ) as function of  $h\nu$  (Fig. I.16) we can determine the value of  $E_{00}$

$$\ln \alpha = \ln \alpha_0 + \frac{h\nu}{E_{00}}$$

When  $E_{00}$ : is Urbach energy, which determine disorder.

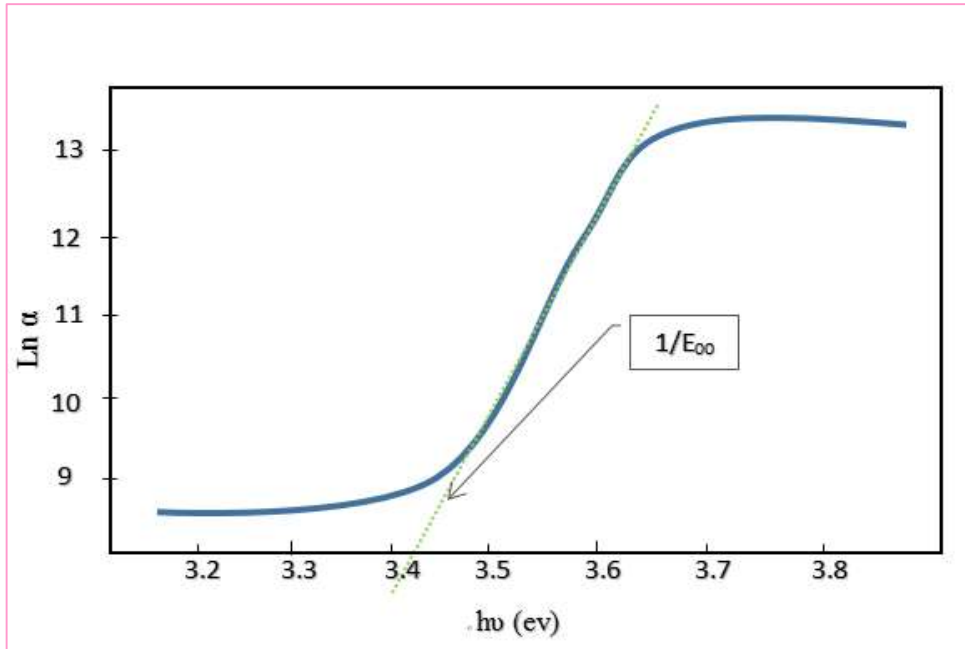


**Fig I.16.** Urbach Energy Determination.

### I.4.3.2. Photoluminescence spectroscopy

Photoluminescence (PL) analysis is a nondestructive technique that requires very little sample manipulation or environmental control; it is the spontaneous emission of light from a material following optical excitation. It is a powerful technique to probe discrete energy levels and to extract valuable information about semiconductor sample composition, quantum well thickness or quantum dot sample monodispersity Fig.I.17.

An electron that has been excited above the conduction band of a material will eventually fall and recombine to the hole that has been excited below the valence band after losing some energy through releasing a phonon to the lowest available non radiative energy level. The efficiency of photoluminescence signal is determined by the nature of optical excitation, properties of material; i.e. radiative and non radiative recombination and defects [36].

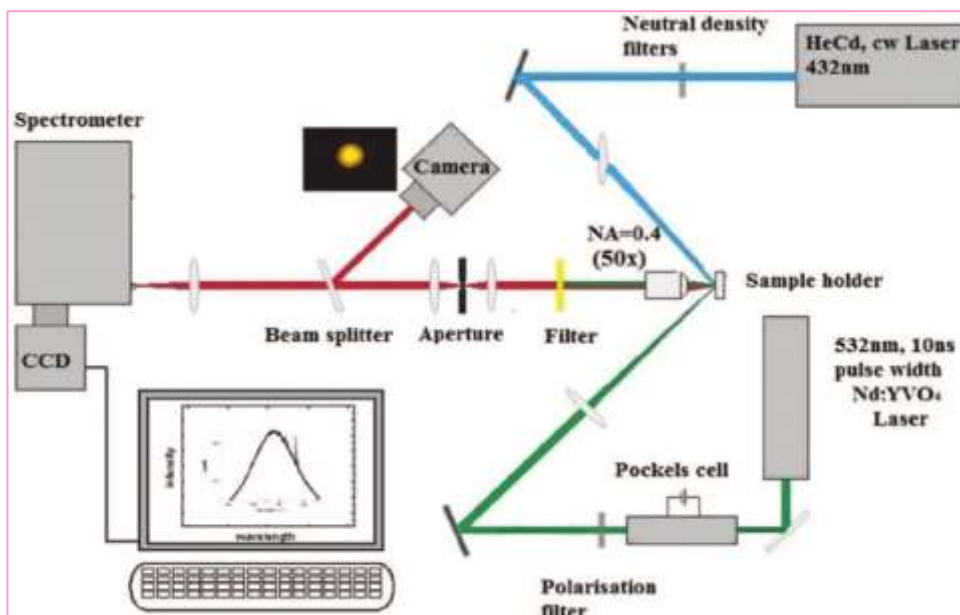


**Fig.I.17** the principle operation of PL spectroscopy [37].

### I.4.4 Four points measurements

Ohmmeter measurements normally made with just a two-point measurement method. However, when measuring very low values of ohms, in the milli or micro ohm range, the two-point method is not satisfactory because test lead resistance becomes a significant factor.

The four-point resistance measurement method eliminates lead resistance. Instruments based on the four-point measurement work on the following principle:

- Two current leads, C<sub>1</sub> and C<sub>2</sub>, comprise a two-wire current source that circulates current through the resistance under test.
- Two potential leads, P<sub>1</sub> and P<sub>2</sub>, provide a two-wire voltage measurement circuit that measures the voltage drop across the resistance under test.
- The instrument computes the value of resistance from the measured values of current and voltage.

The conduction is considered and given as [38]:

$$\frac{U}{I} = K \frac{\rho}{t}$$

When:

$\rho$  is the resistivity of the layer;  $t$ : thickness; the coefficient  $K = \frac{\ln 2}{\pi}$

Therefore, the resistivity of the measurement four points when the thickness is known:

$$\rho = \left[ \frac{\pi}{\ln 2} \frac{U}{I} \right] t$$

The ratio  $\rho/t = R_s$  and it is expressed in  $\Omega$ .

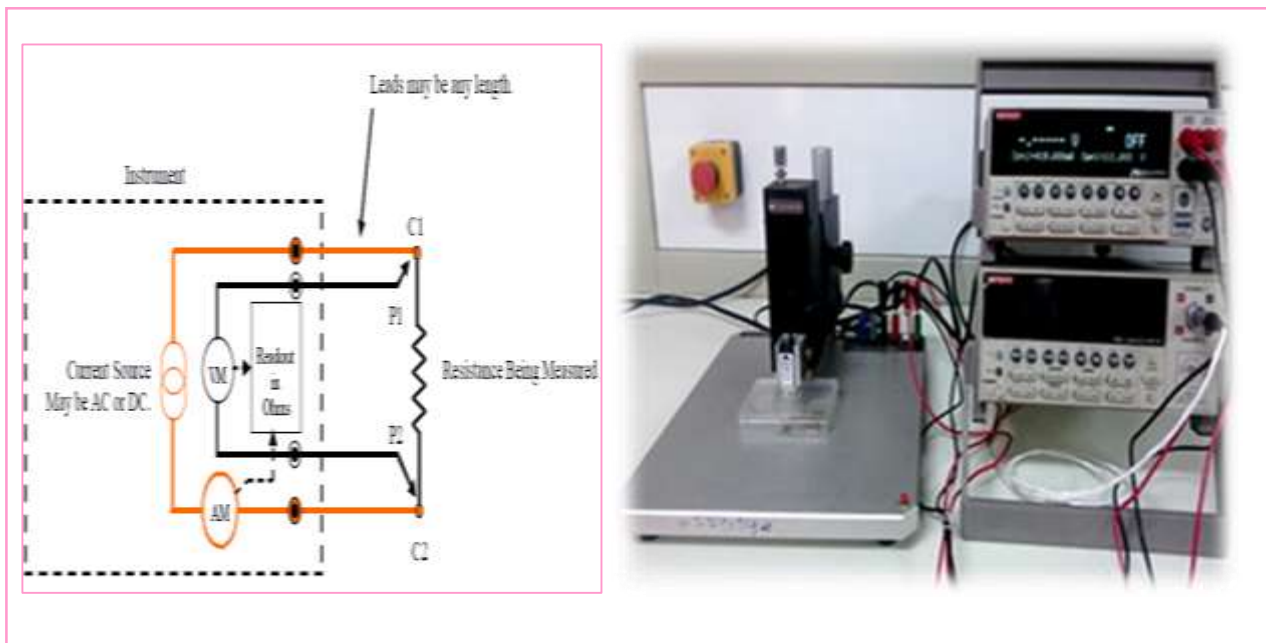


**Fig I.18.** Four Points Measurement Diagram.



***Chapter II:***  
***Effect of solution flow on the***  
***properties of tin dioxide  $\text{SnO}_2$***   
***thin films***

This chapter, is about the study of flow rate effect on the properties of SnO<sub>2</sub> thin films deposited by ultrasonic spray technique, then it describe some characterizations of their structural, optical and electrical properties.

## **II.1. The Deposition Process**

This study investigated the effect of the solution flow on the structural, optical and electrical properties of SnO<sub>2</sub> thin films prepared by spray deposition method. The films were deposited at various solution flow ranging from 50–175ml/h.

### **II.1.1. Preparation of substrates**

#### **II.1.1.1 Choice of the substrate**

The studied films are deposited onto substrates of solid glass, the choice of glass for reasons:

- Glass is the most commonly selected substrate for all TCO films.
- The good agreement of thermal dilation between glass and SnO<sub>2</sub> to minimize the stress interface film/substrate.
- For their transparency that adapts well for the optical characterization of films in the visible.
- For economic reasons.

#### **II.1.1.2. Cleaning of the substrates**

Cleaning of the Glass substrates is in order to eliminate the traces from greases and impurities onto the surface of glass then ameliorate the film adhesion.

The process of cleaning the surface substrates in all my studies is as follows:

- ✚ Firstly using a pen with diamond point to cut the substrates.
- ✚ Rinsing with double distilled water and then with acetone during 10 min.
- ✚ Rinsing with double distilled water.
- ✚ Washing in methanol at ambient temperature.
- ✚ Cleaning in a double distilled water bath
- ✚ Drying by using a drier.

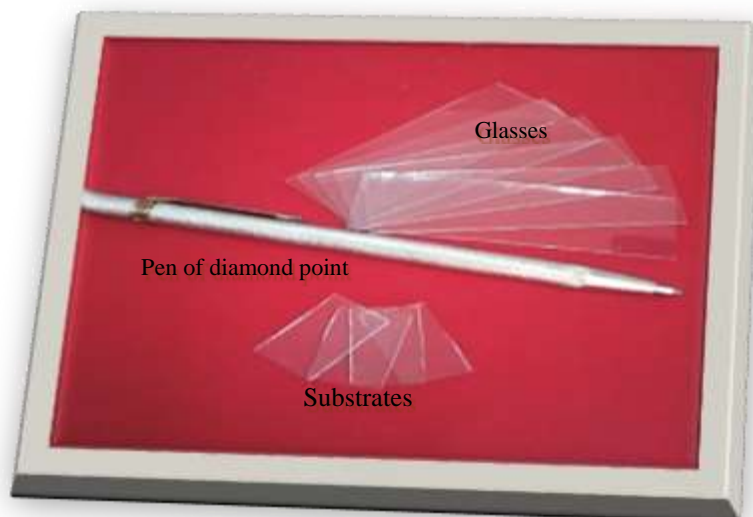
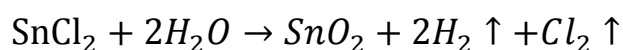


**Fig.II.1.** The used Glasses substrates and diamond pen.

### **II.1.2 Experimental methodology**

For depositing SnO<sub>2</sub> thin films, take 0.57g of Tin (II) chloride (SnCl<sub>2</sub>) dissolved in water to obtain 0.1 mol/l solution concentration. Two droplets concentrated HCl was added to the solution. The addition of HCl rendered the solution transparent, mostly due to the breakdown of the intermediate polymer molecules [39]. Generally, in spray pyrolysis, thin films of SnO<sub>2</sub> are prepared by the reaction:



Tin dioxide was deposited onto glass substrates, which cleaned for 20 min approximately. In order to be able to analyze the effect of solution flow on the properties of SnO<sub>2</sub> thin films, other deposition parameters must be fixed when the flow rate ranging from 50 to 175 ml/h with step of 25 ml/h as follow:

**Table II.1.** The fixed parameters used at the deposition processes:

Parameter	Substrate Temperature	Deposition time	Concentration	Nozzle-substrate distance	Ultrasonic wave amplitude
The values	400 °C	5 min	0.1 M	5 cm	40 %

### II.1.3. Deposition of thin films

We used ultrasonic spray pyrolysis technique to deposit SnO<sub>2</sub> thin films using the following setup “ultrasonic spray technique” in LPCMA laboratory, Biskra University ( thin films laboratory ) Fig II.2:



**FigII.2.** ultrasonic spray technique setup that used.

Where:

(1): ultrasonic generator with 40 % frequency permit to generate the ultrasonic waves and submit them to the atomizer. (2): electrical resistance to heat the substrate. (3): substrate holder, (4): temperature regulator related to a thermocouple to control the temperature. (5): syringe pump Model PHOENIX D-CP (GF-FOURES) to control the precursor solution flow rate. (6): atomizer to decompose the solution to fine droplets. (7): syringe contains the solution. (8): thermocouple.

### II.1.4 The film deposition

After cleaning the substrates, place it onto the ohmic resistance, which linked with temperature controller. Heat the substrate from room temperature to deposition temperature (400°C). When the recommended temperature is reached, start the deposition processes. Very fine droplets are sprayed onto the heated substrate; that caused activation of the chemical reaction between the compounds such as oxygen, tin chloride...

At the end after 5 min, stop heating and leave the substrates to cool slowly until a room temperature, to prevent thermal shock that may crack the glass, then finely you will have tin dioxide thin film samples.

We can summarize the steps to obtain SnO<sub>2</sub> thin films in the following chart:

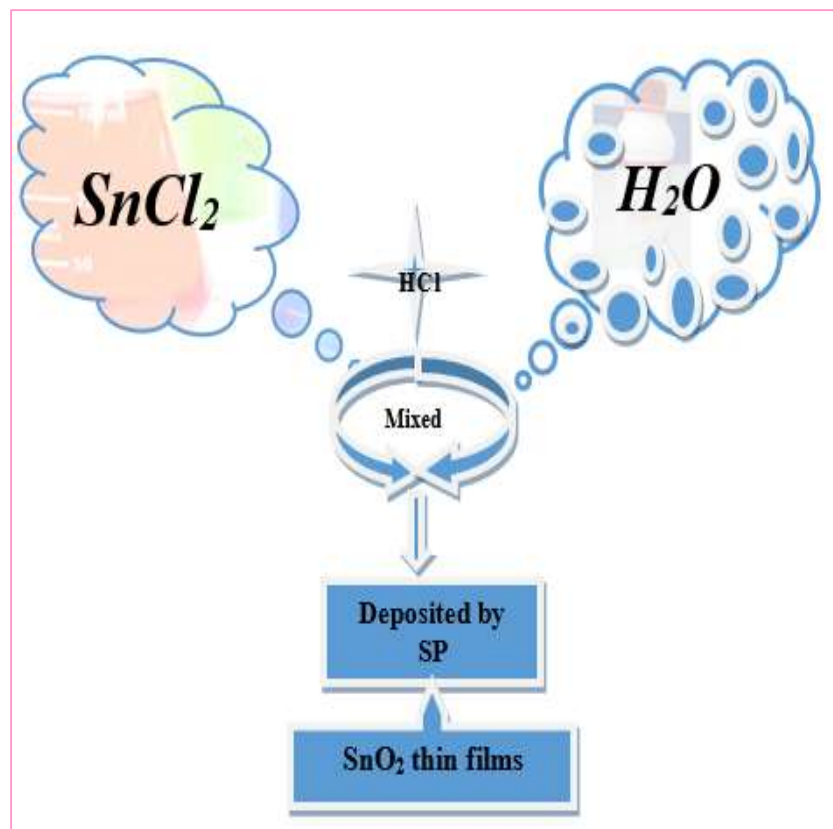


**Fig. II.3** Chart summarize how to obtain SnO<sub>2</sub> thin films.

## **II.2 Results and discussion**

After the deposition of the films, we used the characterization techniques mentioned in the previous chapter. The X-rays diffraction analysis indicated that we have SnO<sub>2</sub> films; they are amorphous or crystalline and permit to calculate other parameters like. The electrical characterization indicated how the films are resistive; UV-visible spectroscopy measures the transmittance, band gap and thickness of the samples.

Before doing any characterization technique, we applied the Stick tape test on the deposited films and it confirmed that the adhesion strength of the pure SnO<sub>2</sub> films considered being "good".

### **II.2.1 Growth Velocity**

Thickness of deposited samples prepared at fixed deposition time of 5 min with different solution flow rates was calculated using both of interference fringes method and gravimetric method [33]. Using relation between thickness and deposition time we could determine the growth rate of our tin dioxide thin films as showing in the following table:

**Table II.2** different values of growth rate, thickness and deposition time of SnO<sub>2</sub> prepared at different flow rates.

<b>Samples</b>	<b>S1</b>	<b>S2</b>	<b>S3</b>	<b>S4</b>	<b>S5</b>	<b>S6</b>
<b>Flow rate (ml/h)</b>	<b>50</b>	<b>75</b>	<b>100</b>	<b>125</b>	<b>150</b>	<b>175</b>
<b>Thickness (nm)</b>	<b>517.15</b>	<b>546.7</b>	<b>598.76</b>	<b>600</b>	<b>750</b>	<b>1066.05</b>
<b>Growth rate (nm/min)</b>	<b>103.43</b>	<b>109.34</b>	<b>119.75</b>	<b>120</b>	<b>150</b>	<b>213.21</b>

Using these results, we plot the variation of the thickness and growth rate as function of flow rates, which is represented in the Fig II.4:

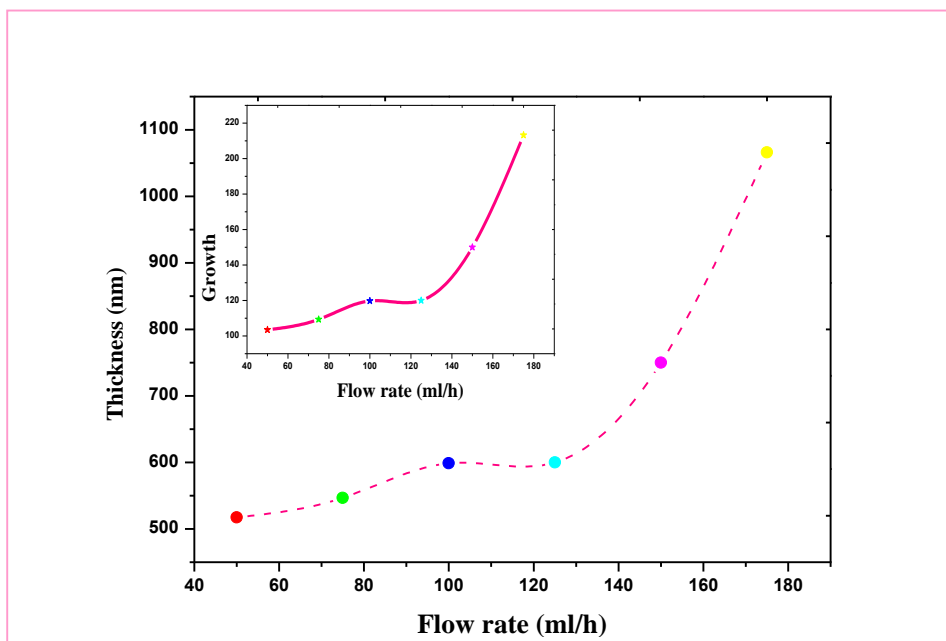


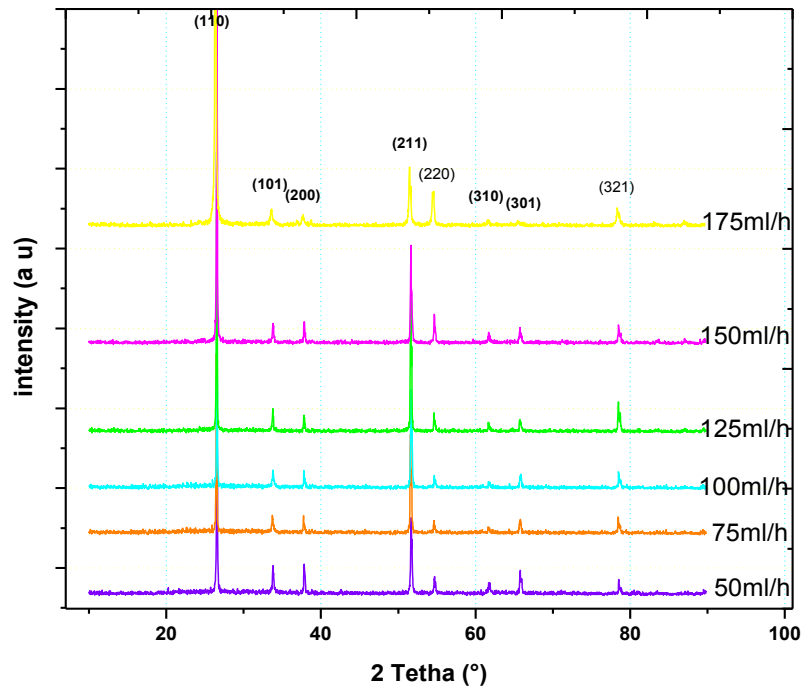
**Fig. II. 4.** Films thickness and growth rate variations as function of the flow rates.

We can see proportion between increasing of thickness as increasing in flow rates, it is indicate that our films were growth uniformly then it will be thick whenever flow rate augment to saturation after outside rates.

We have reported the prepared films thickness variation as a function of flow rate. In figure inset, we have presented the variation of the growth rate that deduced from the ratio of film thickness on the deposition time fixed at 5 min, the deposition rate increase when thickness increasing that because spray volume flux over substrate increasing due to rise in solution flow rate from 50 to 175 ml/h. As can be seen, bellow 125 ml/h the growth rate variation slowly, while above this value the deposition rate varies linearly with the flow rate. That is because in the beginning the growth of the film was onto the surface area then after it will be perpendicular to the substrate; these results were founded too by many research such as C.M. Mahajan [40]; M. L. Zeggar [41].

## II.2.2 Structural characterization

XRD spectra of SnO<sub>2</sub> films prepared with various solution flow with Miller indices of the tetragonal phase of SnO<sub>2</sub> are noted in Fig II.5:



**FigII.5.** XRD results at various flow rates.

The experimental results indicate that at 400 °C these films are polycrystalline in nature.

The XRD spectra show predominant diffractions from the crystallographic (110), (211), this indicates that a film growth muchness in those specific direction (110) which have the most intensity in all the samples. In the present studies, the most conspicuous feature observed in the XRD analysis of the SnO<sub>2</sub> films is orientation along the (110) plane [42]. The same results obtained by S. Gürakar [42]; H .Adel; O. Alkhayatt [43] and C. Sankar [44].

The intensities of the reflections from other main planes of cassiterite (101), (310) are small, this indicate that the films have a strong crystallographic texture along (110) this is why it is the preferred one (Fig II.6). Depending on these results and current studies, we found that a degree of texturing related on both of flow rate, film thickness or nature of the solution; Saji Chacko and all [45] affirmed that a weak peaks indicate that SnO<sub>2</sub> has very small crystalline size or that SnO<sub>2</sub> particles are semi crystalline in nature.

Following figure, summarize these variations in intensities of some plans as function of flow rates:

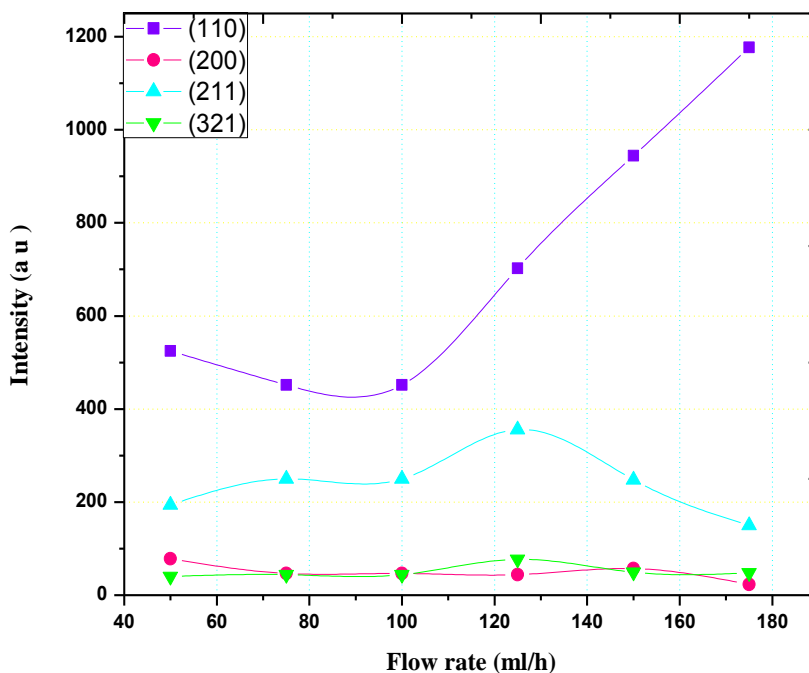


**Fig II.6** Intensity variations of some SnO<sub>2</sub> main pics.

Fig II.6 shows that maximum intensity is 1177 (a u) at 175 ml/h, in the plan (110). We can see also that in the beginning at 50ml/h, a film growth in this plan with 527 (a u) intensity then it fixed at 452 (a u) at 75, 100 ml/h, this indicate that a direction growth changed to other plan. After, at 125, 150, 175 ml/h it turn back to (110) plan with augmentation intensities 702, 944, 1177 (a u).

Using the JCPDS file of SnO<sub>2</sub> (N° 00-041-1445) and compared it with my results confirmed that our samples crystallize as “cassiterite”.

The results of XRD also show that the full width at half maximum (FWHM) of peaks increase with increasing the flow rate to 175ml/h. Consequently, the  $\tau$  will be decreases.

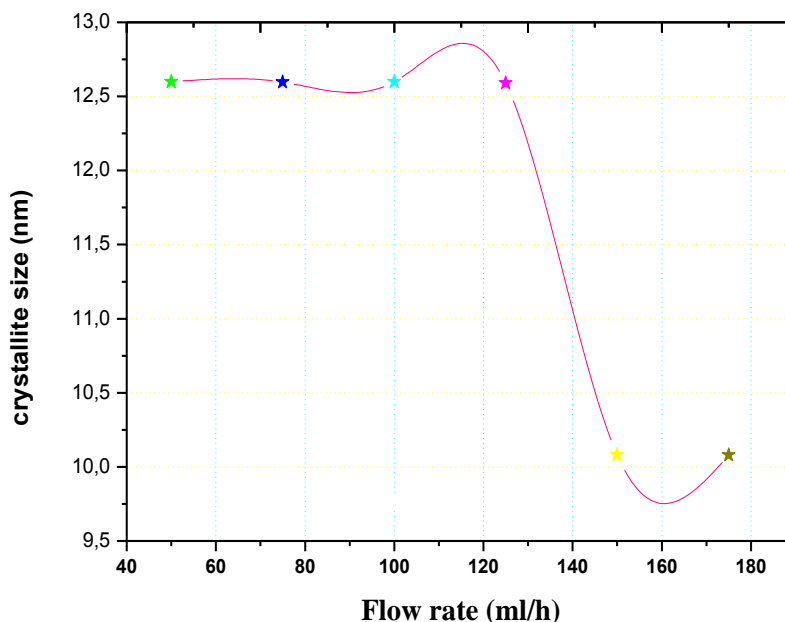
### **II.2.3 The grains size**

The grains size of the various SnO<sub>2</sub> thin films was calculated starting from the width with semi height of the most intense peak, using Scherrer formula. The calculated values of the  $\tau$  at different flow rate are showing in the table II.3:

**Table II.3** of SnO<sub>2</sub> thin films prepared at different flow rates:

Samples	S1	S2	S3	S4	S5	S6
Flow rate ml/h)	50	75	100	125	150	175
(nm)	12.599	12.597	12.599	12.59	10.082	10.08

Using these results, we plot the variation of the crystallites size as function of flow rates, which is represented in the figure II.7:

**Fig II.7.** Average crystallite size of the SnO<sub>2</sub> thin film as a function of flow rates.

At small flow rates values, when elements solution fall onto the substrates, it will find more places to locate at; with increasing of flow, the places will be filled and tin atoms takes interstitial sites then it will be pressed; consequently, effected deformations in near grains then it will be smaller, also it will be have non-stoichiometry structure [46] . Moreover, with increasing in thickness substrate temperature will be not suffice to have complete crystallite structure.

It is well known that the mean measured by this method is usually less than the actual value. This is the consequence of internal stress and defects in deposited thin films.

### II.2.4 Dislocation density

Dislocations are a matter of importance; they are not likely to play a major role in the variation of electrical resistance because increase in dislocation density gives rise in disorders, crystal defects in lattice and decreasing crystallite. The dislocation density ( $\delta$ ) is defined as the length of dislocation lines per unit area as defined in literature [47], which can be estimated from the following relation using the simple approach of Williamson and Smallman:

$$\delta = \frac{1}{D^2}$$

Where D: is the crystallite size

**Table II.4** Dislocations of SnO<sub>2</sub> thin films at different flow rates:

Samples	S1	S2	S3	S4	S5	S6
Flow rate (ml/h)	50	75	100	125	150	175
Dislocations (line/m <sup>2</sup> )*10 <sup>15</sup>	6.29	6.30	6.29	6.30	9.83	9.84

Using these results, we plot following graph:

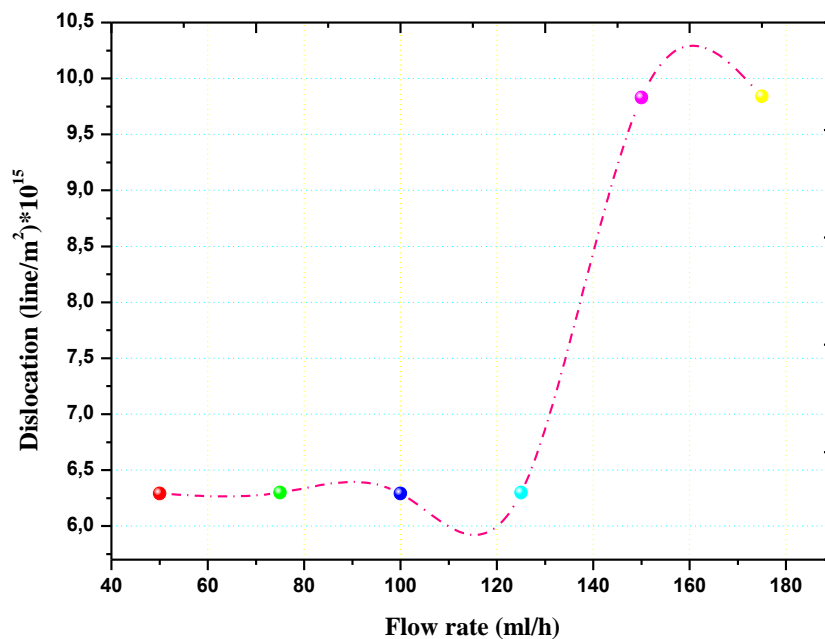


**Fig.II.8** Dislocation of SnO<sub>2</sub> thin films as function of flow rates.

As can be seen, dislocation density was small and stable approximately  $6.10^{15}$  line/m<sup>2</sup> at flow rates between [50-125ml/h], after it was increasing to  $9.84.10^{15}$  line/m<sup>2</sup>, that is because accumulation of O<sub>2</sub> in thick films stop [48], then we will observe non-stoichiometry structure which indicated, increasing of defect in high flow rates.

### **II.2.5 Constraint and deformation**

The lattice parameters are important; they provide information on the state of stress on the samples. The difference between the value of natural lattice parameter solid and the value measured by X-ray diffraction gives the constraint  $\epsilon^{hkl}$  [49].

$$\epsilon^{hkl} = \frac{a_{\text{exp}} - a_{\text{theo}}}{a_{\text{theo}}}$$

$a_{\text{theo}}$  : The lattice constant from ASTM file is  $4.738 \text{ \AA}$

It can take three values of  $\epsilon^{hkl}$ : positive, zero and negative

- ✚  $\epsilon^{hkl} > 0$  : the film subjected to stresses of dilation.
- ✚  $\epsilon^{hkl} = 0$  : absence of stress.
- ✚  $\epsilon^{hkl} < 0$  : the film is subjected to compressive stresses.

We can calculate  $a_{\text{exp}}$  using the following relation:

$$d_{hkl} = \frac{a}{\sqrt{h^2 + k^2 + l^2} \left(\frac{a^2}{c}\right)}$$

I chose the plan (110) in my samples to calculate a:

$$d_{110} = \frac{a}{\sqrt{1^2 + 1^2 + 0}} = \frac{a}{\sqrt{2}}$$

$$a_{\text{exp}} = d_{hkl} \sqrt{2}$$

Following table summarizes (a) and ( $\epsilon$ ) results:

**Table II.5.** Stresses results of SnO<sub>2</sub> thin films for all flow rates:

Samples	S1	S2	S3	S4	S5	S6
Flow rate (ml/h)	50	75	100	125	150	175
$d_{110}(A^\circ)$	3.335	3.341	3.333	3.331	3.328	3.337
$a_{\text{exp}}(A^\circ)$	4.716	4.726	4.714	4.710	4.706	4.719
$\varepsilon^{\text{hkl}} \cdot 10^{-3}$	-4.53	-2.49	-5.00	-5.71	-6.64	-3.92

We can see that all  $\varepsilon^{\text{hkl}}$  were negative that indicate that our SnO<sub>2</sub> thin films prepared by different flow rates were subjected to **compressive stresses**, and this is good agreement with the results.

## II.2.6 Optical study

### II.2.6.1 The transmittance

We were using UV-Visible spectroscopy characterization to indicate how the films are transparent in the visible region then to calculate other parameter such as, band gap, thickness and disorder.

The optical transmittance measurements of SnO<sub>2</sub> films with different flow rates are showing in Fig.II.9:

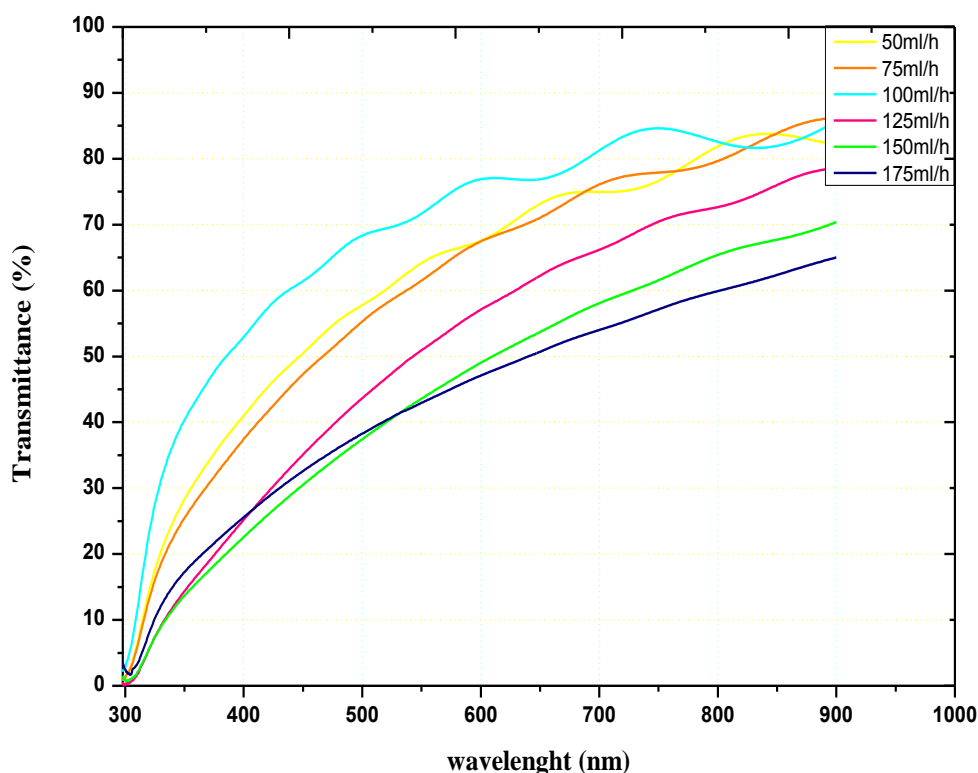


**Fig II.9.**The transmittance spectra of SnO<sub>2</sub> films prepared at various flow rates.

The picture shows that prepared films are fully transparent in the visible region, and the highest value 80% is observed at 100 ml/h; which have most fringes.

It is seen that a values of transmittance is high in the visible and IR region and minimum at wavelength in the absorbance edge (300-400 nm), the same results obtained by other researcher [50]. Also, the transmittances of all the films had common tendency that the values increased with the increase in the wavelength; then we can see that, before 100 ml/h the fringes increasing with flow rate; then after this critical values they decreasing. The most important feature in the transmission spectra is the absence of interference fringes in the spectra of film deposited at 150 and 175 ml/h, despite that the latter is the thicker one [51]. The interference

fringes are due to the multiple reflections at the two film edges, i.e. at the film/air and the film/substrate interfaces. The interference fringes absence in film deposited at 150 and 175 ml/h due to the roughness of the interface air/film, thus at this interface, incident light is diffused rather than reflected in one direction. Moreover, their presence in the other film transmission spectra is a clear indication of the films surface smooth aspect [52].

### **II.2.6.2 Disorder calculating (Energy Urbach)**

Urbach energy is an important parameter, which characterizes the material disorder, according to the Urbach law as we determined in the previous chapter.

The plot of Urbach is the same thing as the band gap, by plotting ( $\ln\alpha$ ) as function of  $h\nu$  we can determine the value of  $E_{00}$  as function of flow rates, the obtain results showing in the following table:

**Table II.6.** Urbach energy of SnO<sub>2</sub> thin films prepared at different flow rate:

<b>Samples</b>	<b>S1</b>	<b>S2</b>	<b>S3</b>	<b>S4</b>	<b>S5</b>	<b>S6</b>
<b>Flow rate (ml/h)</b>	<b>50</b>	<b>75</b>	<b>100</b>	<b>125</b>	<b>150</b>	<b>175</b>
<b>1/E<sub>00</sub></b>	<b>1.40</b>	<b>1.38</b>	<b>1.33</b>	<b>1.64</b>	<b>1.07</b>	<b>0.96</b>
<b>E<sub>00</sub> (eV)</b>	<b>0.71</b>	<b>0.72</b>	<b>0.75</b>	<b>0.61</b>	<b>0.93</b>	<b>1.04</b>

Using these results, we plot the variation of Urbach energy as function of flow rates, which is represented in the Fig.II.10:

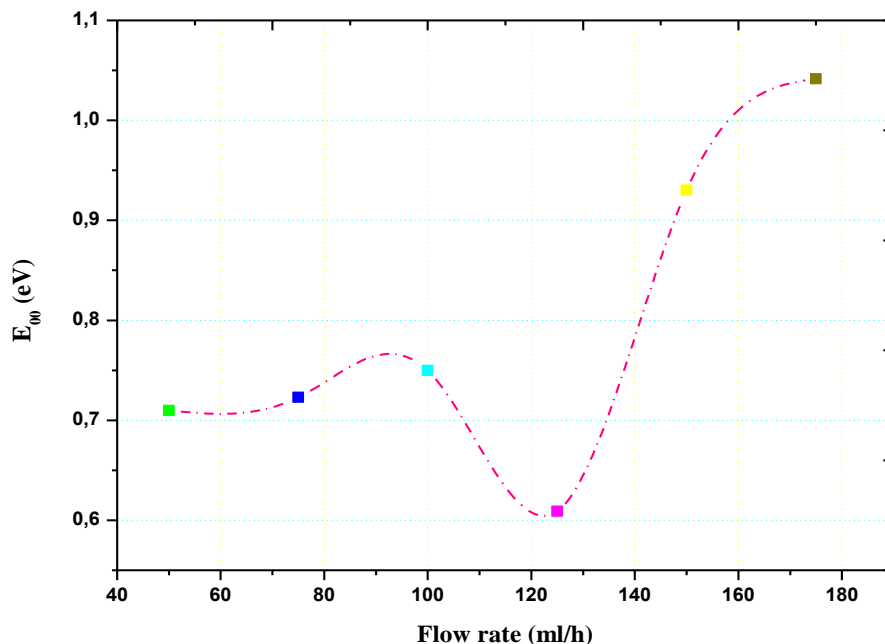


**Fig II.10.** The  $E_{00}$  value of SnO<sub>2</sub> thin film as a function of flow rates.

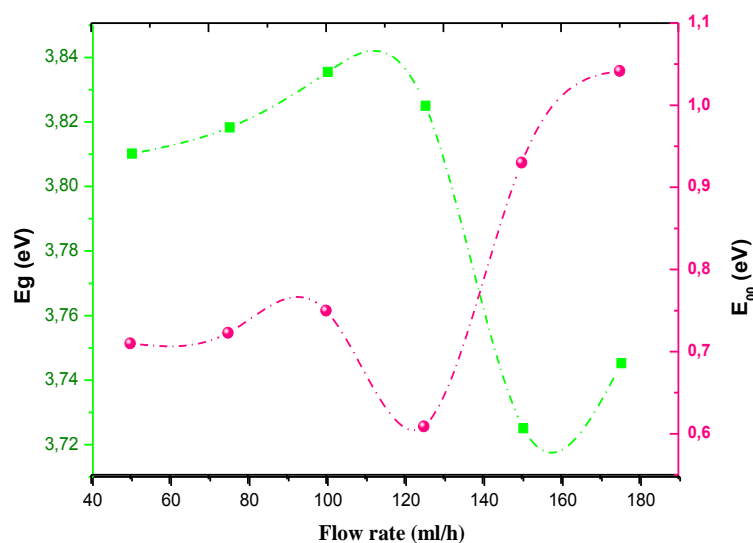
We observe that disorder is running between 609-1041 meV; we can see also the relation between disorder and  $E_{00}$  is inversely; increasing of one of them mean decreasing of the second; which indicate that disorder is less at large  $E_{00}$ , which has good crystalline structure.

### II.2.6.3 Optical Gap

The optical band gap of SnO<sub>2</sub> films has been determined on the basis of UV–VIS transmission measurements by plotting  $(\alpha h\nu)^2$  as function of  $h\nu$  using the relation indicated in previous chapter .

**Table II.7** Band gap energy of SnO<sub>2</sub> thin films prepared at different flow rates:

Samples	S1	S2	S3	S4	S5	S6
Flow rate(ml/h)	50	75	100	125	150	175
Band gap (eV)	3.810	3.818	3.835	3.825	3.725	3.745



**FigII.11.** Variation of band gap for SnO<sub>2</sub> thin films with various flow rates.

It is found that the Optical gap increased with increasing flow rate in the beginning, after 100ml/h it was decrease then it turn back increasing after 150ml/h, that is related with carrier concentration.

The measured optical band gap values were in the range of 3.72–3.83 eV, it seen that a band gap variation and  $E_{00}$  are proportionally [53], while it is inversely with disorder variation; increasing of disorder means decreasing of band gap; these values of band gap were obtained too in the literature [45].

### **II.2.7. Electrical properties**

Using four points measurements determined in the previous chapter permit to indicate how the films are resistive or conductive.

**Table II.8.** Electrical properties of SnO<sub>2</sub> thin films prepared at different flow rate:

<b>Samples</b>	<b>S1</b>	<b>S2</b>	<b>S3</b>	<b>S4</b>	<b>S5</b>	<b>S6</b>
<b>Flow rate (ml/h)</b>	<b>50</b>	<b>75</b>	<b>100</b>	<b>125</b>	<b>150</b>	<b>175</b>
<b>Resistivity <math>\rho</math> (<math>\Omega</math>.cm).10<sup>-2</sup></b>	<b>12.7</b>	<b>74.28</b>	<b>4590.83</b>	<b>75</b>	<b>14.3</b>	<b>11.1</b>
<b>Conductivity <math>\sigma</math> (<math>\Omega</math>.cm)<sup>-1</sup></b>	<b>7.87</b>	<b>1.34</b>	<b>0.021</b>	<b>1.333</b>	<b>6.993</b>	<b>9.00</b>

Using these results, we plot the variation of the resistivity as function of flow rates, which is represented in the Fig II.12

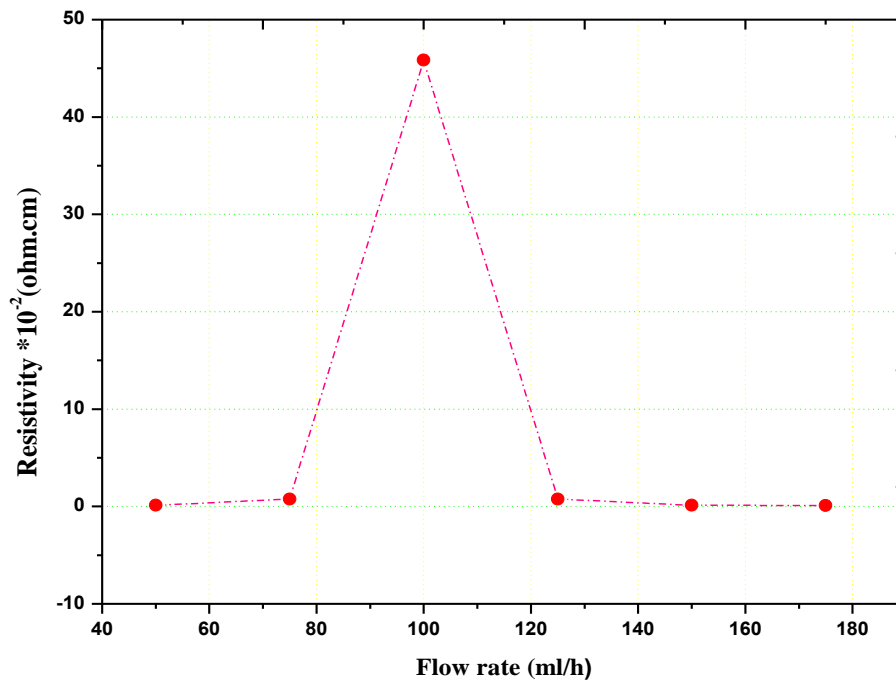


**Fig II.12.** Films resistivity variations as function of the flow rates.

We can see that a graph divided to two parts:

The first from 50 to 100 ml/h when the resistivity increasing that is because the existence defects of the O<sub>2</sub> transferred from substrate to the films by temperature effect are muchness.

The second from 100 to 175ml/h, the resistivity decrease that is because when thickness increase effect of O<sub>2</sub> decrease [48].

### **II.3 Conclusion**

Many researches had done to study the effect of solution flow on the properties of pure SnO<sub>2</sub> thin films deposited by ultrasonic spray. The X-ray diffraction determinate that our films poly crystalline tetragonal structure, with favorable growth direction (110) and crystallite size between 10.08–12.59 nm. The films subjected to compressive stresses which caused deformation of the mesh parameter  $a$ , dislocation density changed from  $6.29 \cdot 10^{15}$  to  $9.84 \cdot 10^{15}$  line/m<sup>2</sup>. While UV–vis results showed that a transmittance decrease when the flow rate increase in the visible region from 80% to 50% approximately; thus thickness increase too from 510.17 to 1066.5 nm. We found that our films have direct energy band gap between 3.72 eV for 3.83 eV with presence of disorder ranging from 609 to 1041 meV and growth rate between 103.43–213.21 nm/min. The electrical study using 4-point technique gave maximum values of conduction at 100 ml/h is  $45.90 (\Omega\text{-cm})^{-1}$ .



***Chapter III:***  
***Realization of Ti doped SnO<sub>2</sub>***  
***thin films properties***

In This chapter we have used ultrasonic spray technique to prepare our Ti-SnO<sub>2</sub> thin films, in order to have high quality of films with greater transmittance and high conductivity. This work based on doped the SnO<sub>2</sub> films and study their properties.

### **III.1. Experimental methodology**

For depositing Ti-SnO<sub>2</sub> thin films, we using an alcoholic precursor solution consisting of stannic chloride SnCl<sub>4</sub>, dissolving in methanol, which served as a starting solution. The Titanium (IV) isopropoxide (C<sub>12</sub>H<sub>28</sub>O<sub>4</sub>Ti) was added to the starting solution as source of titanium. Spray pyrolysis was done at different Ti concentration varied from 0 to 5 at% onto glass substrate heated when the deposition parameters are fixed as follow:

**Table III.1.** The fixed parameters used at the deposition processes

Parameter	temperature	Deposition time	concentration	Nozzle-substrate	Ultrasonic wave
The values	400 °C	5 min	0.1 M	5 cm	40 %

### **III.2 Results and discussion**

Always in thin films before doing any characterization we applied the Stick tape test on the deposited films, it confirmed that the adhesion strength of the Ti-SnO<sub>2</sub> films considered being "good".

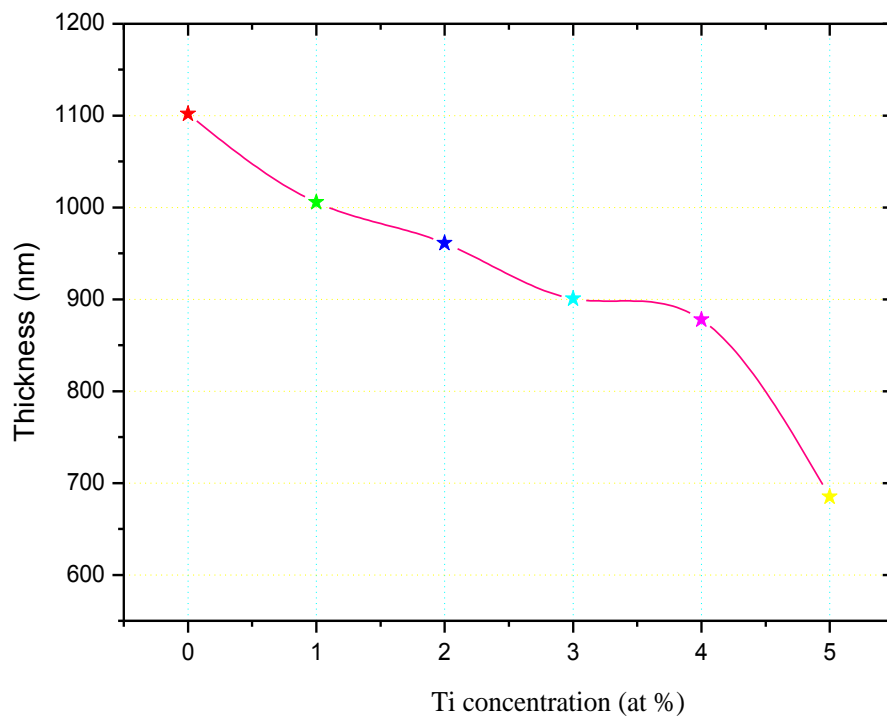
#### **III.2.1 Growth Velocity**

Thickness of Ti-SnO<sub>2</sub> samples prepared at different Ti doping was calculated using both of interference fringes method and gravimetric method to confirm the real results and the same variation. The calculated results obtained showing in the following table:

**Table III.2** different thickness values of SnO<sub>2</sub> prepared at different Titanium doping:

Ti-SnO <sub>2</sub> %	0	1	2	3	4	5
Thickness (nm)	1102	1005.5	961.12	900.8	877.91	685

Using these results, we plot the variation of the thickness as function of Titanium concentration, which is represented in the Fig III.1:



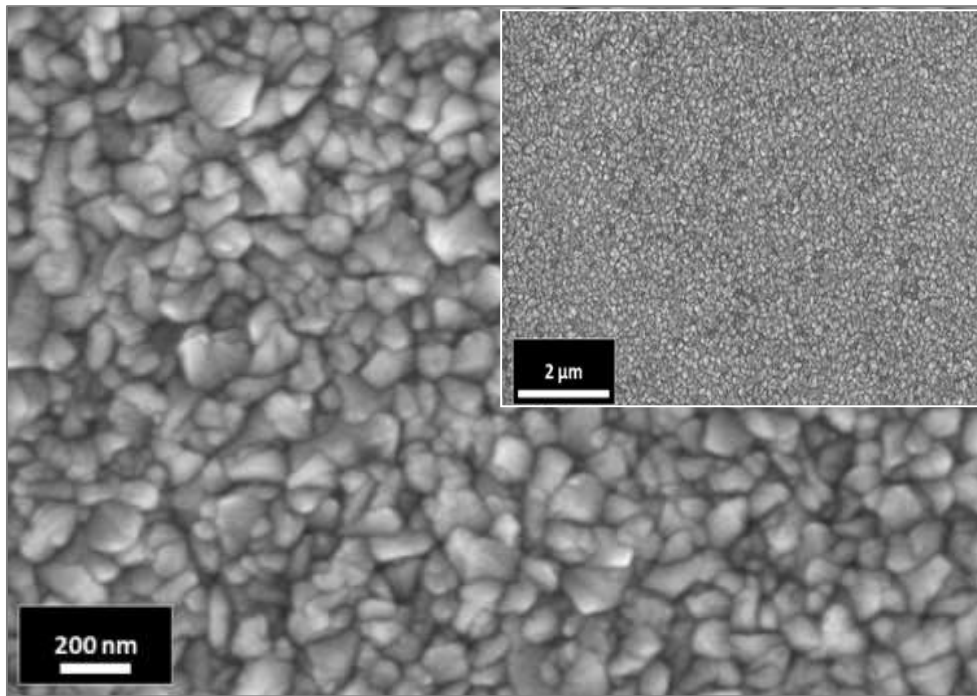
**Fig.III.1.** Ti-SnO<sub>2</sub> films thicknesses at different Ti concentration.

Fig.III.1 shows proportion between decreasing in thickness as increasing Ti concentration uniformly, may that is due to Ti atom size that is smaller than Sn and O atoms. With augmentation of the quantity of titanium, they occupy substitution sites of Sn, as the rayon of Ti is smaller than Sn so, the size of the mesh decreases and consequently the thickness decreases too. In addition, the growth orientation was changed with doping thus made small grains.

### **III.2.2 Scanning Electron Microscopy**

The scanning electron microscopy is enable to observe the surface topography of bulk samples by sweeping their surfaces. The film was studied by using Zeiss-SMT LEO 1540 XB scanning electron microscopy at Hungarian Academy of Sciences, Centre for Energy Research.

Fig.III.2 shows the surface morphology of spray deposited Ti- SnO<sub>2</sub> thin film at 5 at% concentration:



**Fig III.2.** Scanning electron micrographs of nanocrystalline Ti-SnO<sub>2</sub> sample at 5 at% Ti doping.

It is clear in the SEM image that the 5 at% Ti doped SnO<sub>2</sub> film has big homogenous with middle size grains of the order 50 nm approximately. In addition, with the incorporation of Ti the surface became very smooth with less roughness which giving rise to increase the transmittance to 80% in the visible region.

### III.2.3 Structural Characteristics

The crystal structure was determined by XRD of spray deposited SnO<sub>2</sub> and Ti-SnO<sub>2</sub> thin films with different titanium doping concentration shown in Fig.III.3:

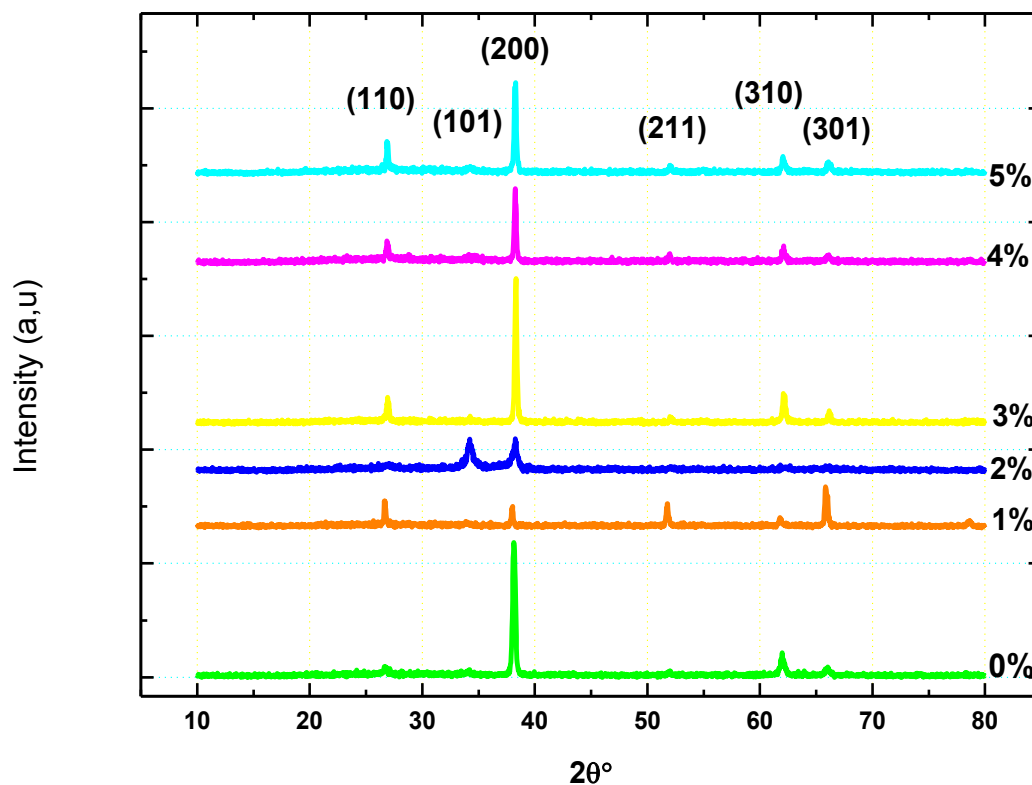


**Fig.III.3** XRD spectrum of Ti doped SnO<sub>2</sub> thin films at various Ti doping.

It is interesting to note that from a general view, all X-ray diffraction patterns look like the same as the pure SnO<sub>2</sub> sample. These peaks found are in good agreement with the ASTM data, which confirm the tetragonal (cassiterite) structure of our deposits as Batzill et al [54] found it.

The diagram in Fig.III.3 shows that several peaks are present with a preferential orientation according to (200) which determines a strong crystallographic texture or low energy. There are minority peaks according to (110), (101), (211), (310) and (301) reflecting the poly crystallinity of the pure structure.

More that, by comparing our results with the ASTM files, we notice a slight shift of the peaks that reflects the creation of the constraints.

### III.2.4 Crystallite Size and Dislocation Density

Generally, the average crystallites size evaluated from XRD results according to the Scherrer formula.

The crystallite size  $D$  and dislocation  $\delta$  results as a function of Ti concentrations are presenting in the Fig.III.4, when  $\delta$  is defined as the length of dislocations lines per unit of the crystal volume estimated by using Williamson and Smallman's relation.

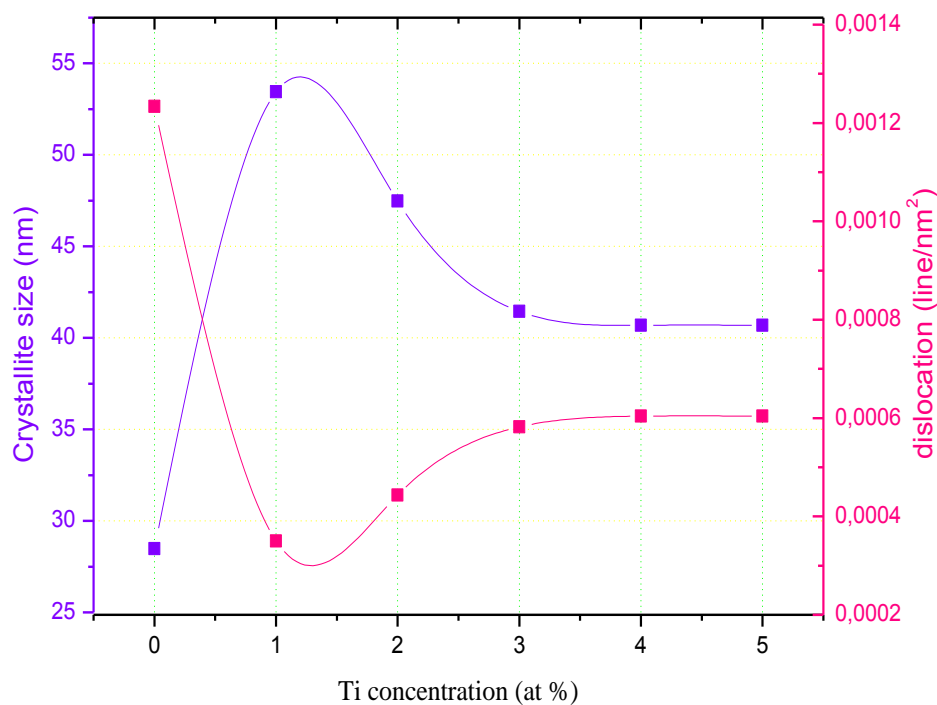


**Fig.III.4** Variation of crystallite size and dislocation of Ti-SnO<sub>2</sub> with different titanium doping.

The variation in  $D$  shows an increase in the beginning then after it was decrease when the dopant concentration augment. It is observed that the  $D$  increases to the value 47.48 nm for a percentage of 1 and 2% when the larger grains are required for the fabrication of high efficiency solar cells [55]. After this value, it was decreases and stabilized at 40.69 nm.

We can interpret the increase of the grains size by the reconstruction nucleation sites through the increase of titanium atoms so the quality of crystalline improves. In addition, the decrease in the  $D$  is due to the decrease in thickness because we have increase dislocation in our films or less density of grains that responsible to do a complete nucleation [56]. More that the calculation of deformation was negative (compression), which explains that decrease is due to the compression stress.

### III.2.5 The transmittance

The transmittance spectra obtained by UV-visible spectroscopy as function of wavelength over spectral range 350-1100 nm are showing in Fig.III.5:

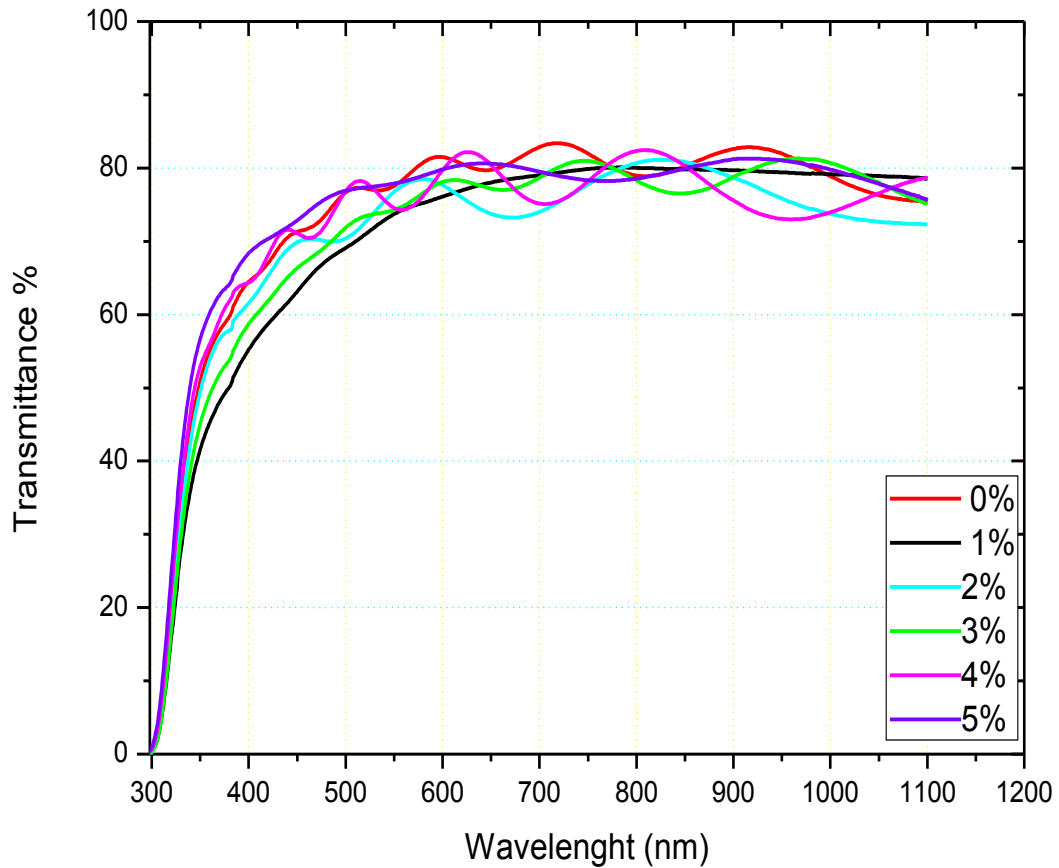


**Fig.III.5** Optical transmittance spectra of Ti-SnO<sub>2</sub> thin films at different Ti concentration.

Fig.III.5 represents the optical transmission spectra of pure and Ti-doped SnO<sub>2</sub> thin films deposited at different Ti concentrations. It is clear that the films show high transparency in the range of [400 - 1100 nm], where the highest transmittance values up to 84% approximately. At first the transmittance decrease with the augmentation of Ti then after it started to increase but with less fringes, however 4% represents high transparency with more fringes, which confirm that the film prepared under these conditions is very smooth and uniform due to the multiple reflections on the different interfaces [57].

The decrease is due to the existence of defects in the lattice, which made deformation and no homogeneity structure thus affect the morphology and consequently decrease the transmittance

by scattering of light. However, the increase of transmittance is due to the decrease both of the defects and the film thickness and that was clear in Fig.III.1, vice versa is happened with the decrease.

### III.2.5.1 Band Gap Energy

The optical band gap energy  $E_g$  was calculated according to the Tauc's formula. The plot of  $(\alpha h\nu)^2$  as function of  $h\nu$  illustrated in the Fig.III.6, which determine the typical Tauc's plot then, Fig.III.7 shows the obtainable values and the variation of the band Gap  $E_g$ :

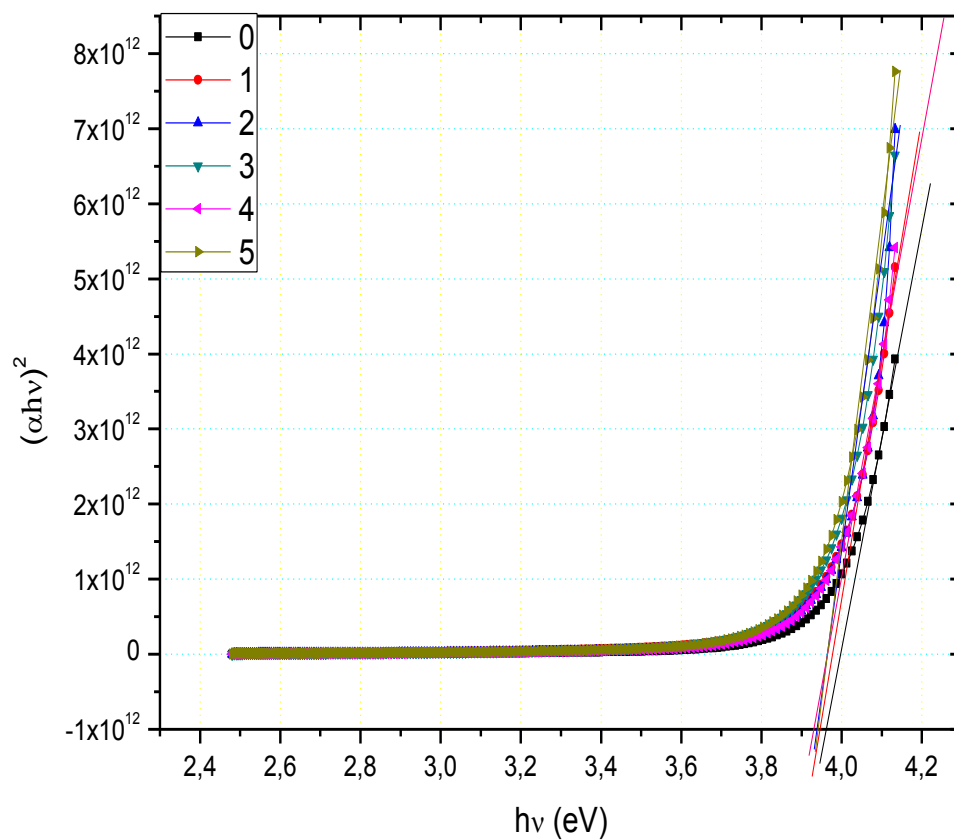


**Fig.III.6** Typical Tauc plot used for optical band gap determination of Ti-SnO<sub>2</sub> films at different Ti concentration.

We can summarize and plot the  $E_g$  values variation as function of the titanium doping concentration in the Fig.III.7:

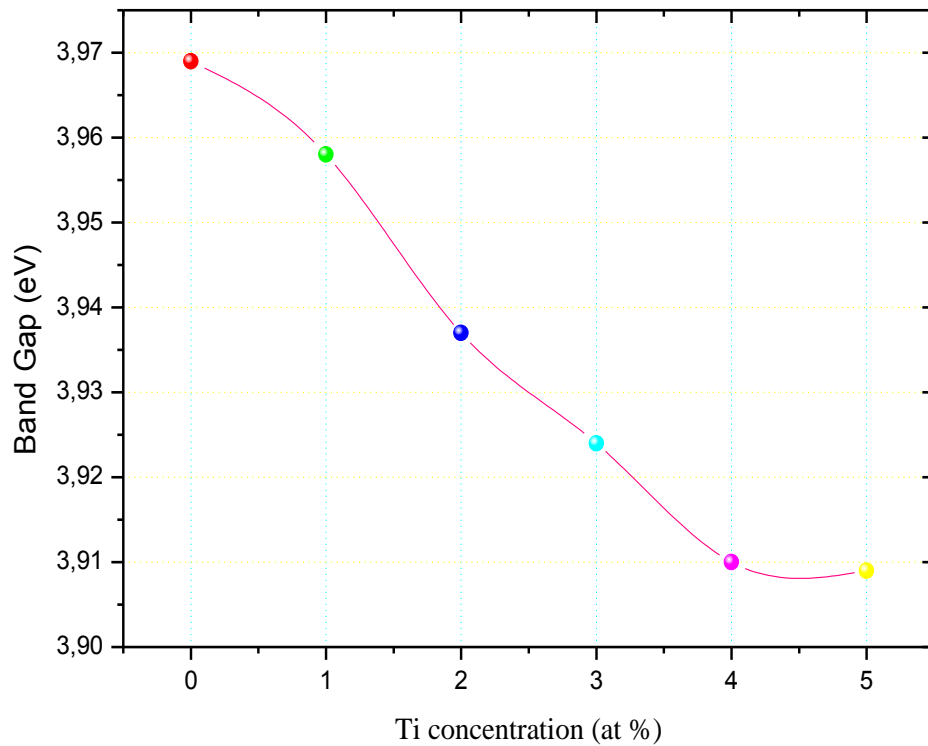


**Fig.III.7** The optical band gap variation of Ti-SnO<sub>2</sub> films at different Ti concentrations.

The decrease in optical band gap with increasing Ti doping, can be due to the decrease that decline the films crystallinity and increase the dislocation. More that, the blue emission of PL spectroscopy confirm that the injection of Ti ions in the crystal lattice, created an energy level presented into the band gap so that level maybe near the valence band of SnO<sub>2</sub>, then it make a decrease in the band gap. The compressive stress and the decrease of thickness too can be related and responsible to this shift of band gap.

### **III.2.5.2 Figure of Merit**

In order to evaluate the efficiency of Ti-SnO<sub>2</sub> films and when they present the best condition for their applications as in widow and collector in solar cells. Figure of merit  $\phi$  was obtained by using Haacke's formula [58]:

$$\phi = T^{10} / R_{sh}$$

Fig.III.8 represents the variation of figure of merit as function of wavelength at different Ti doping:

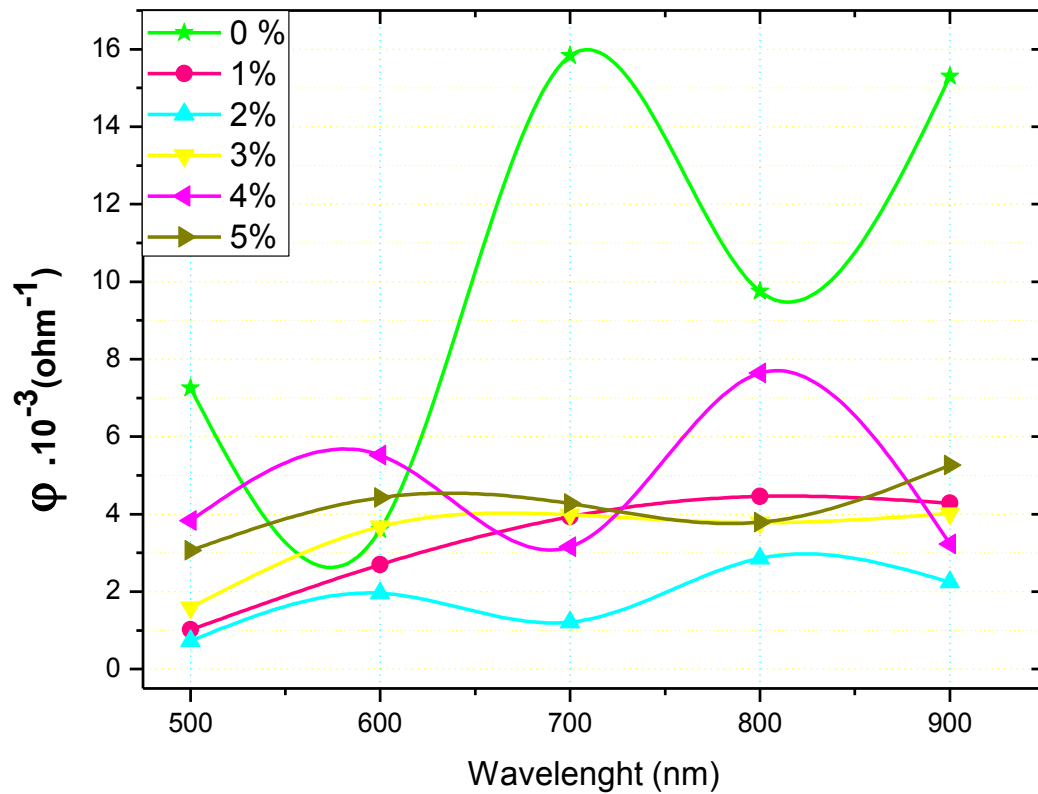


**Fig.III.8** Figure of merit values of Ti-SnO<sub>2</sub> at different Ti concentrations.

It is clear in Fig.III.8 that figure of merit values decrease when the Ti concentration increase, and the best values are at the pure SnO<sub>2</sub>. When the 4 at% Ti-SnO<sub>2</sub> seem better than the others doping values.

### III.2.6 Photoluminescence

We used photoluminescence (PL) spectroscopy technique for investigating the structure, defect, impurity levels and quality of thin films. Fig.III.9 represents the photoluminescence spectra of the pure and Ti-SnO<sub>2</sub> films:

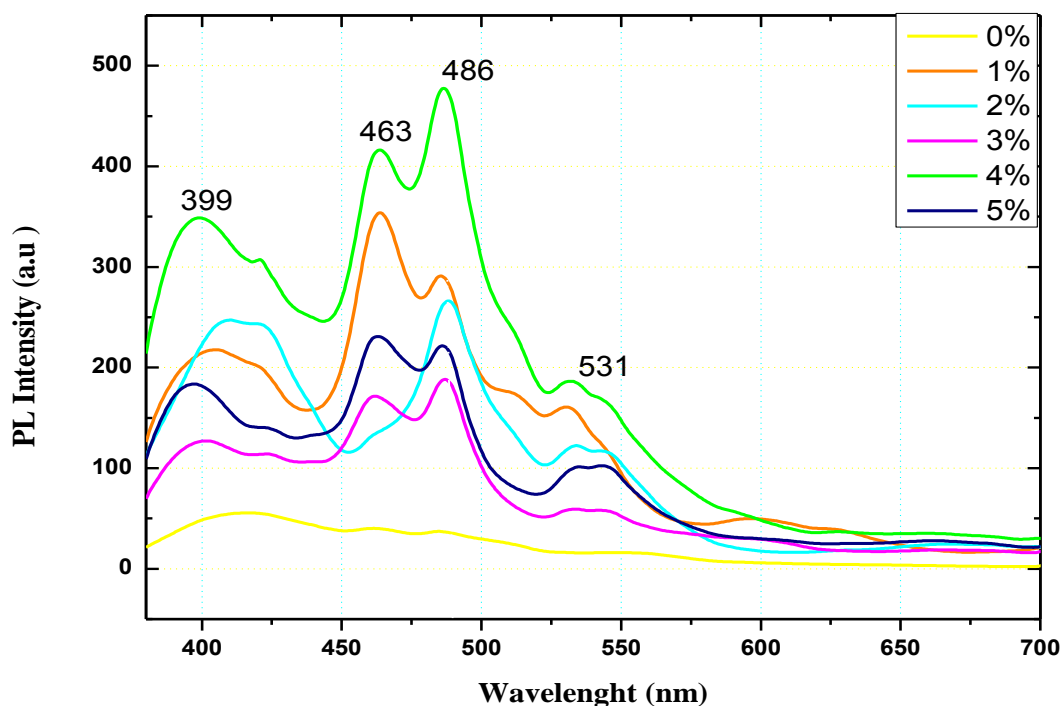


Fig.III.9 Photoluminescence spectra of Ti doped SnO<sub>2</sub> thin films.

A broad dominant peak is observed in the range 390-540 nm show three emissions bands, as presented in Fig.III.9, this no homogeneity broadened luminescence might be due to all the luminescent centers, such as Nano crystals and defects in the Ti-SnO<sub>2</sub> films [59].

The first peak at 399 nm corresponding to the UV emissions band due to oxygen vacancies that forms the donor levels and were the responsible for available electrons in the CB [60]. The second peak positioned at 486 nm with shoulder peak at 463 nm, corresponding to the blue emissions signal that a new defect level presented into the band gap by the Ti doping and that peak is absence in the pure, which confirm that a new defect in the others is caused by Ti doping. A very low intensity pic at 531 agreeing to the green, which created from the electron-hole recombination at the defect sites due to electron transition from the oxygen vacancy [61]. The increase in PL intensity with the increasing Ti doping concentration maybe due to the decrease of band gap energy of Ti-SnO<sub>2</sub> samples [62].

### III.2.7 Electrical properties

Using 4-point measurements that permit to indicate how Ti-SnO<sub>2</sub> films are resistive, the obtained results are showing in Fig.III.10.

Fig.III.10 shows plot of electrical resistivity ( $\rho$ ) and the electrical conductivity ( $\sigma$ ) as function of Ti concentration:

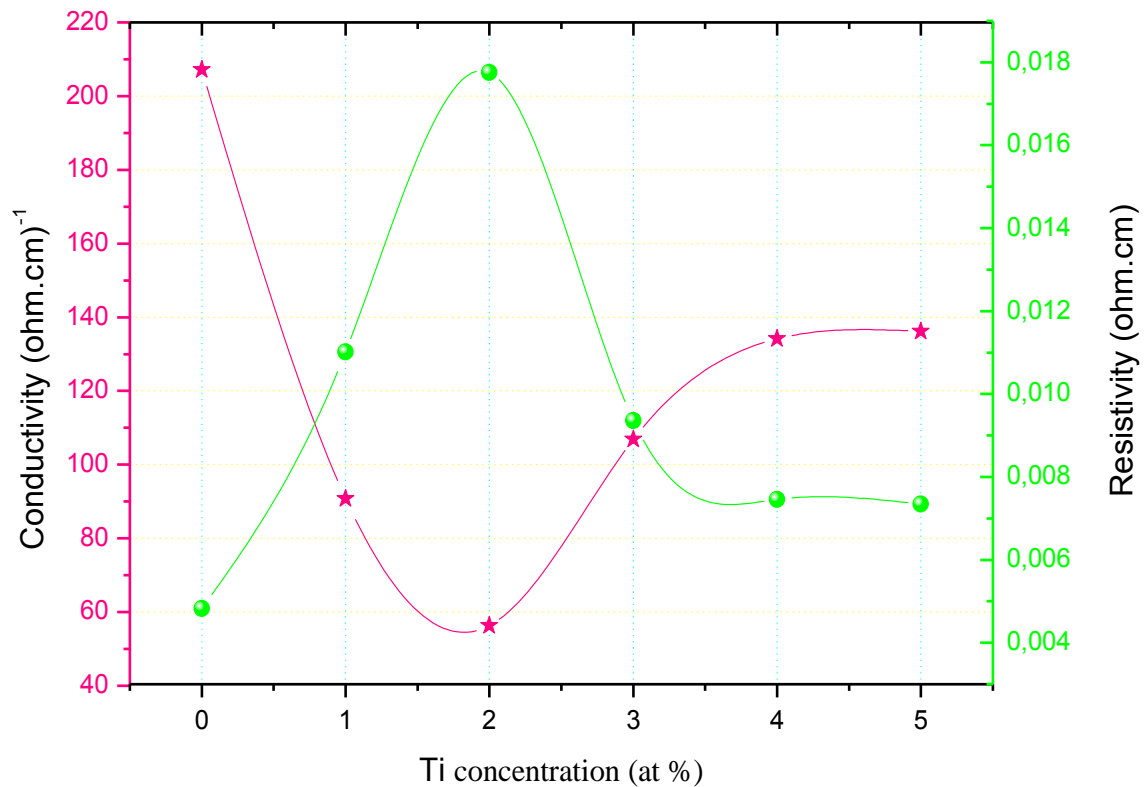


**Fig.III.10** Variation of conductivity and resistivity of Ti-SnO<sub>2</sub> with different Ti doping.

Fig.III.10 shows that the electrical conductivity started to decrease until 2 at% of Ti doping then after it started to increase up to  $140 (\Omega.\text{cm})^{-1}$  but the augmentation was slowly and less than the speed of decrease.

The decrease of conductivity is due to the incorporation of Ti in the beginning that caused disorder in the SnO<sub>2</sub> lattice with some defects. By the other hand the existence of O<sub>2</sub> transferred from substrate to the films by temperature effect are muchness. Also in the beginning Takumi Tomita [63] confirm that in some cases, the oxygen vacancies cannot act as a native donor that is due to its defect level which is much lower than the conductive band.

The increase of conductivity is due to the decrease of the band gap. More that, the existence of the oxygen vacancy at these concentrations may act the role of donor, so that increase the carrier concentration due to more free electrons transferred from the defect level of O, which became located near the conductive band in the lattice.

### **III.3. Conclusion**

Many researches had done on Ti-SnO<sub>2</sub> thin films prepared by ultrasonic spray. The characterizations techniques show that all Ti-SnO<sub>2</sub> films are Polycrystalline with strong orientation along (200) which confirm the highest texture along these orientations. The best values of the figure of merit are seen at 4 at% reached to 7,  $64.10^{-3}\Omega^{-1}$  at 800 wavelength.

Photoluminescence spectroscopy confirm that we have UV emission which due to the existence of the oxygen vacancies in one hand, and the presence of new defect level in the band gap due to the incorporation of the titanium. Few changes were noted in the optical band gap between 3.91-3.97 eV that seem constant approximately.

The Ti-SnO<sub>2</sub> films revealed the maximum transmittance up 84% in the visible region with maximum conductivity about  $1.4 \times 10^2 (\Omega\text{-cm})^{-1}$  at 5 at %.



***Chapter IV:***  
***Investigation of F doped SnO<sub>2</sub>***  
***thin films properties***

This chapter presents undoped tin dioxide and fluorine doped tin dioxide thin films deposited onto glass substrates, to investigate the effect of the F concentration on the properties of SnO<sub>2</sub> films using XRD, SEM, UV-Visible, PL and 4-point.

### **VI.1. Experimental methodology**

For depositing F-SnO<sub>2</sub> thin films by easy and low cost spray, we have been prepared using pyrolysis technique an alcoholic precursor solution consisting of stannic chloride SnCl<sub>4</sub>, dissolving in methanol, which served as a starting solution. The ammonium fluoride (NH<sub>4</sub>F) was added to the starting solution as source of fluorine. Spray pyrolysis was done at different F concentration varied from 0 to 5 at% onto heated glass substrate when the deposition parameters are fixed as follow:

**Table VI.1.** The fixed parameters used at the deposition processes

Parameter	temperature	Deposition time	concentration	Nozzle-substrate	Ultrasonic wave
The values	450 °C	5 min	0.1 M	5 cm	40 %

### **VI.2 Results and discussion**

As usual before doing any characterization, we applied the Stick tape test on the deposited F-SnO<sub>2</sub> films to confirm that the adhesion strength of these films considered being "good".

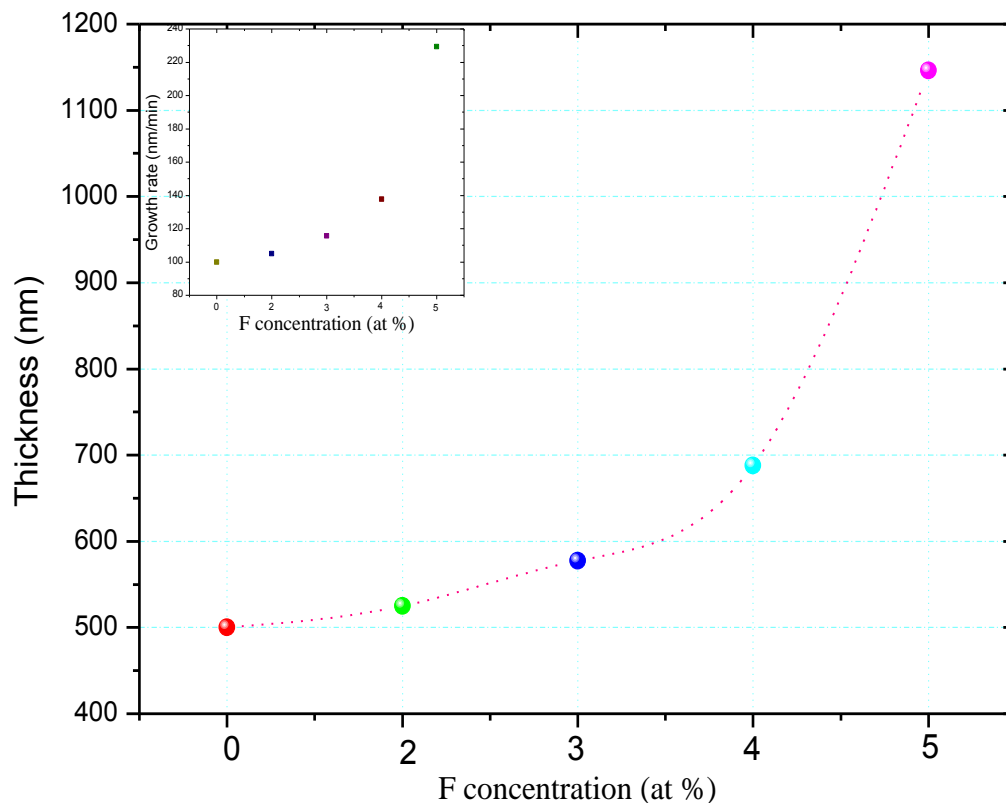
#### **VI.2.1 Growth Velocity**

Thickness of F-SnO<sub>2</sub> deposited samples prepared at different F doping was calculated using both of interference fringes method and gravimetric method to confirm the real results and the same variation. The calculated results obtained are showing in the following table:

**Table VI.2** different thickness values of SnO<sub>2</sub> prepared at different F doping.

F-SnO <sub>2</sub> %	0	2	3	4	5
Thickness (nm)	500	524.97	577.60	688	1146

Using these results, we plot the variation of the thickness as function of fluorine concentration, which is represented in the Fig VI.1:



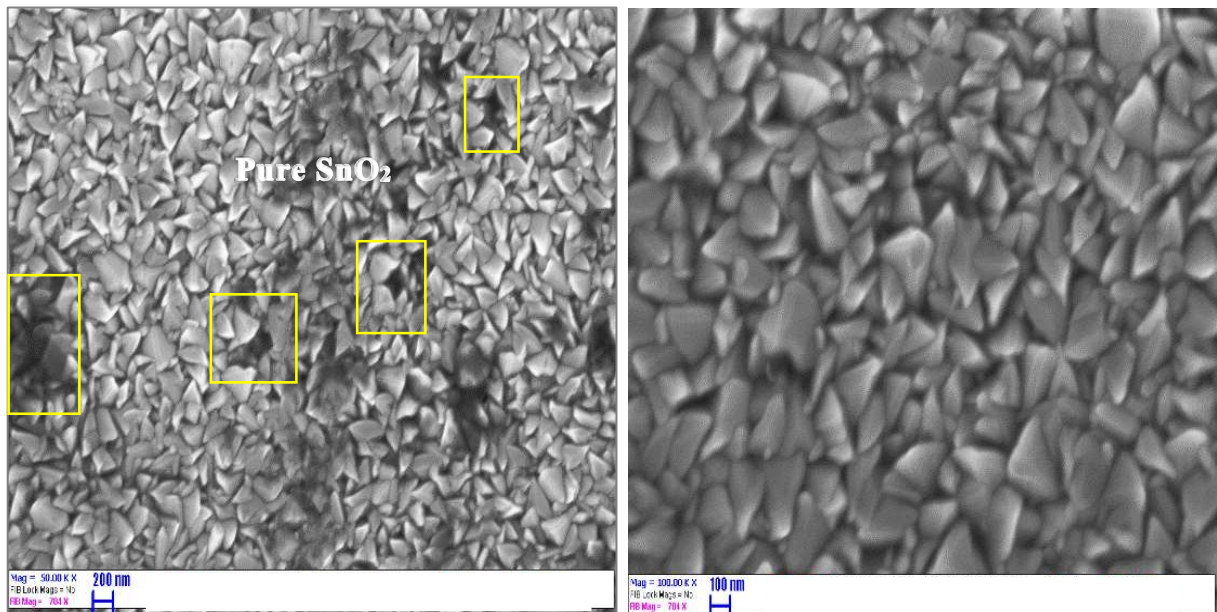
**Fig.VI.1.** F-SnO<sub>2</sub> films thicknesses and growth rate variations at different F concentration.

Fig.VI.1 shows proportion between increasing in thickness as increasing F concentration uniformly. In the figure insert, the growth rate (thickness/5 min) variation was slowly then it will be thicker and linearly after outside concentration, because in the beginning the growth of the film was onto the surface area (2D) then after it will be perpendicular to the substrate (3D) [64]. By other, hand with increase in solution amount, the fluorine atoms will take oxygen vacancies. By way of F size is large thereby, enhancement quantity of F atoms caused an increase in thickness.

## **VI.2.2 Scanning Electron Microscopy**

The scanning electron microscopy is enable to observe the surface topography of bulk samples by sweeping these surfaces. The film was studied by using Zeiss-SMT LEO 1540 XB scanning electron microscopy at the Hungarian Academy of Sciences, Centre for Energy Research.

Fig.VI.2 shows the surface morphology of spray deposited pure SnO<sub>2</sub> thin film at various magnifications:



**Fig VI.2.** Scanning electron micrographs of nanocrystalline pure SnO<sub>2</sub> samples.

It is clear in the SEM image that the pure SnO<sub>2</sub> film has grains with different sizes whereas intergranular region appears dark. In addition, the grains are randomly distributed with some porosity and roughness surface which giving rise to a scattering effect, thereby reducing transmittance [65].

### VI.2.3 Structural Characteristics

The crystal structure was determined by XRD of spray deposited SnO<sub>2</sub> and F-SnO<sub>2</sub> thin films with different fluorine doping concentration shown in Fig.VI.3:

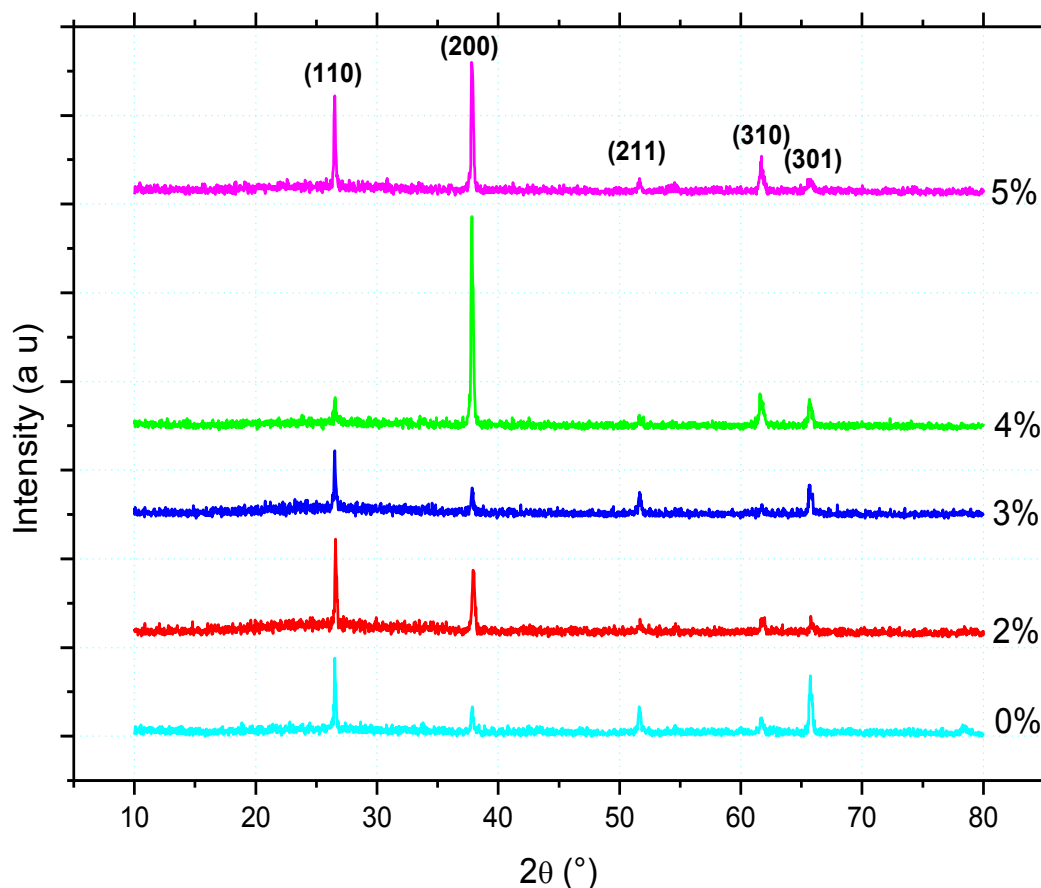


**Fig.VI.3** XRD spectrum of F doped SnO<sub>2</sub> thin films at various F doping.

The results clearly indicate that all the films are tetragonal Rutile structure with a polycrystalline nature. The major peaks located at 26.75, 38.09, 51.64, 61.88 and 65.81 corresponding to (110), (200), (211), (310) and (301) diffraction planes respectively. A strong (110) orientation is observed at 0, 2 and 3% which indicate that the films have a strong crystallographic texture along (110) where the formation energy was lower. Above these values at 4 and 5 at%, we can see that the orientation was changed to (200) which has high texture growth confirmed by TC in Fig.VI.4 With the increasing of fluorine doping concentration the rutile structure remains the same, other main planes of cassiterite have also been detected but with substantially lower intensities. It is evident from the XRD spectra there is no diffraction peaks of any other impurity phases are detected in the prepared samples such as Sn and SnF<sub>2</sub>, indicating the O atoms were replaced by F atoms in the F-SnO<sub>2</sub> films [43].

The inserting of fluorine does not affect the structural properties of the films, however, the increase in the intensities of the main XRD peaks with increasing fluorine doping levels, is probably attributed to the change in the growth rate which leads to an increase in the thickness of the films[64] or the change of solution concentration . These explications were obtained well in other papers [66] and confirmed by Demet Tatar [67].

#### **VI.2.4 Texture Coefficient (TC)**

Texture coefficient, measures the relative degree of preferred orientation of the SnO<sub>2</sub> films among crystal planes, which is obtained from the X-ray data using the following expression [68] :

$$TC_{(hkl)} = [I_{(hkl)} / I_0(hkl)] / [N^{-1} \sum_N (I_{(hkl)} / I_0(hkl))]$$

Where  $I_{(hkl)}$  is the measured intensity of the plane (hkl),  $I_0(hkl)$  is the standard intensity of the plane (hkl) according to the JCPDS data then N is the number of diffraction peaks. The texture coefficient was calculated for (110), (200) and (310) peaks, shown in following Table:

**Table.VI.3** Texture coefficient results at different F-SnO<sub>2</sub> concentration:

F-SnO <sub>2</sub> %	TC <sub>(110)</sub>	TC <sub>(200)</sub>	TC <sub>(310)</sub>
0	0.5820	1.1645	1.2534
2	0.6145	1.6803	0.7050
3	0.7658	1.6187	0.6154
4	0.0635	2.336	0.5996
5	0.2878	1.9871	0.7249

The obtained results of TC were plotted as a function of F concentration in Fig VI.4:

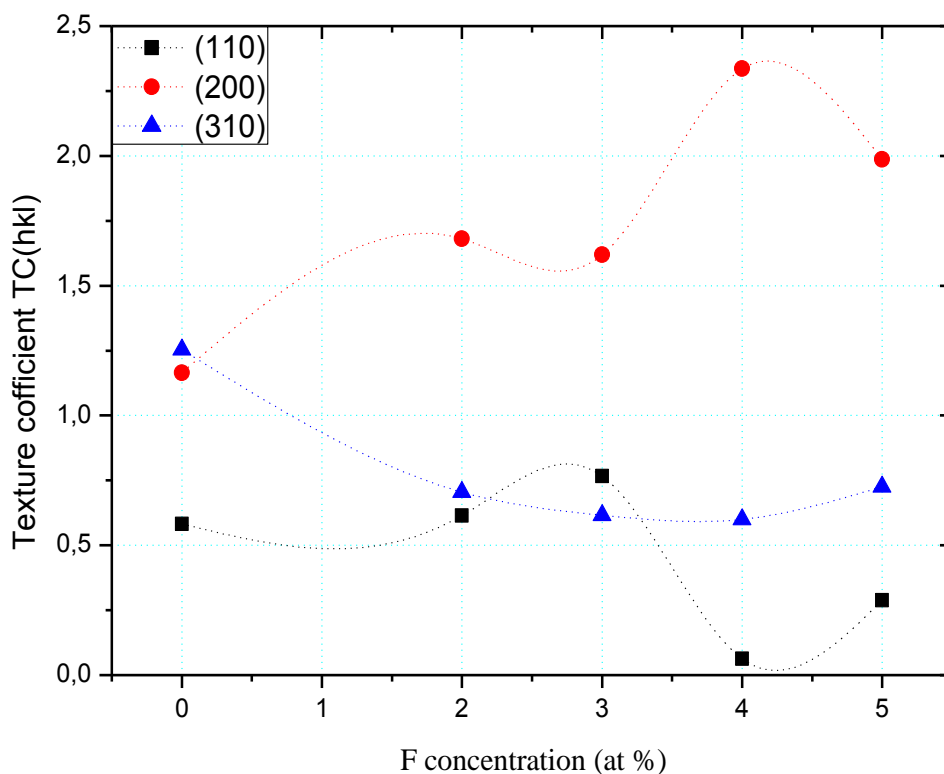


**Fig.VI.4** Texture coefficient plot of F-SnO<sub>2</sub> as function of F doping.

The higher values in TC<sub>(200)</sub> means that the preferential orientation is along (200) lattice plane, and this is good agreement with XRD results which confirmed that the (200) plane shows highly textured growth than (110) plane.

The relation between the energy minimization and the morphology is of great importance in texture development; Yaqin Wang and all see that the value of TC decreases as the film thickness or average crystalline size goes up [69].

### VI.2.5 Crystallite Size and Dislocation Density

Generally, the average crystallites size was evaluated from XRD results according to Scherrer formula [70].

The results of the crystallite size  $D$  and dislocation  $\delta$  as a function of F concentrations are presenting in the Fig.VI.5 when  $\delta$  is defined as the length of dislocations lines per volume unit of the crystal and was estimated using Williamson and Smallman's relation [71] :

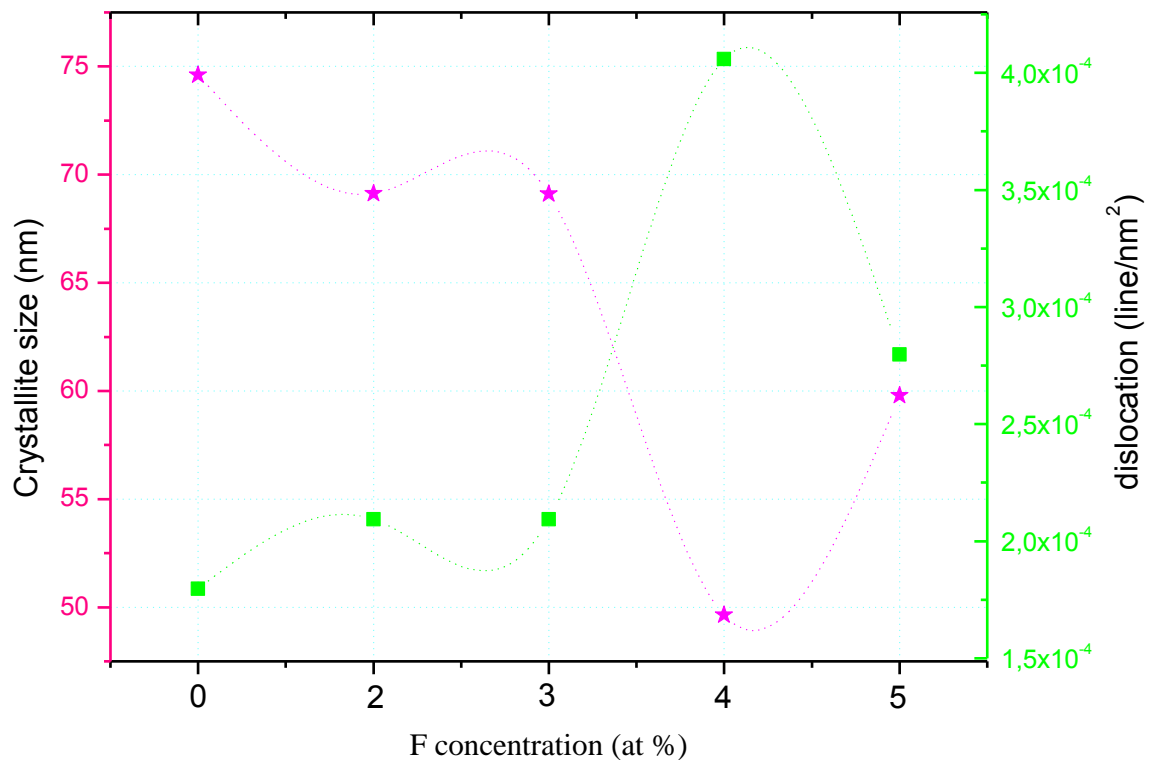


**Fig.VI.5** Variation of crystallite size and dislocation of F-SnO<sub>2</sub> with different fluorine doping.

In the beginning until 4 % the FWHM increase with increasing F concentrations this indicates a decrease of  $D$  due to the incorporation of F ions into the SnO<sub>2</sub> lattice which take interstitial sites then pressed there on one hand, and the augmentation of dislocation density by the other hand. At 5 % the  $D$  is increase when dislocation decrease due to the O atoms which replaced by F in the F-SnO<sub>2</sub> lattice [43]. Also, above 4 % as the fluorine injected increase, the  $D$  increase too and this is probably due to the increasing in fluorine atoms arriving to the substrate which have big atomic rayon, thereby causing an increase in the nucleation numbers which combine together to form larger grains [72]. Therefore, the crystalline quality improves and that is clear in XRD results.

### VI.2.6 The transmittance

The transmittance spectra obtained with UV-visible spectroscopy as function of wavelength over spectral range 350-1100 nm are showed in Fig.VI.6:

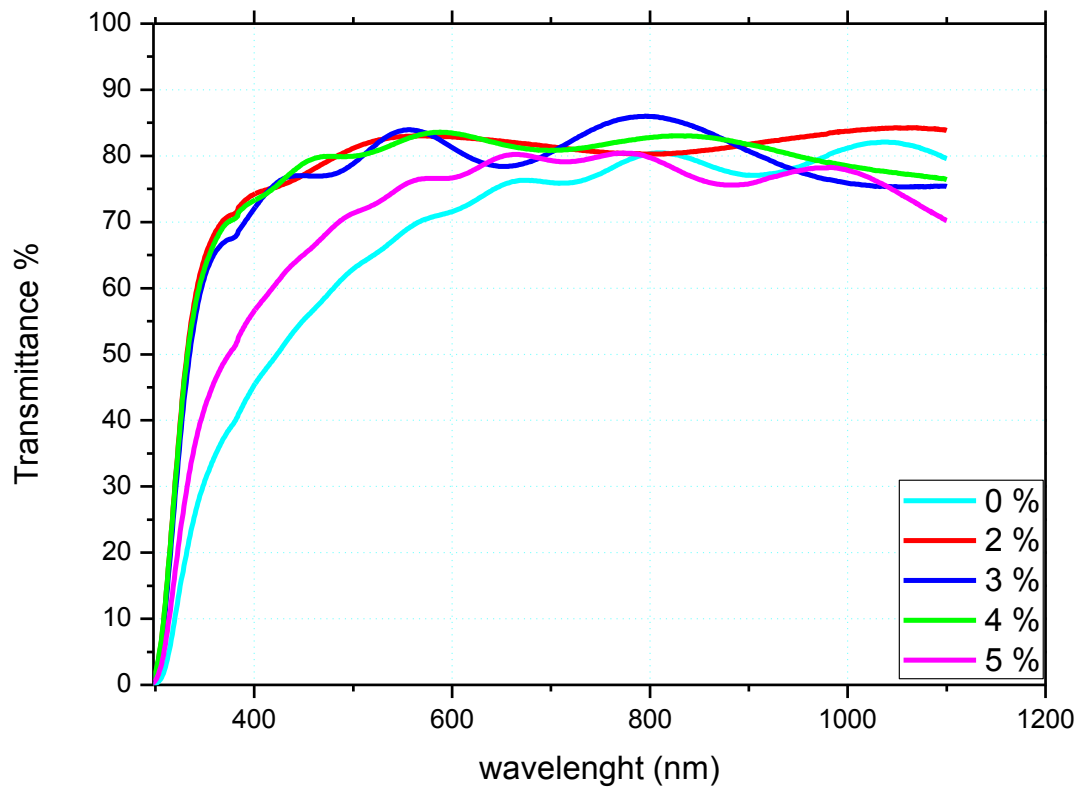


**Fig.VI.6** Optical transmittance spectra of F-SnO<sub>2</sub> thin films at different F concentration.

It is clearly that an average optical transparency is about 85 % in the visible range. As the doping concentration increases, the transmittance increase too, which indicate the good crystallization with high structural homogeneity [73]. At 5% the transmittance decreases, but it remains bigger than the pure SnO<sub>2</sub>, this decrease probably due to the diffusion photon by crystal defects or due to free carrier as A. Arunachalam and all supposed [74].

### VI.2.6.1 Figure of Merit

In order to evaluate the efficiency of F-SnO<sub>2</sub> films and when they present the best condition for their applications as window and collector in solar cells. Figure of merit  $\phi$  was obtained by using Haacke's formula [75] to evaluate the F-SnO<sub>2</sub> films.

Fig.VI.7 presents the variation of figure of merit as function of wavelength at different F doping:

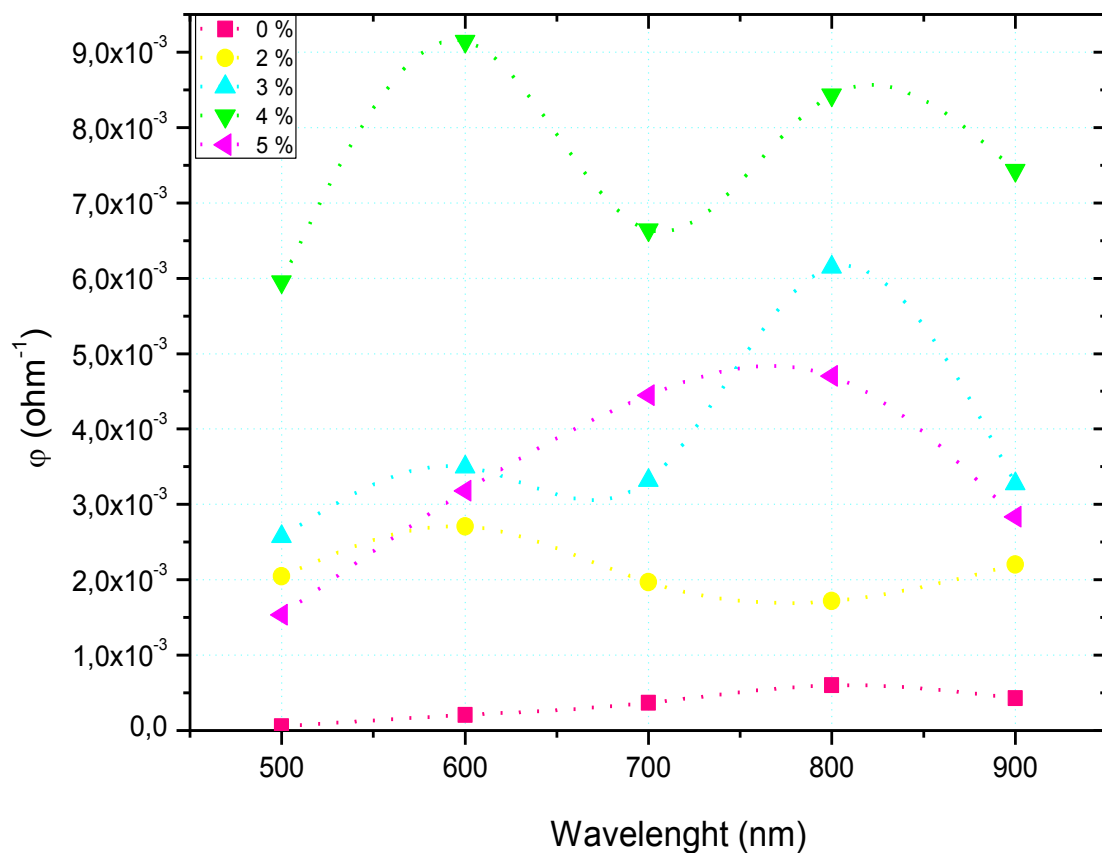


Fig.VI.7 Figure of merit values of F-SnO<sub>2</sub> at different F concentrations.

It is clear from Fig.VI.7 that the augmentation in figure of merit values in the visible region was well observed when the F concentration increase as well, and the best values are at 4 %.

M.N. Yusnidar and all [58] see that ultrasonic spray pyrolysis method may produce thin films with high figure of merit due to their high electrical conductivities, which result from their large grain and crystallite sizes with enhanced oxygen vacancies.

### VI.2.6.2 Band Gap Energy

The optical band gap energy  $E_g$  was calculated according to Tauc's formula [76]. The plot of  $(\alpha h\nu)^2$  as function of  $h\nu$  illustrated in the Fig. VI.8 which determine the typical Tauc's plot then, Fig. VI.9 shows the obtainable values and the variation of the band Gap  $E_g$ :

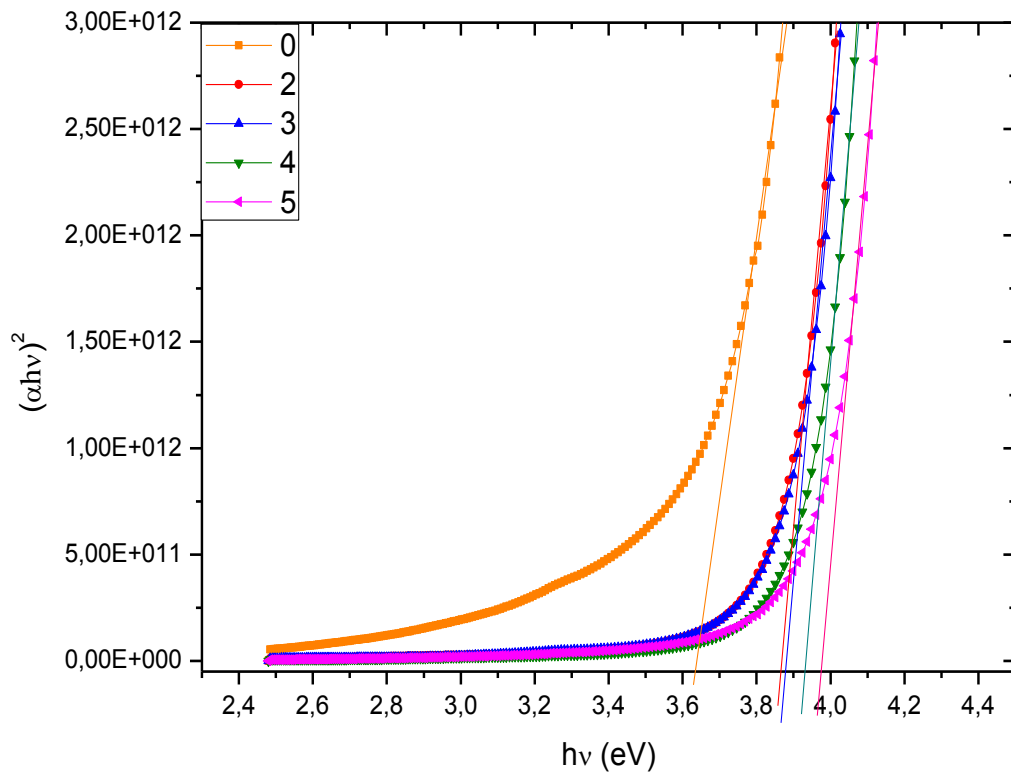


**Fig. VI.8** Typical Tauc plot used for optical band gap determination of F-SnO<sub>2</sub> films at different F concentration.

We can summarize and plot the  $E_g$  values variation as function of the fluorine doping concentration in the Fig. VI.9:

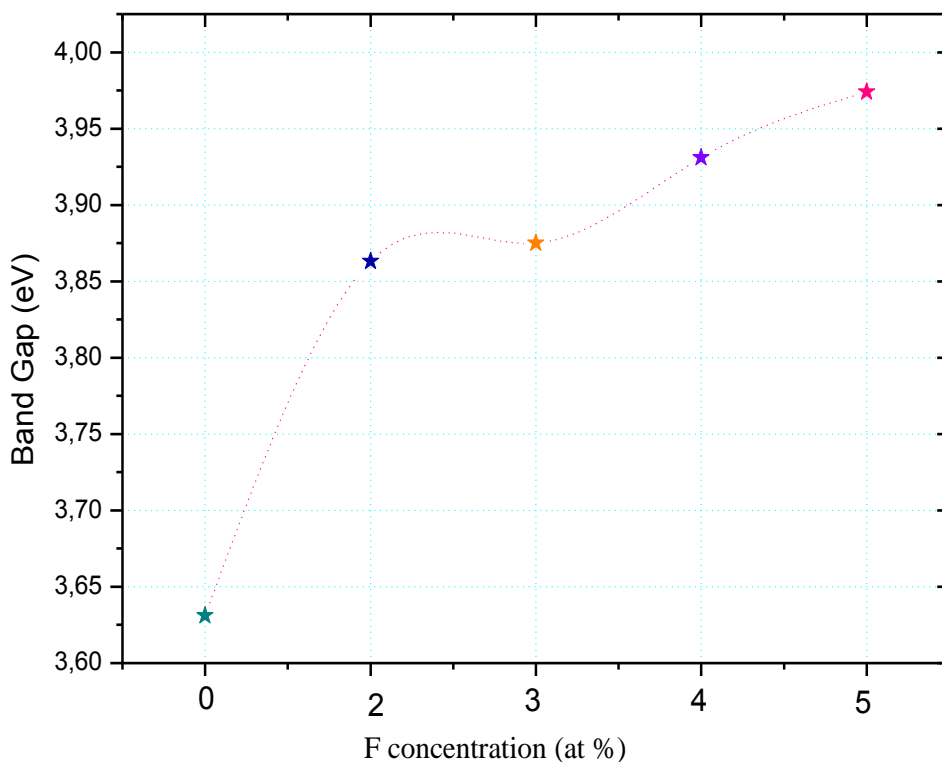


**Fig.VI.9** The optical band gap variation of F-SnO<sub>2</sub> films at different F concentrations.

The injection of F ions in the crystal lattice and the existence of oxygen vacancies induced during the film growth increase the electrons near the conduction band edge, which created donor levels in the conductive band of SnO<sub>2</sub>, then will increase the band gap [77]. The widening effect in band gap can be attributed to Burstein-Moss effect which states that: carrier concentration is due to the high doping levels, fills blank states belonging to CB of the thin films so increasing the energy magnitude necessary for the valence band to conduction band transitions [78].

In other hand, the change in crystallite size or structural phase and carrier concentration [79] with the increase of F doping, make large band gap and caused the increase of the crystal defects existed in the band gap of the F-SnO<sub>2</sub> films [80].

### VI.2.7 Photoluminescence

Photoluminescence (PL) spectroscopy technique used for investigating the structure, defect, impurity levels and quality of thin films. Fig.VI.10 represents the photoluminescence spectra of the pure and F-SnO<sub>2</sub> films:

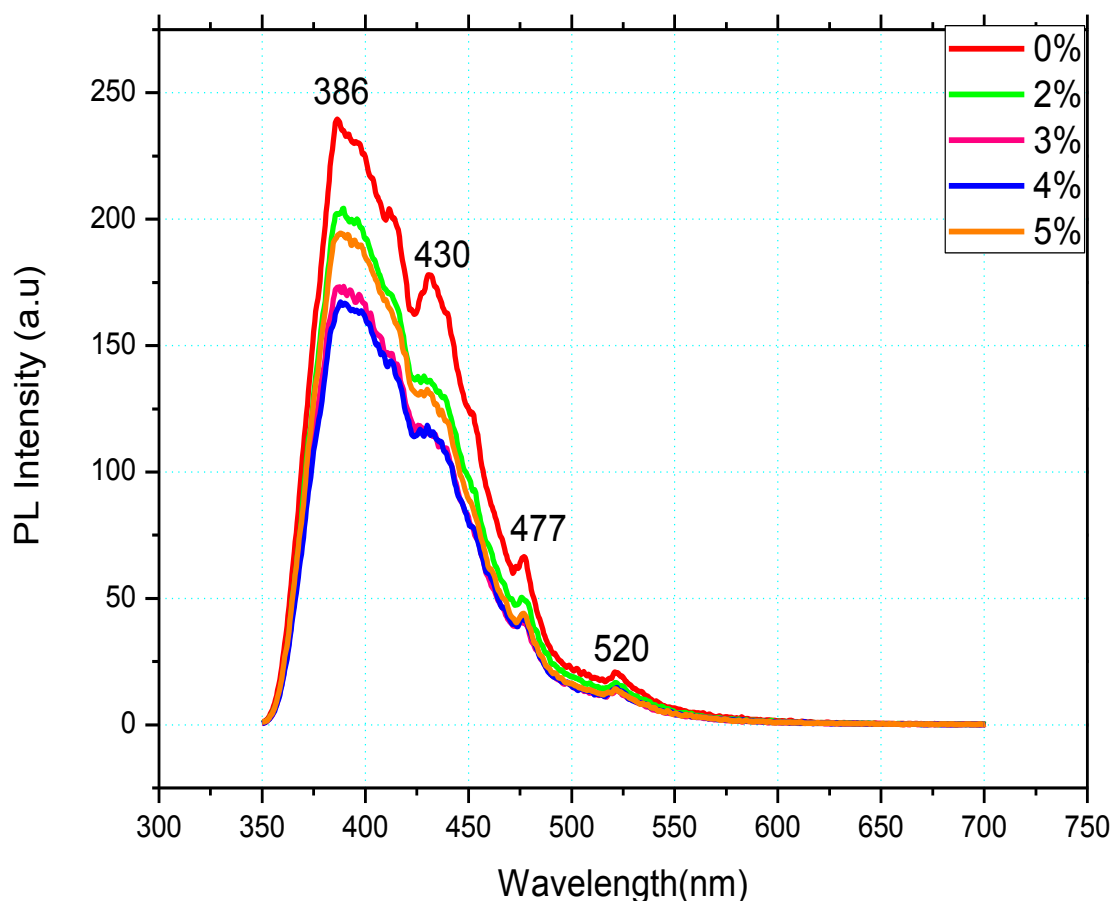


**Fig.VI.10** Photoluminescence spectra of F doped SnO<sub>2</sub> thin films.

All the F-SnO<sub>2</sub> samples in the range 350-550 nm show four emissions bands. The first peak at 386 nm corresponding to the UV emissions band due to oxygen vacancies [81] which forms the donor levels and were the responsible for available electrons in the CB. The second peak positioned at 430 nm corresponding to the violet emissions band. The third low intensity pic centered at 477 nm corresponding to the blue emissions signal that a new defect level presented into the band gap by the F doping [61]. A very low intensity pic at 520 agreeing to the green, which created from the electron-hole recombination at the defect sites due to electron transition from the oxygen vacancy [61]. The decrease in PL intensity with the increasing F doping concentration may

be due to the increase of band gap energy of F-SnO<sub>2</sub> samples or could be attributed to the energy exchange between a pair of F ions [62].

### **VI.2.8 Electrical properties**

The electrical properties are showed using 4-point technique to indicate how F-SnO<sub>2</sub> films are resistive; and the obtained results are showing in Fig.VI.11

Fig.VI.11 shows plot of electrical resistivity ( $\rho$ ) and the conductivity ( $\sigma$ ) as function of F concentration:

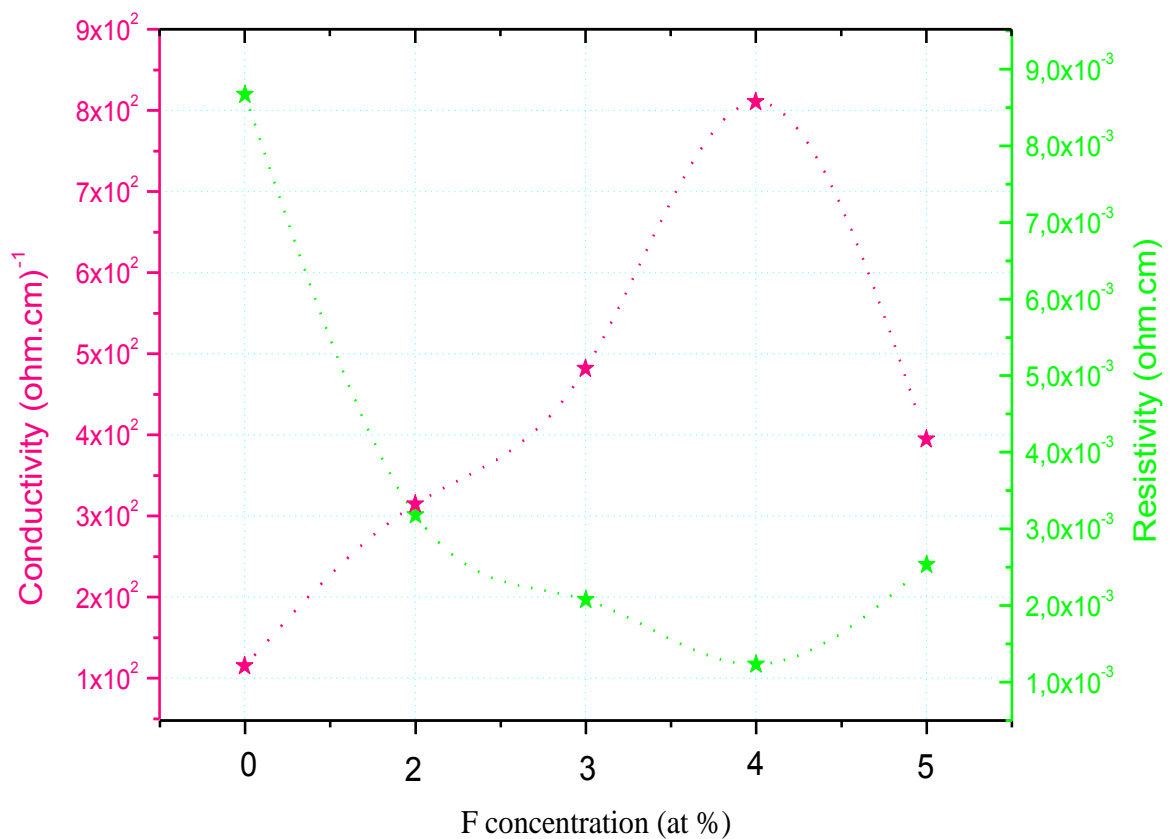


**Fig.VI.11** Variation of conductivity and resistivity of F-SnO<sub>2</sub> with different fluorine doping.

As usual the resistivity variation is opposite to the conductivity, it is found that, the conductivity increase with increasing fluorine concentration and reaches a saturate value  $8.11 \times 10^2$  ( $\Omega.\text{cm}$ )<sup>-1</sup> at 4 %. However, at 5% the conductivity is started decrease. The conductivity increase due to the oxygen vacancies, which caused no stoichiometry in SnO<sub>2</sub> lattice in one hand, and the increase of carrier concentration by the other hand. The increase of the carrier concentration may be due to more free electrons provided by substitution of O<sup>-2</sup> by F<sup>-</sup> ion in the lattice[81].

The fluorine too create donor level below the conduction band (that confirmed by PL technique), allowed an increase in the number of electrons transferred from the donor level to the CB, which caused the increase of the conductivity [82].

### **VI.3. Conclusion**

Major research has been performed on F-SnO<sub>2</sub> thin films prepared by easy and low cost chemical technique, ultrasonic spray at 450 °C. Several characterizations techniques were done to the prepared films such as XRD, UV-visible, PL, 4-point. The Polycrystalline F-SnO<sub>2</sub> films showed strong orientation along (110) at 0, 2 and 3%, which changed to (200) at 4 and 5% when they have higher values of TC<sub>(200)</sub>, that indicate a strong crystallographic texture along these orientations. The best values of figure of merit are seen at 4% reached to  $9.10^{-3}\Omega^{-1}$ .

The F-SnO<sub>2</sub> films revealed the maximum transmittance of 85 % in the visible range and maximum conductivity about  $8.11 \times 10^2 (\Omega\text{-cm})^{-1}$  at 4 %.

Photoluminescence spectroscopy shows UV emission that due to the existence of the oxygen vacancies and the presence of new defect level in the band gap due to the incorporation of the fluorine thus increase the band gap from 3.6 to 3.97eV approximately.



## ***Chapter V:***

# ***Tuning the Opto-electrical properties of SnO<sub>2</sub> thin films by F and Ti Co-doping***

In This chapter we have prepared F-Ti: SnO<sub>2</sub> Co-doping thin films. In order to have both of high transparency and of conductivity, we study how the inclusion of Ti and F to the pure SnO<sub>2</sub> affect the structural, optical and electrical properties.

### **V.1. Experimental methodology**

For depositing SnO<sub>2</sub> with F and Ti Co-doping thin films via easy and low cost spray, we have been prepared using pyrolysis technique, an alcoholic precursor solution consisting of stannic chloride SnCl<sub>4</sub>, dissolving in methanol, which served as a starting solution. The ammonium fluoride (NH<sub>4</sub>F) was added to the starting solution as source of fluorine and the Titanium (IV) isopropoxide (C<sub>12</sub>H<sub>28</sub>O<sub>4</sub>Ti) was added as source of titanium. F and Ti Co-doping SnO<sub>2</sub> films were done at different F concentration varied from 2 to 6 at% when Ti fixed at 5 at% (F-Ti: SnO<sub>2</sub>) onto glass substrate. Then they were done at different Ti concentration varied from 2 to 6 at% too when F fixed at 4 % (Ti-F: SnO<sub>2</sub>) in order to compare between their properties and explore the best F and Ti Co- doping characteristics. The other deposition parameters are fixed as follow:

**Table V.1.** The fixed parameters used at the deposition processes

Parameter	temperature	Deposition time	concentration	Nozzle-substrate	Ultrasonic wave
The values	450 °C	5 min	0.1 M	5 cm	40 %

### **V.2 Results and discussion**

As habitual, before doing any characterization we applied the Stick tape test on the deposited films. The test clearly indicated that the adhesion strength of the F-Ti: SnO<sub>2</sub> films considered being “good”.

#### **V.2.1 Growth Velocity**

Thickness of F and Ti Co-doped SnO<sub>2</sub> samples prepared at different F and Ti doping were calculated using both of interference fringes method and gravimetric method to confirm the real results and a same variation, the calculated results obtained showing in the following table:

**Table V.2** thickness values of SnO<sub>2</sub> prepared at different fluorine and Titanium Co- doping:

F %	2F5T	3F5T	4F5T	5F5T	6F5T
<b>F-Ti: SnO<sub>2</sub> thickness (nm)</b>	<b>553.94</b>	<b>608.06</b>	<b>627.8</b>	<b>985.77</b>	<b>992.38</b>
Ti %	2T4F	3T4F	4T4F	5T4F	6T4F
<b>Ti-F: SnO<sub>2</sub> thickness (nm)</b>	<b>1167.28</b>	<b>800</b>	<b>787</b>	<b>627.8</b>	<b>555.36</b>

Using these results, we plot the variation of the thickness as function of fluorine and Titanium Co-doping, which is represented in the Fig V.1:

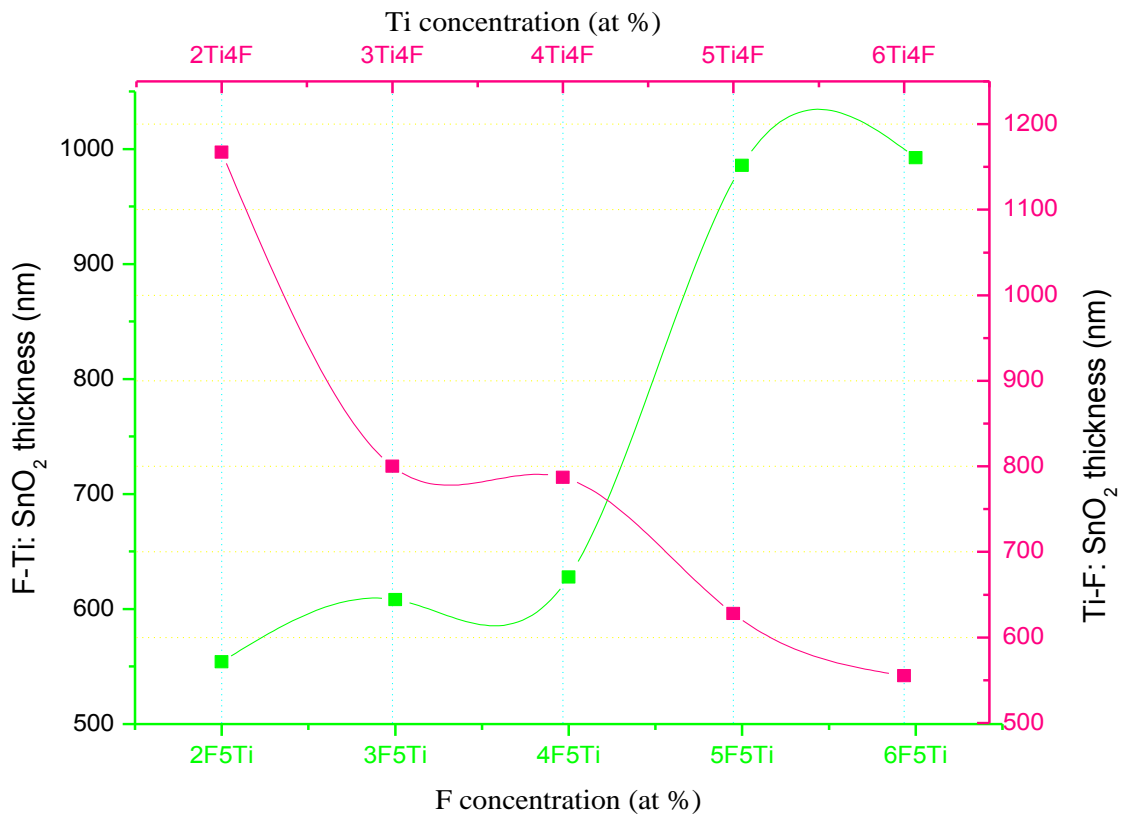
**Fig.V.1.** F-Ti: SnO<sub>2</sub> and Ti-F: SnO<sub>2</sub> films thicknesses at different F and Ti Co-doping.

Fig.V.1 shows proportion between increasing in thickness as increasing F concentration uniformly however; it is decrease with increase of Ti so, we have the same variation of previous studies when thickness decrease with Ti-SnO<sub>2</sub> and increase with F-SnO<sub>2</sub>.

At F-Ti: SnO<sub>2</sub> films, with the increase in solution amount, the fluorine atoms will take oxygen vacancies and Ti will take interstitial sites, by way of fluorine size is large; thereby enhancement quantity of F atoms caused an increase in thickness. However, at Ti-F: SnO<sub>2</sub> films with the increase in solution amount the fluorine atoms take the oxygen vacancies or substitution sites of O so with augmentation of the titanium quantity; they occupy substitution sites of Sn, and as the rayon of Ti is smaller than Sn, the size of the mesh parameter decreases and consequently the thickness decreases too.

### **V.2.2 Scanning Electron Microscopy**

The scanning electron microscopy facilitate to observe the surface topography of bulk samples by sweeping these surfaces, the films are studied by using Zeiss-SMT LEO 1540 XB scanning electron microscopy (SEM) at Hungarian Academy of Sciences, Centre for Energy Research.

Fig.V.2 shows the surface morphology of spray deposited F-Ti: SnO<sub>2</sub> thin films at various F and Ti concentrations:

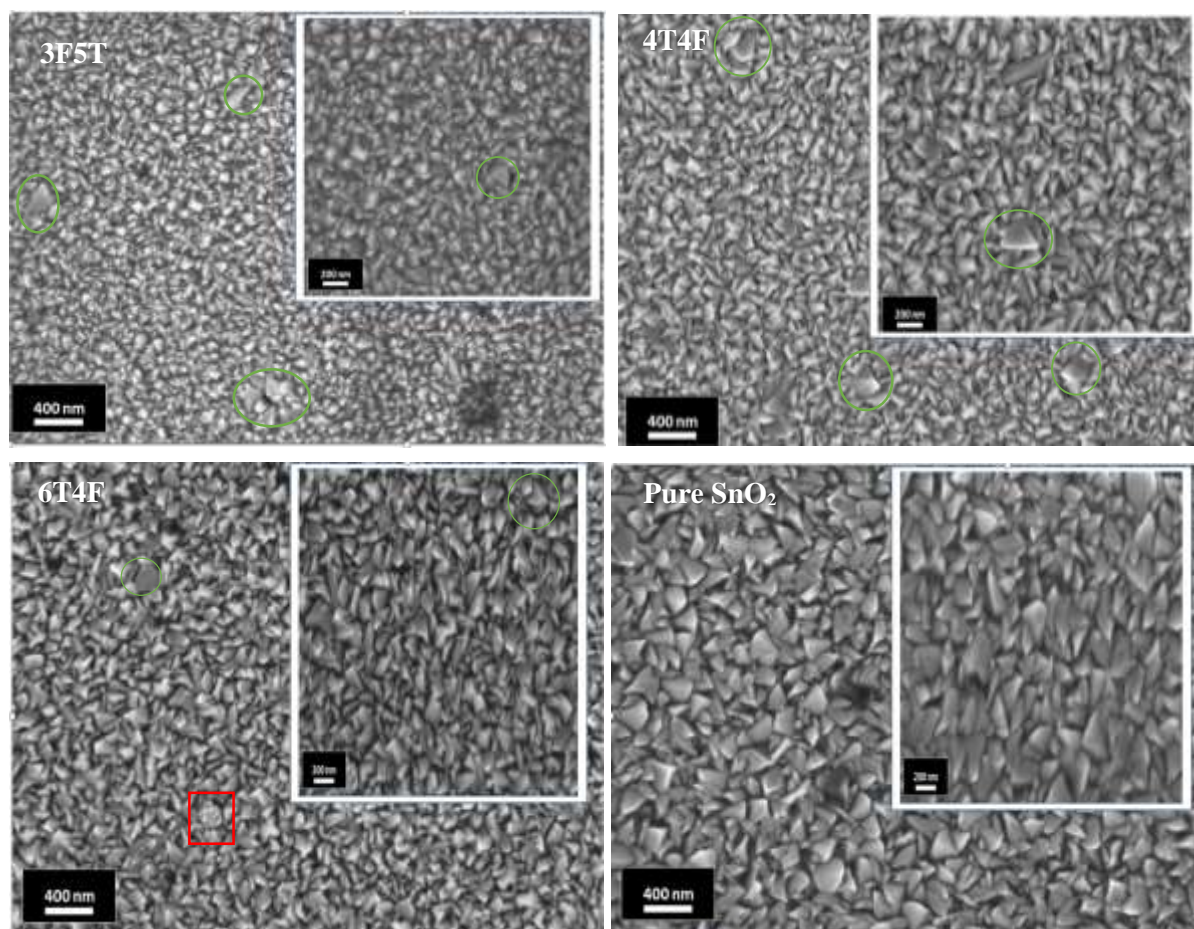


**Fig V.2.** Scanning electron micrographs of nanocrystalline F-Ti: SnO<sub>2</sub> samples at different F and Ti Co-doping.

It is clear in the SEM image that the Co-doping films are better than the pure .they are uniform, smooth without cracks and with big homogeneity. The pure SnO<sub>2</sub> film has grains with different sizes whereas intergranular region appears dark. In addition, the grains are randomly distributed with some porosity and roughness surface which giving rise to a scattering effect, thereby reducing transmittance to 70% in visible region with low electrical conductivity about  $1.10^2 (\Omega.cm)^{-1}$  (in the previous chapter). The red square is a grain of titanium, when the green circles show grains bigger than the others grain, due to the fluorine doped atoms.

3F5T presents some homogeneity with different size of grains that caused roughness in the surface and make the transmittance 78% in the visible region with  $7.10^2 (\Omega.cm)^{-1}$  electrical conductivity.

4T4F, this sample with the same concentration of Ti and F have big homogenous than the pure SnO<sub>2</sub> with smaller grains sizes. In addition, the surface seem smooth which giving rise to increase the transmittance to 80% in the visible region with high electrical conductivity about  $7.7.10^2 (\Omega.cm)^{-1}$ .

6T4F shows homogeneous surface with some different size of grains that caused roughness in the surface giving rise to the scattering of light which affect the transmittance and make it 70% in the visible. However, this sample and those conditions make 6T4F have the highest electrical conductivity  $10.10^2 (\Omega.cm)^{-1}$  approximately.

### V.2.3 Structural Characteristics

The crystal structure was determined by XRD of spray deposited SnO<sub>2</sub> and F-Ti: SnO<sub>2</sub> Co-doping thin films with different fluorine and titanium Co-doping concentration shown in Fig.V.3:

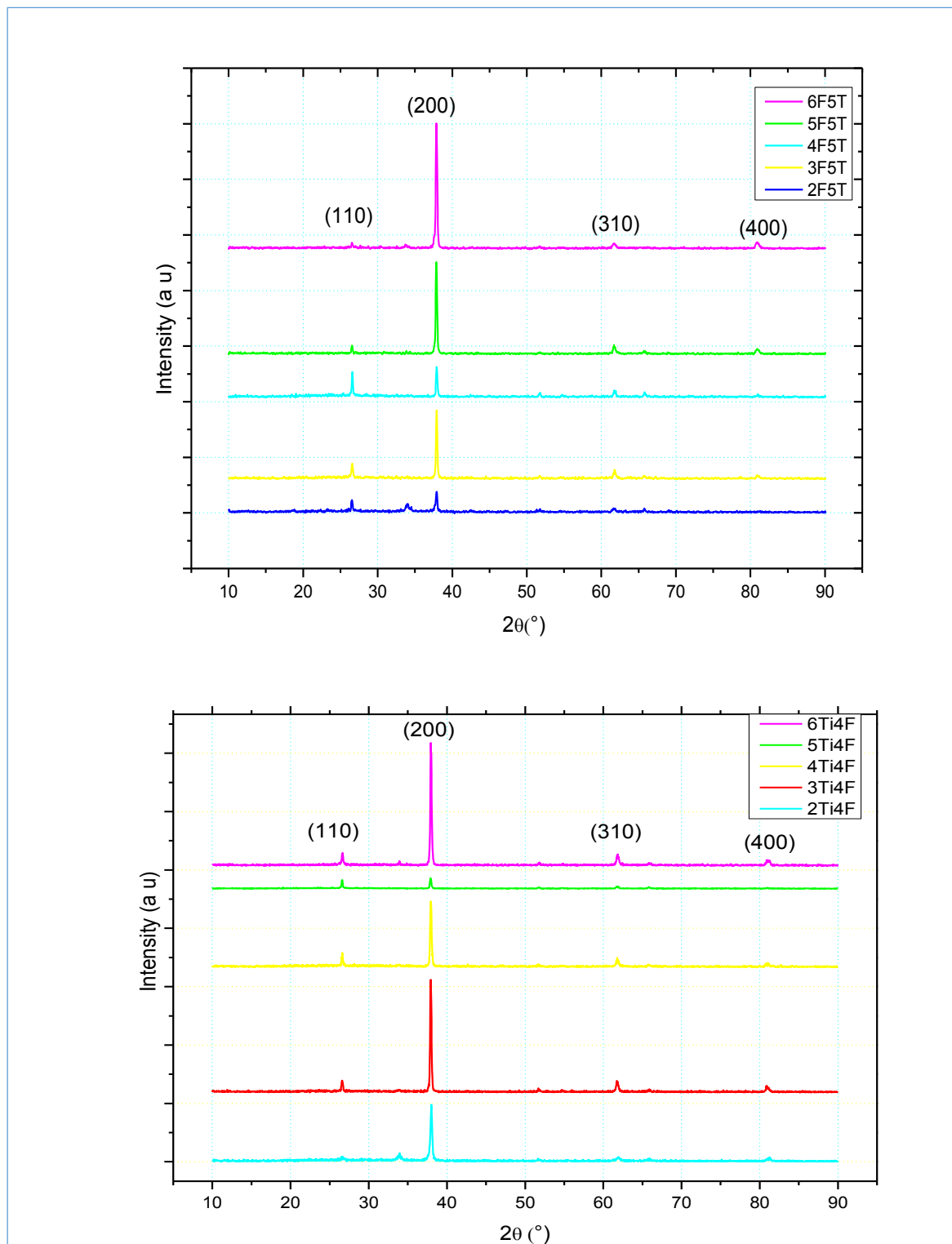


Fig.V.3 F-Ti: SnO<sub>2</sub> and Ti-F: SnO<sub>2</sub> films XRD at different F and Ti Co-doping.

The results clearly indicate that with the increasing of fluorine and titanium Co-doping concentration the tetragonal Rutile structure remains the same and polycrystalline nature.

The major peaks located approximately at 26°, 38°, 61° and 80° corresponding to (110), (200), (310) and (400) diffraction planes respectively. More that, there is no diffraction peaks of any other impurity phases are detected in the prepared samples such as SnO or Sn phases observed, showing that the films were completely oxidized. A strong (200) orientation is observed at F-Ti: SnO<sub>2</sub> and Ti-F: SnO<sub>2</sub>, which indicate that the films have a strong crystallographic texture along (200) where the formation energy was lower. Usually in the literature, we find that (200) and (110) orientations are the preferred one[42] [83] because they has strong texture that confirmed in the previous chapter by TC.

The inserting of fluorine and titanium does not affect the structural properties of the films, however, the increase in the intensities of the main XRD peaks with increasing doping levels, is probably attributed to the change in the growth rate. In general, the intensity of the diffraction peaks increase greatly with the increase of doping concentration, indicating acquire of crystallinity and the lattice is not distortion [84].

### V.2.4 Crystallite Size

Generally, the average crystallites size were evaluated from XRD results according to Scherrer formula.

The results of the crystallite size *D* of Co-doping SnO<sub>2</sub> as a function of F and Ti concentrations is presenting in the Fig.V.4:

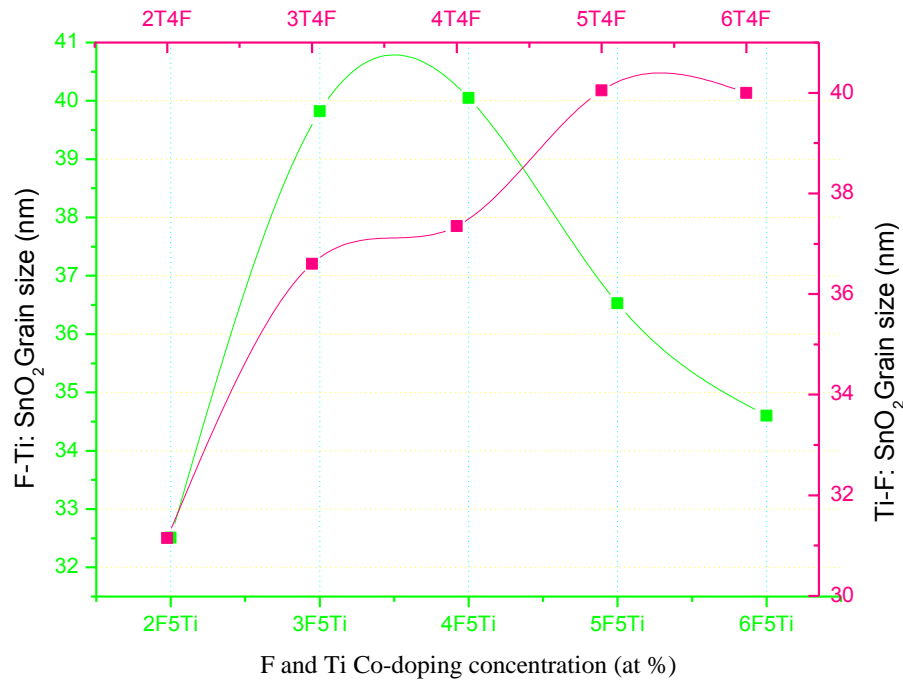


**Fig.V.4** Variation of crystallite size of F-Ti:SnO<sub>2</sub> at different F and Ti Co-doping.

The figure shows that in Ti-F:SnO<sub>2</sub> the increase with doping when in the previous study of Ti-SnO<sub>2</sub> it was decrease however, the orientation (200) remain the same, which indicate that the crystallization improve with Co-doping Ti-F:SnO<sub>2</sub>. The increase of the indicate the good crystallization without defects and less dislocation. More that, the injection of F by their big size atoms is a part that affect in the increase of crystal size.

The same thing happened with F-Ti: SnO<sub>2</sub>, we have one fixed preferred orientation (200) when the previous study of F-SnO<sub>2</sub> changed from (110) to (200), also the XRD results confirm that F-Ti: SnO<sub>2</sub> have crystallization better then F-SnO<sub>2</sub>. The increase of crystal size with increase of doping probably due to the increasing in fluorine atoms arriving to the substrate, which have big atomic rayon, thereby causing an increase in the nucleation numbers that combine together to form larger grains thereby the electron mobility should be increase. The decrease of is due to the augmentation of dislocation density or the incorporation of F ions into the SnO<sub>2</sub> lattice, which take

interstitial sites then pressed there in the lattice. In addition, the smaller increases the specific surface area [85], that is needed in the photo catalytic applications.

### **V.2.5 The transmittance**

The transmittance spectra obtained by UV-visible spectroscopy as function of wavelength over spectral range 350-1100 nm are showing in Fig.V.5:

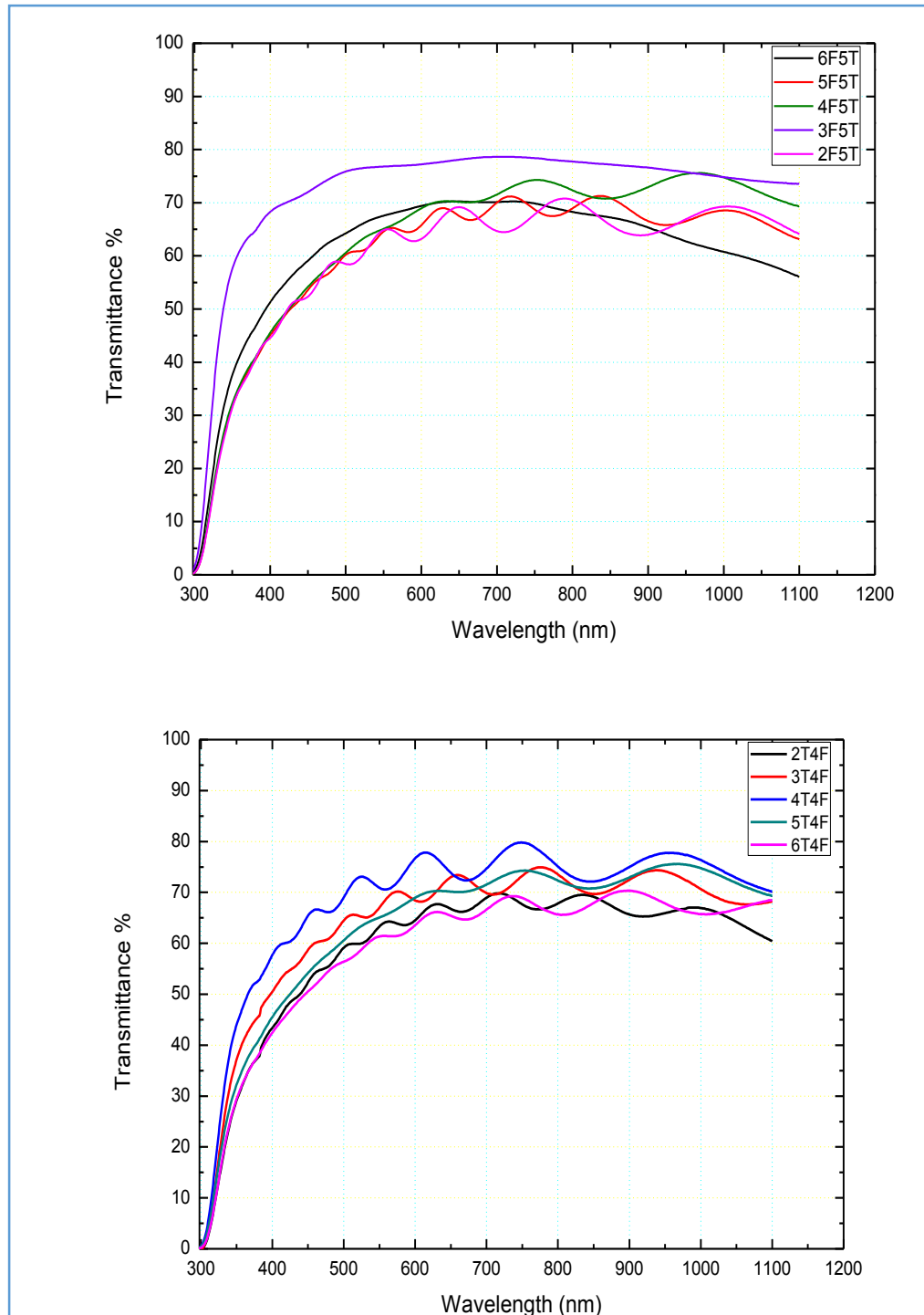


**Fig.V.5** Optical transmittance spectra of F-Ti: SnO<sub>2</sub> thin films at different F and Ti Co-doping.

With an overview, the Fig.V.5 shows highest transmittance is about 80% at 3F5Ti with F-Ti: SnO<sub>2</sub> and it is 80% too at 4Ti4F with Ti-F: SnO<sub>2</sub> however, the first was without fringes when the second was full of fringes. Which, indicate that 4% is very smooth than 3% that rough so, we can say that Ti-F: SnO<sub>2</sub> films are very smooth than F-Ti:SnO<sub>2</sub> due to the appearance of fringes with all its samples [86].

The increase of dopant in F-Ti: SnO<sub>2</sub> make a decrease of fringes consequently the films were roughness that is probably due to the crystal defects thus giving rise to the scattering effect however, Ti - F: SnO<sub>2</sub> represents big homogenous with their smooth surfaces specially 4Ti4F.

### V.2.5.1 Figure of Merit

The calculation of figure of merit is in order to evaluate the efficiency of F-Ti: SnO<sub>2</sub> Co-doping films, then when they present the best condition for their applications as window and collector in solar cells.

Fig.V.6 represents the variation of figure of merit as function of wavelength at different F and Ti Co-doping:

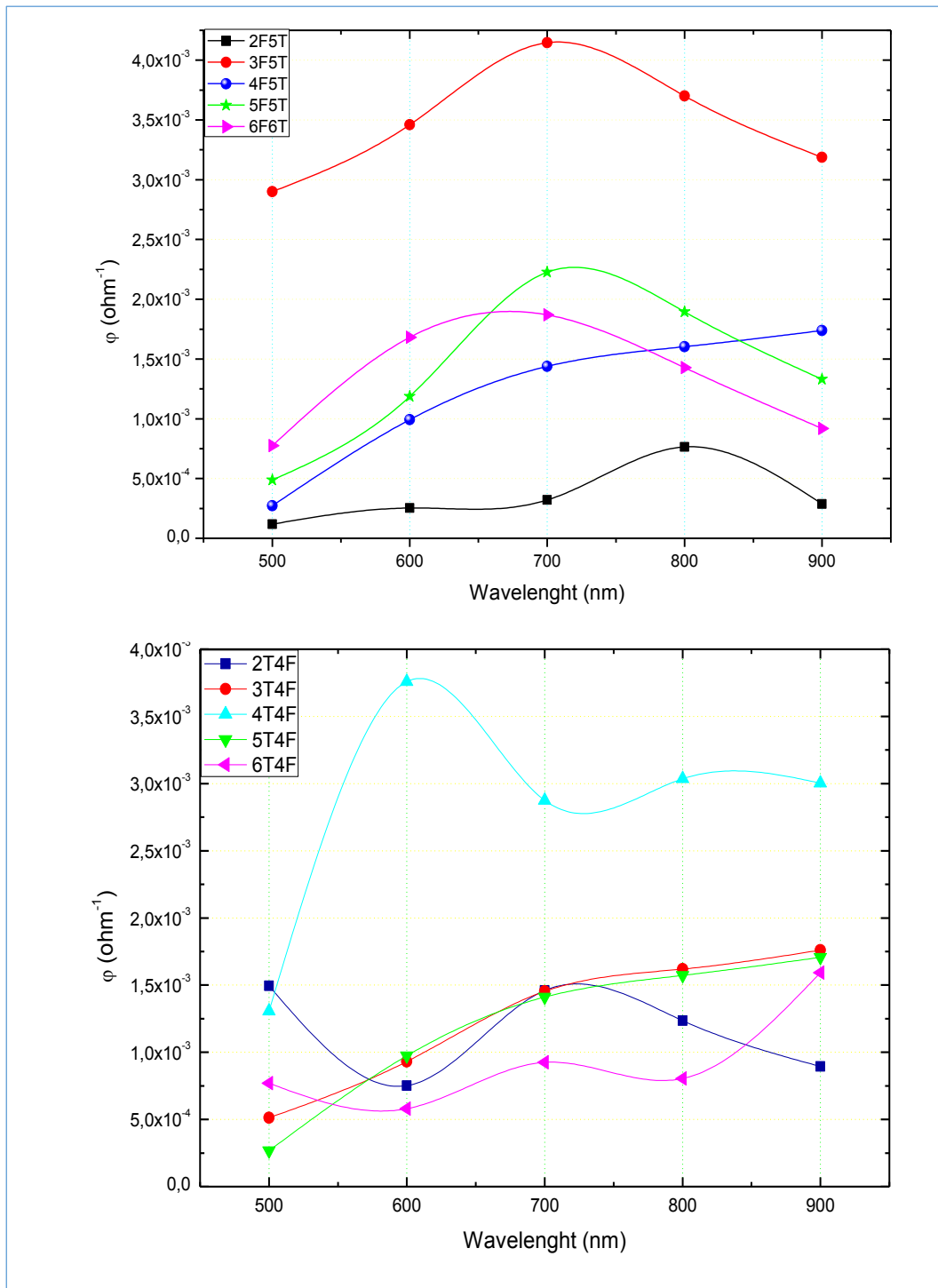


**Fig.V.6** Figure of merit values of F-Ti:-SnO<sub>2</sub> at different F and Ti Co- doping.

It is clear in Fig.V.6 that the augmentation in figure of merit values in the visible region was well observed when the F and Ti doping increase as well and the best values are 3F5Ti reached  $4.10^{-3} \Omega$  at 700 nm wavelength and 4T4F reached  $3.7.10^{-3} \Omega$  at 600 nm wavelength.

### V.2.5.2 Band Gap Energy

The optical band gap energy  $E_g$  was calculated according to Tauc's formula. The plot of  $(\alpha h\nu)^2$  as function of  $h\nu$  illustrated in the Fig.V.7. when the obtainable values of the band Gap  $E_g$  as function of F-Ti: Co-doping are showing in Fig.V.8:

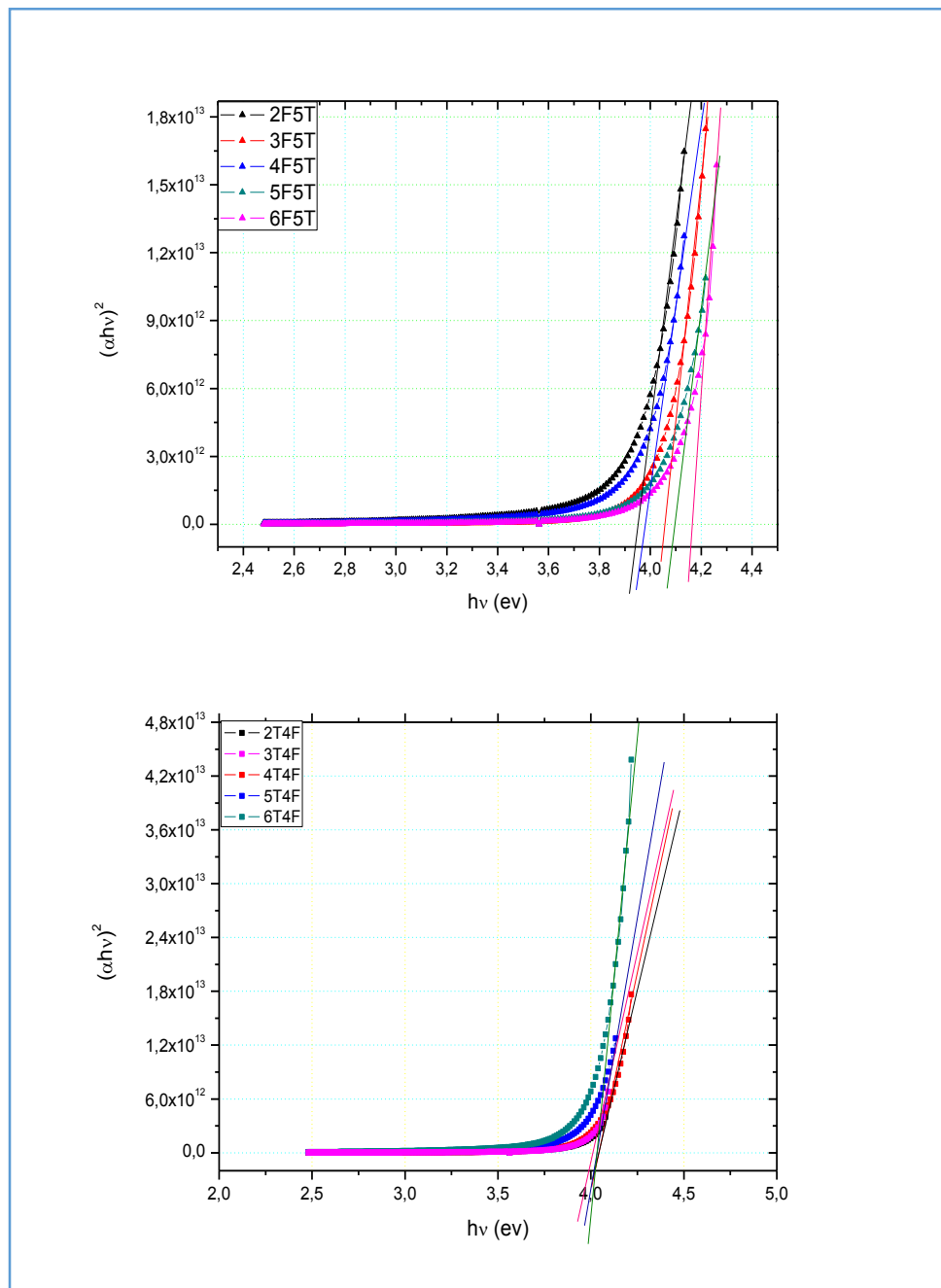


**Fig.V.7** optical band gap determination of F-Ti:SnO<sub>2</sub> with different F and Ti Co-doping concentrations.

The figure above shows that the band gap variation of Ti-F: SnO<sub>2</sub> seem constant approximately at 4 eV like that with Ti: SnO<sub>2</sub> films in the previous study (third chapter). When the F-Ti: SnO<sub>2</sub> presents noteworthy increase so, we summarize and plot the E<sub>g</sub> values variation of F-Ti: SnO<sub>2</sub> as function of the fluorine and titanium tin dioxide doping concentration in the following figure:

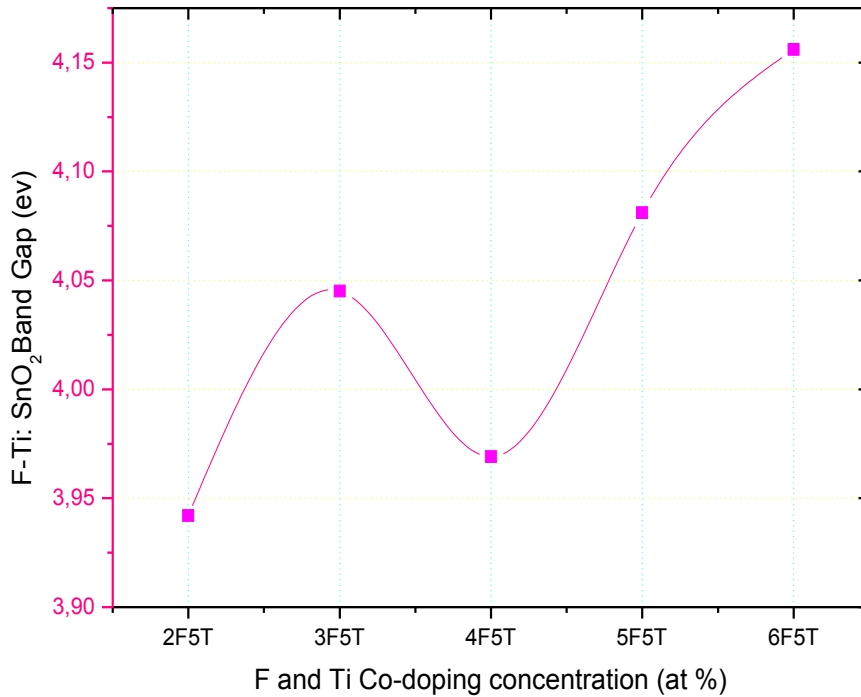


**Fig.V.8** optical band gap variation as function of F-Ti Co-doping SnO<sub>2</sub>.

The Ti-F: SnO<sub>2</sub> shows high optical band gap, approximately 4 eV due to the small atoms of Ti; as the lattice constant decrease the interatomic distance will be reduced thus the band gap increase and will be high [87]. However, with F-Ti: SnO<sub>2</sub> the band gap increase that related with defect level created by the F atoms level, which located in the conductive band in the lattice[88].

The carrier concentration is due to the high doping levels, fills blank states belonging to CB of the thin films so increasing the energy magnitude necessary for the valence band to conduction band transitions [78] [89].

### V.2.6 Photoluminescence

Used photoluminescence (PL) spectroscopy technique for investigating the structure, defect, impurity levels and quality of thin films. Fig.V.9 represents the photoluminescence spectra of F-Ti:SnO<sub>2</sub> with different F and Ti Co- doping:

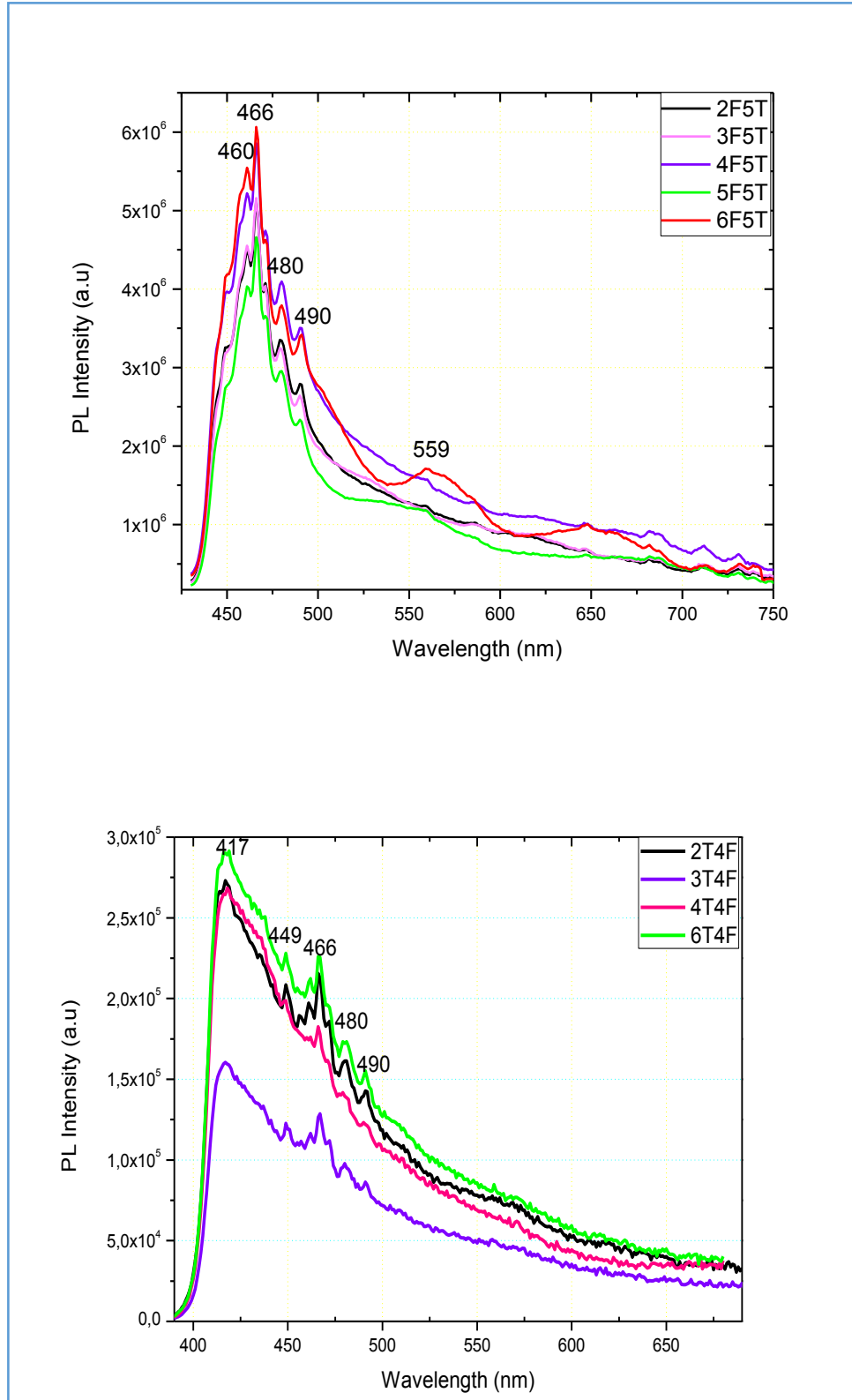


**Fig.V.9** Photoluminescence spectra of F-Ti doped SnO<sub>2</sub> thin films at different doping.

All the F-Ti: SnO<sub>2</sub> samples show emissions bands in the range 450-560 nm. The UV emissions band is absent here, that confirm nonexistence of oxygen vacancies. The peaks positioned at 460, 466, 480, 490 nm are corresponding to the blue emissions signal that a new defect level presented into the band gap by the F and Ti doping [61].

A very low intensity pic at 559 agreeing to the green, which created from the electron-hole recombination at the defect sites [61].

The Ti-F: SnO<sub>2</sub> samples show emissions bands in the range 417-490 nm. The UV emissions band is absent too. The first peak located at 417 corresponding to the violet emissions band, the other peaks are positioned at 449, 466, 480, 490 nm corresponding to the blue emissions signal too that a new defect level presented into the band gap by the Ti and F doping.

### V.2.7 Electrical properties

The electrical properties are showing using 4-point technique to indicate how F-SnO<sub>2</sub> films are resistive; and the obtained results are showing in Fig.V.10.

Fig.V.10 represents a plot of electrical conductivity ( $\sigma$ ) of SnO<sub>2</sub> thin films as function of F and Ti Co-doping concentrations:

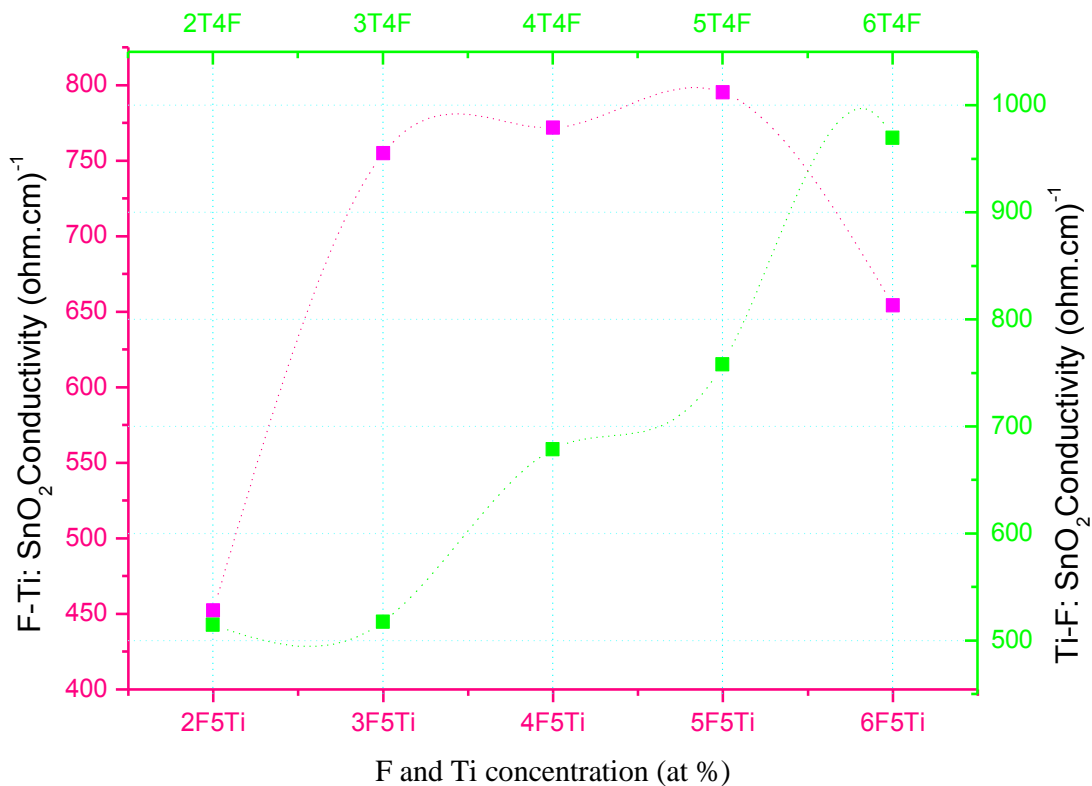


**Fig.V.10** Conductivity variation of F-Ti:-SnO<sub>2</sub> with different F and Ti Co- doping.

It is clear that the electrical conductivity increase with both of F-Ti: SnO<sub>2</sub> and Ti-F: SnO<sub>2</sub>; Jian Tao Wang found that the preferred orientation (200) enhance the carrier concentration thus the conductivity [83]. More that the high crystallization and the increase of crystal size too take responsible for that increase.

In addition, the incorporation of F increase the conductivity, especially with F-Ti: SnO<sub>2</sub> because the F create donor level in the CB, so increase the free electrons thus increase conductivity.

### **V.3. Conclusion**

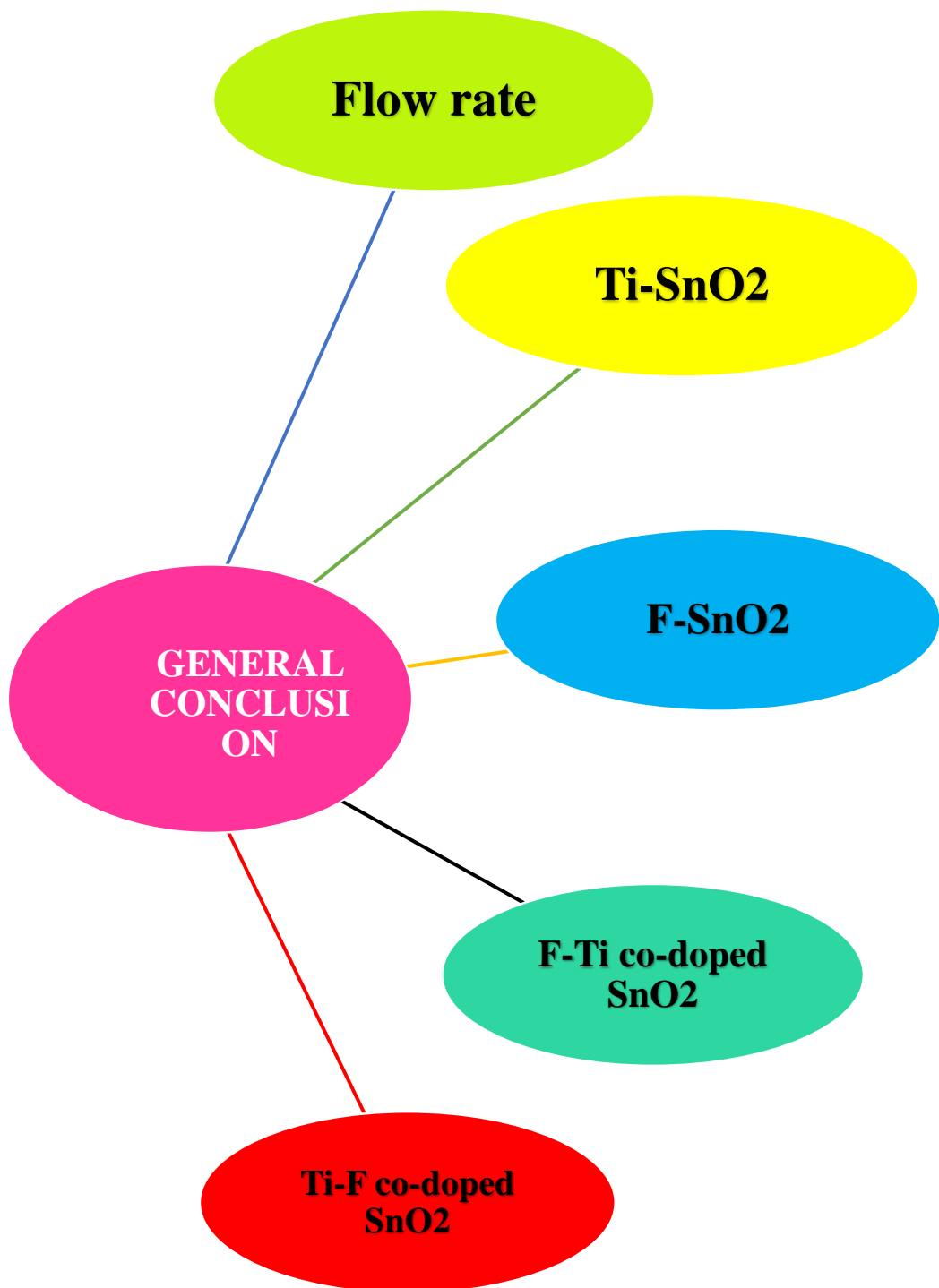
Major research has been performed on on F-Ti:SnO<sub>2</sub> thin films prepared by easy and low cost chemical technique, ultrasonic spray at 450 °C. Several characterizations techniques were done to the prepared films such as XRD, SEM, UV-visible, PL, 4-point.

The Polycrystalline F-Ti: SnO<sub>2</sub> films showed strong orientation along (200) that indicate a strong crystallographic texture along these orientations. Figure of merit represent the best values are 3F5Ti reached  $4.10^{-3} \Omega$  at 700 nm wavelength and 4T4F reached  $3.7.10^{-3} \Omega$  at 600 nm wavelength.

The F-Ti: SnO<sub>2</sub> and Ti-F: SnO<sub>2</sub> films both revealed the maximum transmittance of 80 % in the visible range when the first represents maximum conductivity about  $7.2 \times 10^2 (\Omega\text{-cm})^{-1}$  at 5F5T and the second presents  $9.69 \times 10^2 (\Omega\text{-cm})^{-1}$  at 6T4F.

The 6Ti4F sample shows high conductivity, good crystallization and the most important high transparency with less thickness so that make it the best one approximately.

Photoluminescence spectroscopy shows that UV emissions band is absent that confirm nonexistence of oxygen when the presence of blue emissions signal that a new defect level presented into the band gap by the F and Ti doping.



# General Conclusion



Major researches have done on the SnO<sub>2</sub> thin films deposited by easy and low cost chemical technique, ultrasonic spray to have high quality of thin films such as both of high transmittance and high conductivity.

The effect of solution flow rate, represent poly crystalline tetragonal structure, with favorable growth direction (110) and between 10–12.6 nm. The films subjected to compressive stresses which caused deformation of the mesh parameter *a*. While UV–vis results showed that a transmittance decrease when the flow rate increase in the visible area from 80% to 50% approximately with 45.90 (Ω·cm)<sup>-1</sup> electrical conductivity at 100 ml/h. The film thickness increase from 510 to 1066.5 nm. We found that our films have direct energy band gap between 3.72 eV for 3.83 eV.

The pure SnO<sub>2</sub> film had grains with different sizes. In addition, the grains are randomly distributed with some porosity and roughness surface which giving rise to a scattering effect, thereby reducing transmittance to 70% in visible region with low electrical conductivity about 10<sup>2</sup> (Ω·cm)<sup>-1</sup>

The Ti-SnO<sub>2</sub> films show Polycrystalline structure with strong orientation along (200) which confirm the highest texture along these orientations. The best values in figure of merit are seen at 4 at% reached to 7, 64.10<sup>-3</sup>Ω<sup>-1</sup> at 800 wavelength. The Photoluminescence spectroscopy confirm that we have UV emission, which due to the existence of the oxygen vacancies in one hand, and the presence of new defect level in the band gap due to the incorporation of the titanium. Few changes were noted in the optical band gap between 3.91-3.97 eV that seem constant approximately. The Ti-SnO<sub>2</sub> films revealed the maximum transmittance up to 84% in the visible region with maximum conductivity about 1.4 × 10<sup>2</sup> (Ω·cm)<sup>-1</sup> at 5 at %.

The F-SnO<sub>2</sub> thin represented Polycrystalline structure with strong orientation along (110) at 0, 2 and 3 at%, which has been found change to (200) at 4 and 5% when they have higher values of TC<sub>(200)</sub>, that indicate a strong crystallographic texture along these orientations. The best values in figure of merit are seen at 4% reached to 9.10<sup>-3</sup>Ω<sup>-1</sup>. The F-SnO<sub>2</sub> films revealed the maximum transmittance of 85 % in the visible range and maximum conductivity about 8.11 × 10<sup>2</sup> (Ω·cm)<sup>-1</sup> at 4 %. Photoluminescence spectroscopy shows UV emission that due to the existence of the oxygen

vacancies and the presence of new defect level in the band gap due to the incorporation of the fluorine thus increase the band gap from 3.6 to 3.97eV approximately.

After these studies, we decided to take the best values of each one above to prepare the F-Ti: SnO<sub>2</sub> Co-doping thin films at different F concentrations varied from 2 to 6 at% when Ti fixed at 5 at% (F-Ti: SnO<sub>2</sub>) onto glass substrate. Then they were done at different Ti concentration varied from 2 to 6 at% too when F fixed at 4 at% (Ti-F: SnO<sub>2</sub>) in order to compare between their properties and explore the best F and Ti Co- doping values. Several characterizations techniques represent Polycrystalline structure with strong orientation along (200) that indicate a strong crystallographic texture along these orientations. Figure of merit represent the best values are 3F5Ti reached  $4.10^{-3} \Omega$  at 700 nm wavelength and 4T4F reached  $3.7.10^{-3} \Omega$  at 600 nm wavelength.

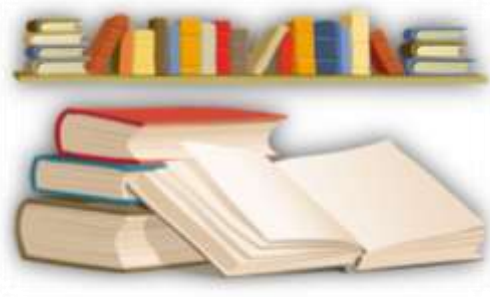
The F-Ti: SnO<sub>2</sub> and Ti-F: SnO<sub>2</sub> films both revealed the maximum transmittance of 80 % in the visible range when the first presents maximum conductivity about  $7.2 \times 10^2 (\Omega\text{-cm})^{-1}$  at 5F5T and the second presents  $9.69 \times 10^2 (\Omega\text{-cm})^{-1}$  at 6T4F.

Photoluminescence spectroscopy shows that UV emissions band is absent that confirm nonexistence of oxygen vacancies when the presence of blue emissions signal that a new defect level presented into the band gap by the F and Ti doping.

In SEM characterization of the samples the 3F5T represents some homogeneity with different size of grains that caused roughness in the surface and reduce the transmittance however, 4T4F have big homogenous than pure SnO<sub>2</sub> with smaller grains sizes. In addition, the surface seem smooth which giving rise to increase the transmittance. More that 6T4F show homogeneity with some different size of grains that affect the surface when it had the scattering effect and that reduce the transmittance to 70% in the visible with highest electrical conductivity  $10.10^2 (\Omega\text{-cm})^{-1}$  approximately.

Generally, we can see that dopant enhance the properties of the pure tin dioxide thin films such as transmittance and the conductivity; however, the Co-doping seem better than dopant because it improve transmittance, conductivity and the structure.

Finally, we can say that both of F: SnO<sub>2</sub>, Ti: SnO<sub>2</sub> doping and F-Ti: SnO<sub>2</sub> Co- doping are good candidate for optoelectronic, solar cells and gas sensor applications due to their high transmittance and conductivity, specially F: SnO<sub>2</sub>, which have the highest transmittance and 6T4F that have the highest conductivity with lowest thickness.



# Bibliography

- [1] H. Bendjedidi; A. Attaf, H. Saidi, M. S. Aida, S. Semmari, A. Bouhdjar, “Properties of n-Type SnO<sub>2</sub> semiconductor prepared by spray ultrasonic technique for photovoltaic applications,” *J. Semicond.*, vol. 36, no. 12, p. 123002, 2015.
- [2] N. Lehraki, M. S. Aida, S. Abed, N. Attaf, A. Attaf, and M. Poulain, “ZnO thin films deposition by spray pyrolysis: Influence of precursor solution properties,” *Curr. Appl. Phys.*, vol. 12, no. 5, pp. 1283–1287, 2012.
- [3] I. Saaddedin, “Preparation and characterization of new transparent conducting oxides based on SnO<sub>2</sub> and In<sub>2</sub>O<sub>3</sub> ceramics and thin films,” Bordeaux I University, 2007.
- [4] J. E. Medvedeva and a. J. Freeman, “Combining high conductivity with complete optical transparency: A band-structure approach,” *Europhys. Lett.*, vol. 69, no. 4, p. 3, 2004.
- [5] B. Palmer, “Phase relations, transparency and conductivity in Ga<sub>2</sub>O<sub>3</sub>-SnO<sub>2</sub>-ZnO,” *Solid State Sci.*, vol. 4, no. 3, pp. 317–322, 2002.
- [6] Y. T. K. Miyake, H. Kaneko, “Electrical and optical properties of reactively sputtered tungsten oxide films,” *Electrochem. Soc.*, vol. 127, no. 4, p. 918, 1980.
- [7] H. Dixit, “First-principles electronic structure calculations of transparent conducting oxide materials,” UNIVERSITEIT ANTWERPEN, 2012.
- [8] X. T. Yin and X. M. Guo, “Selectivity and sensitivity of Pd-loaded and Fe-doped SnO<sub>2</sub> sensor for CO detection,” *Sensors Actuators, B Chem.*, vol. 200, pp. 213–218, 2014.
- [9] G. M. Stoian, “physical properties of magnetic as grown and oxygen annealed SnO<sub>2</sub>: CO thin films,” Florida State University, 2013.
- [10] M. Farida, “Préparation et caractérisation de couches minces d’oxyde de titane(TiO<sub>2</sub>) et du couple d’oxydes (TiO<sub>2</sub>/SnO<sub>2</sub>),” UNIVERSITE MENTOURI CONSTANTINE, 2012.
- [11] K. Rao, “Studies on Tin Oxide Films Prepared By Electron Beam Evaporation and Spray Pyrolysis Methods,” *Bull. Mater. Sci.*, vol. 27, no. 3, pp. 295–301, 2004.
- [12] R. Udayakumar, V. Khanaa, and T. Saravanan, “Synthesis and Structural Characterization of Thin Films of SnO<sub>2</sub> Prepared by Spray Pyrolysis Technique,” *Sci. Technol. Suppl.*, vol. 1, no. 7, pp. 666–669, 2013.
- [13] A. Höling, L. Hultman, M. Odén, J. Sjöln, and L. Karlsson, “Mechanical properties and

- machining performance of Ti<sub>1-x</sub>Al<sub>x</sub>N-coated cutting tools,” *Surf. Coatings Technol.*, vol. 191, no. 2–3, pp. 384–392, 2005.
- [14] D. Magnfält, “Nucleation and stress generation in thin films deposited with a pulsed energetic deposition flux,” Linköping University, Sweden, 2013.
- [15] M. Henini and K. Seshan, *Handbook of thin-film deposition processes and techniques*, vol. 31, no. 3. 2002.
- [16] D. I. Materia, B. Politechniki, and P. Poig, “PVD and CVD Technologies For Surface Processing Of Engineering Materials,” Silesian University of Technology, 2012.
- [17] G. K. Wolf, K. Zucholi, M. Barth, and W. Ensinger, “Equipment for ion beam assisted deposition,” *Nucl. Instruments Methods Phys. Res. Sect. B Beam Interact. with Mater. Atoms*, vol. 21, no. 1–4, pp. 570–573, Jan. 1987.
- [18] R. W. and S. M. A Botman, J J L Mulders, “Purification of platinum and gold structures after electron-beam-induced deposition,” *Nanotechnology*, vol. 17, no. 15, 2006.
- [19] K. M. and M. O. Katsuhiko Yokota, Kazuhiro Nakamura, Tomohiko Kasuya, “Resistivities of titanium nitride films prepared onto silicon by an ion beam assisted deposition method,” *J. Phys. D. Appl. Phys.*, vol. 37, no. 7, 2004.
- [20] J. E. Mellor and Accepted, “Investigation of a Sol-Gel Coating Technique for Polarized 3 He Target Cells,” College of William and Mary in Virginia, 2001.
- [21] K. BEDI, S. MISHRA “Alcohol sensing of tin oxide thin film prepared by sol–gel process,” *thin Film.*, vol. 25, no. 3, pp. 231–234, 2002.
- [22] R. S. Sonawane, S. G. Hegde, and M. K. Dongare, “Preparation of titanium(IV) oxide thin film photocatalyst by sol-gel dip coating,” *Mater. Chem. Phys.*, vol. 77, no. 3, pp. 744–750, 2003.
- [23] D. Perednis and L. J. Gauckler, “Thin Film Deposition Using Spray Pyrolysis,” *Electroceramics*, vol. 14, pp. 103–111, 2005.
- [24] L. Madler, “Liquid-Fed Aerosol Reactors for One-Step Synthesis of Nano-Structured Particles,” *Kona*, vol. 22, pp. 107–20, 2004.
- [25] H. A. Hamedani, “Investigation of Deposition Parameters in Ultrasonic Spray Pyrolysis For Fabrication Of Solid Oxide Fuel Cell Cathodes,” Georgia Institute Of Technology, 2008.
- [26] S. Kaneko, “Spray Pyrolysis Deposition for Thin Film Formation and Its Application to DSC Study,” in *24th EU PVSEC, Hamburug*, 2009, pp. 432–8003.
- [27] C. J. Humphreysa, “The significance of Bragg’s law in electron diffraction and microscopy, and Bragg’s second law,” *Acta Crystallogr. Sect. A*, vol. 69, no. 1, pp. 45–50,

- 2013.
- [28] Y. C. M. Caglar, "The Determination Of The Thickness And Optical Constants Of The ZnO Crystalline Thin Film By Using Envelope Method," *Optoelectron. Adv. Mater.*, vol. 8, no. 4, pp. 1410–1413, 2006.
- [29] D. A. Skoog, *Principles of Instrumental Analysis (6 th Ed.)*. CA : Thomson Brooks/Cole, 2007.
- [30] E. R. Shaaban, I. S. Yahia, and E. G. El-Metwally, "Validity of swanepoel's method for calculating the optical constants of thick films," *Acta Phys. Pol. A*, vol. 121, no. 3, pp. 628–635, 2012.
- [31] P. K. Manoj, B. Joseph, V. K. Vaidyan, and D. S. D. Amma, "Preparation and characterization of indium-doped tin oxide thin films," *Ceram. Int.*, vol. 33, no. 2, pp. 273–278, 2007.
- [32] Y. C. M. Caglar, "The Determination Of The Thickness And Optical Constants Of The ZnO Crystalline Thin Film By Using Envelope Method," *Optoelectron. Adv. Mater.*, vol. 8, no. 4, pp. 1410–1413, 2006.
- [33] A. Abdelkrim, S. Rahmane, O. Abdelouahab, A. Hafida, and K. Nabila, "Optoelectronic properties of SnO<sub>2</sub> thin films sprayed at different deposition times," *Chinese Phys. B*, vol. 25, no. 4, p. 46801, 2016.
- [34] D. B. M. Hoffman., S. Martin; W. Choi, "Environmental Applications of Semiconductor Photo Catalysis," *Chem. Rev.*, vol. 95, no. 1, pp. 69–96, 1995.
- [35] S. J. Ikhmayies and R. N. Ahmad-Bitar, "A study of the optical bandgap energy and Urbach tail of spray-deposited CdS:In thin films," *J. Mater. Res. Technol.*, vol. 2, no. 3, pp. 221–227, Jul. 2013.
- [36] T. H. Gfroerer, "Photoluminescence in Analysis of Surfaces and Interfaces. In Encyclopaedia of Analytical Chemistry," *f Analytical Chemistry*. John Wiley & Sons Ltd, Chichester, pp. 9209–9231, 2000.
- [37] T. B. A. Mengistu, T. Grossmann, "Strongly confining bare core CdTe quantum dots in polymeric microdisk resonators," *APL Mater.*, vol. 2, no. 1, 2013.
- [38] J. Garnier, "Elaboration de couches minces d'oxydes transparents et conducteurs par spray cvd assiste par radiation infrarouge pour applications photovoltaïques l'École Nationale Supérieure d'Arts et Métiers Spécialité 'Énergétique , génie des procédés,'" Angers Bordeaux, Paris, 2009.
- [39] P. K. S. Myint, "Optical and electrical properties of polycrystalline SnO<sub>2</sub>:Sb thin films," *Yangon Inst. Educ. Res. J*, vol. 4, no. 1, 2012.

- [40] M. G. T. C.M. Mahajan, "Intermittent spray pyrolysis growth of nano crystalline and highly oriented transparent conducting ZnO thin films: effect of solution spray rate," *Alloy. Compd.*, vol. 584, pp. 128–135, 2014.
- [41] M. Lamri Zeggar, L. Chabane, M. S. Aida, N. Attaf, and N. Zebbar, "Solution flow rate influence on properties of copper oxide thin films deposited by ultrasonic spray pyrolysis," *Mater. Sci. Semicond. Process.*, vol. 30, pp. 645–650, 2015.
- [42] S. Gürakar, T. Serin, and N. Serin, "Electrical and microstructural properties of (Cu, Al, In)-doped SnO<sub>2</sub> films deposited by spray pyrolysis," *Adv. Mater. Lett.*, vol. 5, no. 6, pp. 309–314, 2014.
- [43] A. H. Omran Alkhayatt and S. K. Hussian, "Fluorine highly doped nanocrystalline SnO<sub>2</sub> thin films prepared by SPD technique," *Mater. Lett.*, vol. 155, pp. 109–113, 2015.
- [44] C. Sankar, V. Ponnuswamy, M. Manickam, R. Mariappan, and R. Suresh, "Structural , morphological , optical and gas sensing properties of pure and Ru doped SnO<sub>2</sub> thin films by nebulizer spray pyrolysis technique," *Appl. Surf. Sci.*, vol. 349, pp. 931–939, 2015.
- [45] N. S. S. Chacko, "Effect of substrate temperature on structural, optical and electrical properties of spray pyrolytically grown nanocrystalline SnO<sub>2</sub> thin films," *Phys. Status Solidi (A)*, vol. 204, no. 10, pp. 3305–3315, 2007.
- [46] T. V. Vimalkumar, "On tuning the orientation of grains of spray pyrolysis ZnO thin films," *Appl. Surf. Sci.*, vol. 256, pp. 6025–6028, 2010.
- [47] B. B. S. Abbas, "Effect of film thickness on the structural, optical and electrical properties of SnO<sub>2</sub>: F thin films prepared by spray ultrasonic for solar cells applications," *Super lattices Microstruct.*, vol. 83, 2015.
- [48] T. P. D. P. V.S. Vaishnava, "Preparation and characterization of indium tin oxide thin films for their application as gas sensors," *Thin Solid Films*, vol. 487, pp. 277–282, 2005.
- [49] A. L. C. Nacereddine, "Structural, electrical and magnetic properties of evaporated Ni/Cu and Ni/glass thin films," *Mater. Sci. Eng. B*, vol. 136, pp. 197–202, 2007.
- [50] B. C. Y. S. Gupta, "Microstructural, optical and electrical investigations of Sb-SnO<sub>2</sub> thin films deposited by spray pyrolysis," *Mater. Res. Bull.*, vol. 48, pp. 3315–3322, 2013.
- [51] M. S. Aida. N. Lehraki a, "ZnO thin films deposition by spray pyrolysis: Influence of precursor solution Properties," *Curr. Appl. Phys.*, vol. 12, pp. 1283–1287, 2012.
- [52] S. A. A. Mosbaha, "Preparation of highly textured surface ZnO thin films," *Mater. Sci. Eng. B*, vol. 129, p. 144–149., 2006.
- [53] S. A. V Soleimanian, "The influence of annealing temperature on the slip plane activity and optical properties of nanostructured ZnO films," *Appl. Surf. Sci.*, vol. 258, no. 4, pp.

- 1495–1504, 2011.
- [54] U. D. M. Batzill, “The surface and materials science of tin oxide,” *Prog. Surf. Sci.*, vol. 79, pp. 47–154, 2005.
- [55] W. Daranfedi, M.S. Aida, N. Attaf, J. Bougdira, *Properties and Characterization of Modern Materials*, vol. 33, no. January. Springer, 2017.
- [56] C. Nacereddine *et al.*, “Structural, electrical and magnetic properties of evaporated Ni/Cu and Ni/glass thin films,” *Mater. Sci. Eng. B Solid-State Mater. Adv. Technol.*, vol. 136, no. 2–3, pp. 197–202, 2007.
- [57] S. Benzitouni *et al.*, “High Sensitivity of Porous Cu-Doped SnO<sub>2</sub> Thin Films to Methanol,” *Adv. Nanoparticles*, vol. 5, no. 5, pp. 140–148, 2016.
- [58] V. Fauzia, M. N. Yusnidar, L. H. Lalasari, A. Subhan, and A. A. Umar, “High figure of merit transparent conducting Sb-doped SnO<sub>2</sub> thin films prepared via ultrasonic spray pyrolysis,” *J. Alloys Compd.*, vol. 720, pp. 79–85, 2017.
- [59] T. W. Kim, D. U. Lee, and Y. S. Yoon, “Microstructural, electrical, and optical properties of SnO<sub>2</sub> nanocrystalline thin films grown on InP (100) substrates for applications as gas sensor devices,” *J. Appl. Phys.*, vol. 88, no. 6, p. 3759, 2000.
- [60] S. Bansal, D. K. Pandya, S. C. Kashyap, and D. Haranath, “Growth ambient dependence of defects, structural disorder and photoluminescence in SnO<sub>2</sub> films deposited by reactive magnetron sputtering,” *J. Alloys Compd.*, vol. 583, pp. 186–190, 2014.
- [61] Y. Cao *et al.*, “Improved photocatalytic activity of Sn<sup>4+</sup>,” *New J. Chem.*, vol. 28, pp. 218–222, 2004.
- [62] R. K. Mishra, A. Kushwaha, and P. P. Sahay, “Influence of Cu doping on the structural, photoluminescence and formaldehyde sensing properties of SnO<sub>2</sub> nanoparticles,” *RSC Adv.*, vol. 4, no. 8, pp. 3904–3912, 2014.
- [63] T. Tomita, K. Yamashita, Y. Hayafuji, and H. Adachi, “The origin of n-type conductivity in undoped In<sub>2</sub>O<sub>3</sub>,” *Appl. Phys. Lett.*, vol. 87, no. 5, pp. 5–8, 2005.
- [64] C. Khelifi, A. Attaf, H. Saidi, A. Yahia, and A. Saadi, “Effect of solution flow on the properties of tin dioxide SnO<sub>2</sub> thin films deposited by spray pyrolysis technique,” *Opt. - Int. J. Light Electron Opt.*, vol. 127, no. 23, pp. 11055–11062, 2016.
- [65] A. A. Yadav, “Influence of film thickness on structural, optical, and electrical properties of spray deposited antimony doped SnO<sub>2</sub> thin films,” *Thin Solid Films*, vol. 591, no. May, pp. 18–24, 2015.
- [66] M. Thirumoorthi and J. T. J. Prakash, “Effect of F doping on physical properties of (211) oriented SnO<sub>2</sub> thin films prepared by jet nebulizer spray pyrolysis technique,”

- Superlattices Microstruct.*, vol. 89, no. 211, pp. 378–389, 2016.
- [67] B. D. DEMET TATAR, GÜVEN TURGUT, “Effect of Substrate Temperature on the Crystal Growth,” *Rom. Journ. Phys*, vol. 58, pp. 143–158, 2013.
- [68] B. Benhaoua, S. Abbas, A. Rahal, A. Benhaoua, and M. S. Aida, “Effect of film thickness on the structural, optical and electrical properties of SnO<sub>2</sub>: F thin films prepared by spray ultrasonic for solar cells applications,” *Superlattices Microstruct.*, vol. 83, pp. 78–88, 2015.
- [69] Y. Wang, W. Tang, and L. Zhang, “Crystalline Size Effects on Texture Coefficient, Electrical and Optical Properties of Sputter-deposited Ga-doped ZnO Thin Films,” *J. Mater. Sci. Technol.*, vol. 31, no. 2, pp. 175–181, 2015.
- [70] N. H. Toudjjen, B. Bendahmane, M. L. Zeggar, F. Mansour, and M. S. Aida, “SnO<sub>2</sub> thin film synthesis for organic vapors sensing at ambient temperature,” *Sens. Bio-Sensing Res.*, vol. 11, no. December, pp. 52–57, 2016.
- [71] Güven and U. T. Sönmez, Erdal S. Aydınb, R. Dilbera, “Synthesis and characterization of Mo doped SnO<sub>2</sub> thin films with spray pyrolysis,” *Superlattices Microstruct.*, vol. 69, no. November, pp. 175–186, 2014.
- [72] A. Bouhdjer, A. Attaf, H. Saidi, H. Bendjedidi, Y. Benkhetta, and I. Bouhaf, “Correlation between the structural, morphological, optical, and electrical properties of In<sub>2</sub>O<sub>3</sub> thin films obtained by an ultrasonic spray CVD process,” *J. Semicond.*, vol. 36, no. 8, p. 82002, 2015.
- [73] S. S. Shinde, A. P. Korade, C. H. Bhosale, and K. Y. Rajpure, “Influence of tin doping onto structural, morphological, optoelectronic and impedance properties of sprayed ZnO thin films,” *J. Alloys Compd.*, vol. 551, pp. 688–693, 2013.
- [74] A. Arunachalam, S. Dhanapandian, and C. Manoharan, “Effect of Sn doping on the structural, optical and electrical properties of TiO<sub>2</sub> films prepared by spray pyrolysis,” *Phys. E Low-Dimensional Syst. Nanostructures*, vol. 76, pp. 35–46, 2015.
- [75] B. Thangaraju, “Structural and electrical studies on highly conducting spray deposited fluorine and antimony doped SnO<sub>2</sub> thin films from SnCl<sub>2</sub> precursor,” *Thin Solid Films*, vol. 402, no. 1–2, pp. 71–78, 2002.
- [76] P. Malik, M. Srivastava, R. Verma, M. Kumar, D. Kumar, and J. Singh, “Nanostructured SnO<sub>2</sub> encapsulated guar-gum hybrid nanocomposites for electrocatalytic determination of hydrazine,” *Mater. Sci. Eng. C*, vol. 58, pp. 432–441, 2016.
- [77] A. R. Paloly, M. Satheesh, M. C. Martinez-Tomas, V. Munoz-Sanjose, S. Rajappan Achary, and M. J. Bushiri, “Growth of tin oxide thin films composed of nanoparticles on

- hydrophilic and hydrophobic glass substrates by spray pyrolysis technique,” *Appl. Surf. Sci.*, vol. 357, pp. 915–921, 2015.
- [78] P. M. Mwathe, “Influence of Surface Passivation on Optical Properties of Spray Pyrolysis Deposited Pd-F:SnO<sub>2</sub>,” *Int. J. Mater. Sci. Appl.*, vol. 3, no. 5, p. 137, 2014.
- [79] F. Moharrami, M. M. Bagheri-Mohagheghi, and H. Azimi-Juybari, “Study of structural, electrical, optical, thermoelectric and photoconductive properties of S and Al co-doped SnO<sub>2</sub> semiconductor thin films prepared by spray pyrolysis,” *Thin Solid Films*, vol. 520, no. 21, pp. 6503–6509, 2012.
- [80] Y. M. Lu *et al.*, “Polycrystalline SnO<sub>2</sub> films grown by chemical vapor deposition on quartz glass,” *Vacuum*, vol. 122, pp. 3–8, 2015.
- [81] M. Thirumoorthi and J. T. J. Prakash, “Effect of F doping on physical properties of (211) oriented SnO<sub>2</sub> thin films prepared by jet nebulizer spray pyrolysis technique,” *Superlattices Microstruct.*, vol. 89, pp. 378–389, 2016.
- [82] S. S. Roy and J. Podder, “Studies on tin oxide ( SnO<sub>2</sub> ) and CU doped SnO<sub>2</sub> Tthin films deposited by spray pyrolysis technique for window materials in solar cells,” *Proc. Int. Conf. Mech. Eng.*, vol. 2009, no. December, pp. 26–28, 2009.
- [83] J. T. Wang *et al.*, “Influence of Preferred Orientation on the Electrical Conductivity of Fluorine-Doped Tin Oxide Films,” *Sci. Rep.*, vol. 4, pp. 1–9, 2015.
- [84] J. M. G. Y. J. and F. P.-R. Mou Pal\*, Umapada Pal, “Effects of crystallization and dopant concentration on the emission behavior of TiO<sub>2</sub>: Eu nanophosphors,” *Nanoscale Res. Lett.*, vol. 7, no. 1, pp. 1–11, 2012.
- [85] M. G. Ilkay Cesar, Andreas Kay, José A. Gonzalez Martinez, “Translucent Thin Film Fe<sub>2</sub>O<sub>3</sub> Photoanodes for Efficient Water Splitting by Sunlight: Nanostructure-Directing Effect of Si-Doping,” *Am. Chem. Soc.*, vol. 128, no. 14, pp. 4582–4583, 2006.
- [86] S. P. S. Cynthia<sup>1</sup>, R. Sivakumar, C. Sanjeeviraja<sup>1</sup>, “Characterization of ZnO:SnO<sub>2</sub> (50:50) thin film deposited by RF magnetron sputtering technique,” *AIP Conf. Proc.*, vol. 1728, no. 1, 2016.
- [87] T. F. John Orton, *Molecular Beam Epitaxy: A Short History*. Oxford University: Press Amazon France, 2015.
- [88] X. Wang, Q. Di, H. Zhao, B. Liang, and J. Yang, “Mutual effects of fluorine dopant and oxygen vacancies on structural and luminescence characteristics of F doped SnO<sub>2</sub>nanoparticles,” *Materials (Basel)*, vol. 10, no. 12, 2017.
- [89] G. Lutz, *semiconductor radiation detectors*. Munich, Germany: springer.

ॐ नमो भगवते वासुदेवाय

गणेशाय नमः

ॐ नमो भगवते वासुदेवाय

## الشرائح الرقيقة لثنائي أكسيد القصدير ( $\text{SnO}_2$ )الموضوعة بتقنية الرش فوق الصوتي: خصائص وتطبيقات

### ملخص

قمنا في هذا العمل بتحضير شرائح رقيقة من ثنائي أكسيد القصدير ( $\text{SnO}_2$ ) فوق مساند من الزجاج الشفاف باستخدام تقنية الرش

فوق الصوتي، حيث في البداية تم تغيير التدفق من 50 الى 175 مل/سا لاختيار أفضل قيمة لنسجتها في باقي الدراسة.

لأجل تحسين خصائص شرائح  $\text{SnO}_2$  النقية قمنا بتطعيمها بالتيتانيوم ثم بالفلور؛ بعد دراسة فعل التطعيم قمنا باختيار الأفضل في كل

منهما وطعمنا بهما معا للحصول على شرائح ذات خصائص أفضل. تمت معالجة تأثير التطعيم على الشرائح المحضرة باستخدام عدة تقنيات للتشخيص

مثل انعراج الأشعة السينية، التي بينت ان بنية الشرائح بقيت رباعية كما هي ومتعددة البلورات ذات اتجاه نمو مفضل (110) في بعضها و (200)

في البعض الآخر؛ كما بينت مطيافية الأشعة فوق البنفسجية والمرئية ان نفاذية الشرائح تحسنت بعد التطعيم، بلغت نسبة 86 % مع ناقلية كهربائية

عالية وصلت الى  $10.10^2$  (اوم. سم)<sup>-1</sup>. كما أن الشرائح المطعمة بالتيتانيوم أظهرت شرائح بسلك صغير وصل الى 600 نانومتر تقريبا مع نفاذية

وناقية عاليتين مما يجعلها جيدة في التطبيقات الكهروضوئية.

بنيت الدراسة بالمجهر الإلكتروني الماسح بنية متجانسة للشرائح المطعمة أفضل من النقية مع حجم حبيبات كبير يتغير بتغير شائبة التطعيم.

كما تميزت شرائح  $\text{SnO}_2$  المطعمة بفواصل طاقي يتراوح بين 3.6 الى 4ev تقريبا.

**الكلمات المفتاحية:** أكسيد القصدير؛ شرائح رقيقة؛ الرش فوق صوتي؛ التدفق؛ التطعيم؛ الخصائص البنيوية، البصرية والكهربائية.

## Tin dioxide $\text{SnO}_2$ thin films deposited by ultrasonic spray technique. Properties and applications

### Abstract

In this work, we have prepared tin dioxide thin films  $\text{SnO}_2$  onto glass substrates, using ultrasonic spray technique. Firstly, the flow rate has been changed from 50 to 175ml/h in order to shows the best values for use it in all the study.

For enhance the properties of the pure  $\text{SnO}_2$ , the films were doped with titanium Ti:  $\text{SnO}_2$  and fluorine (F:  $\text{SnO}_2$ ) then after we shows the best values of each one to prepare Ti-F: Co-doping. Many characterizations techniques had done to explore the properties of all the films. The XRD shows that the tetragonal structure remains the same with good crystallization. The poly crystalline structure represents favorable orientation (110) with some films and (200) with the others. While UV-visible results showed transmittance up to 86% approximately and high electrical conductivity up to  $10.10^2$  ( $\Omega\cdot\text{cm}$ )<sup>-1</sup>.

The Ti- $\text{SnO}_2$  doping represented the smallest thickens 600 nm approximately with high transparency and conductivity that make them good candidate for optoelectronic applications.

The SEM study represent big homogenous with good structure better than the pure  $\text{SnO}_2$  with changed with the dopant. More that the doped films represented optical band gap between 3.6 to 4 eV approximately.

**Keywords:**  $\text{SnO}_2$  thin films, ultrasonic spray pyrolysis, flow, doping, structural, optical and electrical properties.